

A MIXED-INTEGER NONLINEAR PROGRAM FOR THE OPTIMAL
DESIGN AND DISPATCH OF FUEL CELL-BASED DISTRIBUTED
GENERATION SYSTEMS

by

Kristopher A. Pruitt

© Copyright by Kristopher A. Pruitt, 2012

All Rights Reserved

A thesis submitted to the Faculty and the Board of Trustees of the Colorado School of Mines in partial fulfillment of the requirements for the degree of Doctorate of Philosophy (Mineral and Energy Economics).

Golden, Colorado

Date _____

Signed: _____
Kristopher A. Pruitt

Signed: _____
Dr. Alexandra M. Newman
Thesis Advisor

Signed: _____
Dr. Robert J. Braun
Thesis Advisor

Golden, Colorado

Date _____

Signed: _____
Dr. Roderick G. Eggert
Professor and Head
Department of Economics and Business

ABSTRACT

Distributed generation (DG) technologies have promoted interest in alternative sources of energy for buildings due to their potential to supply heat and power at a lower cost and emissions compared to centralized generation. Accordingly, we present an optimization model that determines the mix, capacity, and operational schedule of DG technologies that minimize economic and environmental costs subject to the energy demands of a building and to the performance characteristics of generation and storage technologies.

Modeling the acquisition of discrete technologies requires integer restrictions, while modeling the variable efficiency of generators (e.g., fuel cells) and the variable temperature of thermal storage introduces nonlinear equality constraints. Thus, our model is a nonconvex, mixed-integer nonlinear program (MINLP). Given the difficulties associated with solving nonconvex MINLPs, we present convex underestimation and linearization techniques to bound and solve the problem. The solutions provided by our techniques are close to those provided by existing solvers for small problem instances. However, our methodology offers the possibility to solve larger instances that exceed the capacity of existing solvers and that are critical to the real-world application of the model.

Our MINLP models off-design performance characteristics of generation and storage technologies that are simplified or ignored in existing research. The consideration of these characteristics can be important for applications that require a time-varying dispatch from the technologies. We demonstrate the impact of ignoring off-design performance by comparing the solution prescribed by a simpler model with that of our MINLP for a representative case study. The simpler model overestimates the DG operational costs and underestimates the optimal DG capacity.

Our MINLP provides a means of conducting sensitivity analyses to determine scenarios that are favorable for DG investment. However, the complexity of our MINLP dictates that large instances of the problem are difficult to solve. Also, for many scenarios, the optimal design and dispatch does not include DG. Consequently, significant time and effort could be expended solving instances for which DG is not economically viable. Thus, we perform a comparative static analysis of the objective function of our MINLP to derive parametric conditions for which DG is economically viable.

TABLE OF CONTENTS

ABSTRACT	iii
LIST OF FIGURES	viii
LIST OF TABLES	x
NOMENCLATURE	xii
LIST OF ABBREVIATIONS	xvi
ACKNOWLEDGMENTS	xvii
INTRODUCTION	1
CHAPTER 1 LITERATURE REVIEW	9
1.1 Approaches	9
1.2 Applications	11
CHAPTER 2 MODEL	17
2.1 System Technologies	17
2.2 Model Description	20
2.3 Mathematical Formulation (\mathcal{P})	22
2.3.1 Minimum Total Cost	24
2.3.2 Power and Heating Demand	28
2.3.3 Utility Restrictions	29
2.3.4 Power Capacity	29
2.3.5 Electric Efficiency	29
2.3.6 Natural Gas Consumption	30

2.3.7	Start Up and Ramping	31
2.3.8	Power Storage	31
2.3.9	Heat Capacity	32
2.3.10	Heat Storage	32
2.3.11	Heat Storage Acquisition	33
2.3.12	Non-negativity and Integrality	34
CHAPTER 3 SOLUTION TECHNIQUES		35
3.1	Mathematical Structure	35
3.2	Lower Bounding: Convex Underestimation (\mathcal{U})	38
3.3	Upper Bounding: Linearization Heuristic (\mathcal{H})	41
3.4	Comparison with Existing Solvers	46
CHAPTER 4 SHORTFALLS IN SIMPLER MODELS		53
4.1	System Operating Strategies	54
4.2	Simplified Formulation (\mathcal{S})	58
4.3	Qualitative Differences Between (\mathcal{P}) and (\mathcal{S})	61
4.4	Quantitative Differences Between (\mathcal{P}) and (\mathcal{S})	68
CHAPTER 5 ECONOMIC SCREENING CRITERIA		79
5.1	Cost Analysis	81
5.2	Savings Analysis	87
5.3	Building, Market, and Technology Scenarios	94
5.4	Scenario Analysis	99
5.4.1	Savings Sensitivity Across Scenarios	100
5.4.2	Savings Sensitivity Within Scenarios	109

CHAPTER 6 CONCLUSIONS	121
6.1 Major Findings	121
6.2 Future Work	123
REFERENCES CITED	127
APPENDIX A - AMPL CODE	133
A.1 Model File	133
A.2 Data File	154
A.3 Run File	160
A.4 Out File	167
APPENDIX B - STATE PRICING, EMISSIONS, AND GRID DATA	171

LIST OF FIGURES

Figure 2.1	Combined heat and power, distributed generation system	18
Figure 3.1	Power and heating demands for a large hotel located in southern California	46
Figure 3.2	Electricity and natural gas prices for commercial customers in southern California.	47
Figure 4.1	Baseload strategy	55
Figure 4.2	Reduced, combined heat and power, distributed generation system	57
Figure 4.3	Load-following strategy	58
Figure 4.4	Comparison of SOFC natural gas consumption in (\mathcal{P}) versus (\mathcal{S}) . .	62
Figure 4.5	Comparison of storage tank heat charge in (\mathcal{P}) versus (\mathcal{S})	65
Figure 4.6	Comparison of storage tank heat discharge in (\mathcal{P}) versus (\mathcal{S})	66
Figure 4.7	Power and heating demands for a large hotel located in southern Wisconsin	70
Figure 4.8	Optimal SOFC power output and natural gas consumption as determined by (\mathcal{P}) versus (\mathcal{S}).	73
Figure 4.9	Optimal SOFC exhaust heat transferred to storage tank as determined by (\mathcal{P}) versus (\mathcal{S}).	74
Figure 4.10	Optimal storage tank water flowrate and temperature as determined by (\mathcal{P}).	75
Figure 4.11	Optimal storage tank heat dispatch as determined by (\mathcal{P}) versus (\mathcal{S}).	76
Figure 5.1	Further reduced, combined heat and power, distributed generation system	80
Figure 5.2	Power demands on peak power day for two building types and two locations	95

Figure 5.3	Heating demands on peak heating day for two building types and two locations	96
Figure 5.4	Weekday electricity and natural gas prices for two locations	97
Figure 5.5	Total annual savings for Scenario 5.	107
Figure 5.6	Total annual savings for Scenario 1.	108
Figure 5.7	Total annual savings for Scenario 2.	109
Figure 5.8	Sensitivity of the annual energy savings to changes in the rated electric efficiency of the SOFC.	111
Figure 5.9	Sensitivity of the annual emissions savings to changes in the rated electric efficiency of the SOFC.	112
Figure 5.10	Sensitivity of the annual O&M savings to changes in the rated electric efficiency of the SOFC.	113
Figure 5.11	Sensitivity of the break-even capital and installation cost to changes in the rated electric efficiency of the SOFC.	114
Figure 5.12	Sensitivity of the annual emissions savings to changes in the carbon tax rate.	116
Figure 5.13	Sensitivity of the break-even capital and installation cost to changes in the carbon tax rate.	117

LIST OF TABLES

Table 3.1	Size of (\mathcal{P}) instances for time horizons of interest.	36
Table 3.2	Generator cost and performance parameter values.	48
Table 3.3	Storage cost and performance parameter values.	49
Table 3.4	Comparison of solutions provided by (\mathcal{U}) and (\mathcal{H}) with those provided by MINOTAUR	50
Table 4.1	Annual power and heating demand statistics for a large hotel located in southern Wisconsin.	69
Table 4.2	Cost, emissions, and technology parameter values.	71
Table 4.3	Summary of solution differences between (\mathcal{P}) and (\mathcal{S})	77
Table 5.1	Size and demand statistics for a large hotel and medium office located in southern California (CA) and southern Wisconsin (WI).	94
Table 5.2	Building, market, and design and dispatch scenarios for which we examine the economic viability of a DG system.	99
Table 5.3	Annual energy savings per kW of SOFC system capacity provided in each scenario.	101
Table 5.4	Annual emissions savings per kW of SOFC system capacity provided in each scenario.	103
Table 5.5	Annual O&M savings per kW of SOFC system capacity provided in each scenario.	104
Table 5.6	Annual peak demand savings per kW of SOFC system capacity provided in each scenario.	105
Table 5.7	Total annual savings per kW of SOFC system capacity provided in each scenario.	106
Table B.1	2009 state energy pricing, carbon emissions rates, and net-metering grades for Alabama through Missouri	172

Table B.2	2009 state energy pricing, carbon emissions rates, and net-metering grades for Montana through Wyoming	173
Table B.3	2010 state energy pricing, carbon emissions rates, and net-metering grades for Alabama through Missouri	174
Table B.4	2010 state energy pricing, carbon emissions rates, and net-metering grades for Montana through Wyoming	175

NOMENCLATURE

The sets, parameters, and variables referenced throughout the document are listed alphabetically below. Upper-case letters identify variables or sets, while lower-case letters identify parameters or set indices. Superscripts and accents differentiate parameters and variables that use the same base letter. Subscripts distinguish between elements of a set. Some parameters and variables, which are identified in a given problem formulation, are only defined for certain elements of sets. The units of each parameter and variable are provided in brackets after its definition.

Sets

$i \in \mathcal{I}$	set of all cost elements
$j \in \mathcal{J}$	set of all technologies
$n \in \mathcal{N}$	set of all months
$t \in \mathcal{T}_n$	set of all hours in month n
$t \in \mathcal{T}$	set of all hours ($\mathcal{T} = \bigcup_n \mathcal{T}_n$)

Parameters

α_j	average ambient heat loss of water stored in each technology j [fraction]
γ_j	average exhaust output from each technology j per natural gas input [kg/kWh]
δ	demand time increment [hours]
ε	an arbitrarily small positive quantity
η_j^{\max}	maximum electric efficiency of each technology j [fraction]
η_j^{\min}	minimum electric efficiency of each technology j [fraction]

η_j^P	rated electric efficiency of each technology j [fraction]
η_j^Q	rated thermal efficiency of each technology j [fraction]
μ_j	maximum turn-down of each technology j [fraction]
ν_t	net-metering rate paid by utility for exported power in hour t [fraction]
σ_j	start-up time for each technology j to reach operating temperature [hours]
τ_j^{in}	average temperature of fluid into each technology j [$^{\circ}\text{C}$]
τ_j^{out}	average temperature of fluid out of each technology j [$^{\circ}\text{C}$]
τ^{max}	maximum temperature of water in the system [$^{\circ}\text{C}$]
τ^{min}	minimum temperature of water in the system [$^{\circ}\text{C}$]
a_{jt}	average availability of each technology j based on weather in hour t [fraction]
c_j	amortized capital and install cost of each technology j [\$/kWh, \$/kW, or \$/gal]
d_t^P	average power demand of building in hour t [kW]
d_t^Q	average heating demand of building in hour t [kW]
g_t	price of natural gas from the utility in hour t [\$/kWh]
h_j	specific heat of fluid output from each technology j [kWh/(kg $^{\circ}\text{C}$)]
k_j^{in}	nameplate power rating into each technology j [kW]
k_j^{out}	nameplate power rating out of each technology j [kW]
m_j	average O&M cost of each technology j [\$/kWh]
p_t	price of power from the utility in hour t [\$/kWh]
p_n^{max}	peak demand charge for power from the utility in month n [\$/kW/month]
r_j^{down}	maximum ramp-down rate for each technology j [kW/hr]
r_j^{up}	maximum ramp-up rate for each technology j [kW/hr]

- s_j^{\max} . . . maximum nameplate energy storage capacity of each technology j [kWh]
- s_j^{\min} . . . minimum nameplate energy storage capacity of each technology j [kWh]
- v_j^{\max} . . . maximum nameplate water storage capacity of each technology j [gallons]
- v_j^{\min} . . . minimum nameplate water storage capacity of each technology j [gallons]
- z tax on carbon emissions [\$/kg]
- z^g average carbon emissions rate for natural gas combustion [kg/kWh]
- z^p average carbon emissions rate for utility power [kg/kWh]

Variables

- A_j number of each technology j acquired [integer]
- B_{jt}^{in} . 1 if water in each technology j is above $(\tau_j^{\text{in}} + \varepsilon)$ in hour t , 0 otherwise [binary]
- B_{jt}^{out} . . 1 if water in each technology j is above τ_j^{out} in hour t , 0 otherwise [binary]
- C_i total cost of cost element i over time horizon of length $|\mathcal{T}|$ [\$]
- E_{jt} electric efficiency of each technology j operating in hour t [fraction]
- F_{jt}^{in} flowrate of exhaust gas into each technology j in hour t [kg/hr]
- F_{jt}^{out} flowrate of water out of each technology j in hour t [gal/hr]
- G_{jt} aggregate natural gas input to each technology j in hour t [kW]
- N_{jt} number of each technology j operating in hour t [integer]
- \acute{N}_{jt} . increased number of each technology j operating from hour $t - 1$ to t [integer]
- P_{jt}^{in} aggregate power input to each technology j in hour t [kW]
- P_{jt}^{out} aggregate power output from each technology j in hour t [kW]
- Q_{jt} aggregate thermal energy stored in each technology j at the start of hour t [kWh]
- Q_{jt}^{in} aggregate heat input to each technology j in hour t [kW]

Q_{jt}^{out} aggregate heat output from each technology j in hour t [kW]
 S_{jt} . . . aggregate state-of-charge of each technology j at the start of hour t [kWh]
 T_{jt} temperature of water stored in each technology j in hour t [°C]
 U_t^{in} power sold to the utility in hour t [kW]
 U_t^{out} power purchased from the utility in hour t [kW]
 U_n^{max} peak power purchased from the utility in month n [kW]
 V_j water storage capacity of technology j [gallons]

LIST OF ABBREVIATIONS

California Independent System Operator	CAISO
Combined Heat and Power	CHP
Distributed Energy Resources Customer Adoption Model	DER-CAM
Distributed Generation	DG
Department of Energy	DOE
Evolutionary Algorithm	EA
Energy Information Administration	EIA
Genetic Algorithm	GA
Hybrid Optimization Model for Electric Renewables	HOMER
Lawrence Berkeley National Laboratory	LBNL
Linear Program	LP
Mixed-Integer Linear Program	MILP
Mixed-Integer Nonlinear Program	MINLP
Nonlinear Program	NLP
Network for New Energy Choices	NNEC
National Renewable Energy Laboratory	NREL
Photovoltaic	PV
Solid-Oxide Fuel Cell	SOFC

ACKNOWLEDGMENTS

It is with immense gratitude that I acknowledge the help of my co-advisors, Dr. Alexandra Newman and Dr. Robert Braun. Dr. Newman consistently provided invaluable guidance throughout the research process, particularly regarding mathematical modeling and technical writing. As the perfect complement to Dr. Newman, Dr. Braun was a constant source of expert instruction on engineering and the real-world applications of our mathematical models. I sincerely appreciate their advice throughout my research.

I am also indebted to Dr. Sven Leyffer at Argonne National Laboratory. Dr. Leyffer's expertise in the field of nonlinear programming proved critical to overcoming some of the most difficult roadblocks in my research. His assistance was above and beyond anything I could have asked of a committee member. That said, it is a pleasure to thank the remaining members of my committee, Dr. Daniel Kaffine, Dr. Dinesh Mehta, Dr. Steffen Rebennack, and Dr. Tyrone Vincent, for the time spent reviewing my work during the proposal and final defense process.

I would like to thank the National Science Foundation for partial support of this research effort under award #CNS-0931748. I am also grateful to fellow graduate student Andrew Schmidt for providing the building load data from EnergyPlus.

Finally, and most importantly, I owe my deepest gratitude to my wife, Kelly, and our two children, Layla and Brayden. Kelly was, and continues to be, the most patient, loving, supportive, and encouraging wife any man could ask for. I am deeply sorry for the countless hours I spent on this research that I could have spent with her and our kids. Kelly, I love you!

INTRODUCTION

Distributed generation (DG) has gained interest as an alternative source of power for new and existing buildings in the residential, commercial, and industrial sectors. Rather than solely purchasing electricity from a centralized utility, a building owner can invest in an on-site system to supply power using non-renewable technologies such as reciprocating engines, microturbines, and fuel cells, and renewable technologies such as photovoltaic (PV) cells, wind turbines, and geothermal-based power generators. When integrated with heat recovery equipment, solar thermal collectors, and absorption chillers, on-site systems can also supply some of the heating and cooling demands. In addition to generation, DG systems can include electric and thermal storage technologies to address the uncertainty in the supply available from renewable generators or to take advantage of time periods in which utility prices are low. Our research considers the integration of technologies such as these with existing commercial buildings.

There are a number of reasons why DG systems should be considered for commercial building applications. Between 2005 and 2009, the commercial sector accounted for 36% of electricity consumption across all sectors, which resulted in an average annual cost of roughly \$127 billion (see [1]). Gumerman et al. [2] list benefits to the owner of DG systems, which have the potential to reduce this economic burden. These benefits include a lower cost of electricity (in some markets), protection from utility price volatility, more reliable power, and greater energy efficiency. The authors further describe potential benefits of DG to the local community. When composed of “clean” natural gas-fed or renewable technologies, DG systems emit less carbon dioxide than most centralized power plants. Smaller, on-site generation also addresses much of the opposition in local communities to the construction of large power plants

and transmission lines. Yet, based on Department of Energy projections for electricity consumption and DG market penetration, on-site systems will supply a mere 2% of commercial sector electricity demand in 2035 (see [3]).

This disparity between the noted operational benefits of DG systems and the modest prediction for future market penetration exists for a variety of reasons. From a purely economic standpoint, many power utilities maintain low prices for electricity while the capital and installation costs for DG technologies remain high. This discrepancy has discouraged building owners from investing in DG systems. However, due to their lower emissions rates compared to those of centralized power plants, some DG technologies afford lower environmental costs which building owners often have no economic incentive to internalize. Properly considering *all* of the costs associated with generation, which include environmental costs and other externalities, effectively increases the price of electricity from the utility and may make DG more economically viable. Finally, DG has experienced limited implementation simply due to a lack of understanding regarding how to appropriately design (i.e., configure and size) and dispatch (i.e., operate) complex, mixed-resource systems. We refer to this task of determining the lowest cost mix, capacity, and operational schedule of DG technologies as the design and dispatch problem.

Extant research, which is reviewed in **Chapter 1**, focuses on various aspects of the design and dispatch problem. Many studies address the optimal performance of an individual DG technology, but do not resolve the system-level problem of integrating, sizing, and operating multiple technologies. Other research seeks the optimal operational strategy (i.e., dispatch) of an *existing* system, but does not consider the optimal combination and capacity (i.e., design) of technologies in which to invest. Our research focuses on the optimal design *and* dispatch of a DG system. Similarly focused research in the literature applies simulation models, evolutionary algorithms, or more traditional mathematical programming algorithms, such as branch-and-bound,

to the design and dispatch problem. In general, studies that apply simulation or evolutionary algorithms cannot guarantee global optimality of their solutions. The existing applications of branch-and-bound to the design and dispatch problem provide a guarantee of global optimality, but fail to consider many of the dynamic (i.e., off-design) performance characteristics of the technologies that are required to realistically model the system operation. Our research contributes to the literature by providing techniques for determining the provably globally minimum cost DG system design and dispatch without sacrificing realistic operation of the technologies. In this paper, we outline the contributions of our research in the form of three objectives.

Objective 1: Develop a tractable optimization model which determines how to design (i.e., configure and size) and dispatch (i.e., operate) a combined heat and power (CHP) DG system at the globally minimum economic and environmental cost. This model should include dynamic performance characteristics of the DG technologies.

Tractability is a concern with the development of a model such as this. First, the time fidelity and total time horizon under consideration can make instances of the model quite large. To realistically capture both short-term spikes and long-term seasonal shifts in demand, one might consider model instances with a one-year time horizon at the hourly level of fidelity. However, this results in 8,760 time periods for each time-varying variable and constraint in the model. Second, since the system design involves the acquisition of real technologies which are only manufactured in discrete sizes, the associated variables must assume integer values. Finally, realistically modeling the operation of complex, CHP systems requires constraints to control the operational status (i.e., standby or “on”), ramping (i.e., increasing or decreasing power output), and part-load (i.e., below maximum power output) electric efficiency of the generators. Constraints are also required to control the state-of-charge (i.e., in-

ventory) of electric storage technologies and the time-varying temperature of thermal storage technologies. These constraints can include integer variables in each time period, connections between consecutive time periods, and nonlinear equalities. Given all of these characteristics, the resulting model is a large, nonseparable, nonconvex, mixed-integer, nonlinear programming (MINLP) problem. **Chapter 2** presents the mathematical formulation of this MINLP, which we call (\mathcal{P}) .

There exist few algorithms suitable for solving large, nonconvex MINLPs, such as (\mathcal{P}) . Furthermore, existing algorithms are dependent on the problem structure. The application of a nonlinear branch-and-bound algorithm requires methods to obtain global upper and lower bounds on the objective value at each node in order to converge on the optimal solution. However, these bounds can be difficult to obtain for large, nonconvex problems. Thus, we develop problem-specific convex underestimation techniques, motivated by our engineering insight, to obtain global lower bounds on the objective value of (\mathcal{P}) . We also develop a linearization heuristic to obtain integer-feasible solutions, and thus global upper bounds, for (\mathcal{P}) . These bounding techniques can be applied as part of a nonlinear branch-and-bound algorithm to solve large instances of (\mathcal{P}) to global optimality. **Chapter 3** details our convex underestimation, called (\mathcal{U}) , and our linearization heuristic, called (\mathcal{H}) , and compares the solutions provided by these bounding techniques to those of existing MINLP solvers.

Objective 2: Evaluate the qualitative modeling differences and the quantitative solution differences between (\mathcal{P}) and simpler models which simplify or ignore dynamic performance characteristics of the DG technologies.

Simpler global optimization models for the design and dispatch of DG systems fail to consider many performance characteristics that constrain the dynamic operation of the technologies. Simplifying or ignoring these characteristics permits a mixed-

integer, linear programming (MILP) formulation of the problem with few integer variable restrictions. Thus, even large instances (i.e., long time horizons) of the design and dispatch problem can be solved with relative ease. However, insufficiently modeling the system dynamics could result in the prescription of unrealistic system dispatch schedules and, ultimately, in the recommendation of a suboptimal system design. Hence, a more detailed design and dispatch model is required to validate (or invalidate) the assumptions made in simpler, linear models.

(\mathcal{P}) addresses this requirement by prescribing a globally minimum cost system design and dispatch that includes dynamic performance characteristics of power and heat generation and storage that are not considered in simpler, linear models. In addition to typical constraints on demand, capacity, and inventory balance, (\mathcal{P}) models the maximum turn-down, start-up fuel consumption, ramping capability, and part-load electric efficiency of power generation technologies, and models the time-varying temperature of thermal storage technologies. The consideration of these dynamic performance characteristics can be particularly important when the technologies are operated in a load-following (i.e., time-varying), rather than baseload (i.e., fixed), manner. In some applications, the DG system configuration and capacity, the building's energy demands, and/or the local utility's rates, policies, and procedures may require a time-varying dispatch from the DG technologies. In these instances, (\mathcal{P}) captures the real-world operation of the technologies more accurately than models which simplify or ignore dynamic performance characteristics. **Chapter 4** presents a representative MILP formulation of the design and dispatch problem, which we call (\mathcal{S}), and discusses the qualitative and quantitative differences between (\mathcal{P}) and (\mathcal{S}).

Objective 3: Determine the parametric conditions for energy markets, building demands, and technology performance characteristics that make DG most economically viable.

(\mathcal{P}) provides a means to evaluate the economic viability of various DG technologies, integrated with different building types, which can be located in diverse energy markets. This type of sensitivity analysis can be accomplished by varying the parameter values (e.g., energy pricing, emissions rates, power and heating loads, capital and operational costs, and efficiencies) to create an array of problem instances, and then solving those instances of (\mathcal{P}) to determine which combinations of parameter values result in DG acquisition. However, large instances (e.g., a one-year time horizon at hourly fidelity) of (\mathcal{P}) can be time consuming and computationally expensive to solve. Additionally, for many instances, the combination of energy market, building type, and DG technology under consideration results in an optimal design and dispatch solution that does *not* include the acquisition of DG. This can be due to a variety of factors, including low-cost electricity from the utility, volatile and/or non-coincident electric and thermal loads for the building, and high capital cost and/or low efficiency for the DG technologies. In any case, a great deal of time and computing power can be expended solving various market-building-technology instances of (\mathcal{P}) in order to discover a combination for which DG is economically viable. For this reason, we wish to identify combinations which are likely to be economically viable prior to solving (\mathcal{P}) to determine the optimal design and dispatch.

In **Chapter 5**, we develop parametric conditions for the economic viability of a CHP DG technology. In other words, we determine conditions for which the savings from operating a CHP DG technology outweigh the cost of acquiring that technology. These parametric conditions address (i) the local energy market, via pricing and emissions rates, (ii) the building of interest, via energy demands and existing heating technology characteristics, and (iii) the CHP DG technology under consideration, via costs and performance characteristics. The development of conditions for these model parameters provides us screening criteria for the instances of (\mathcal{P}) we wish to solve.

Finally, **Chapter 6** concludes the paper by reviewing the major findings from each chapter, and by presenting recommendations for future work.

CHAPTER 1

LITERATURE REVIEW

A variety of methods and models, which are reviewed by Manfren et al. [4], are applied to the DG design and dispatch problem. There appear to be three primary solution techniques for existing models. Simulation, evolutionary algorithms, and more traditional mathematical programming algorithms are the most common techniques for determining what DG technologies to acquire and how to operate them to meet a building's energy demands. In this chapter, we discuss these three approaches in more detail and then present a review of the literature which applies each approach.

1.1 Approaches

Simulation models are intended to mimic the behavior of a system given fixed parameters and formulas which relate those parameters. Though the values of these parameters can be varied between runs to determine the sensitivity of the model, a simulation model cannot prescribe what parameter values lead to the desired outcome (i.e., there are no decision variables). When applied to the design and dispatch problem, simulation models can calculate the cost of acquiring a given system and operating it in a set manner, but they cannot determine what design and dispatch produces the lowest cost system within a single run. Instead, such models require the enumeration and simulation of many designs and dispatch schedules, and the selection of the lowest cost system out of those which were simulated. However, simulation models do have advantages when compared to other approaches. Most notably, they are capable of modeling stochastic parameter values and nonlinear relationships between parameters. Given the uncertainty of demand, weather, and pricing, as well as the nonlinearities inherent in modeling the operation of complex systems, simulation models provide a means of capturing aspects of the design and dispatch problem

that other approaches cannot. However, other approaches include algorithms which determine the parameter values (in this case, decision variable values) that result in an optimal outcome. Two classes of optimization algorithms applied in the DG literature are evolutionary algorithms and more traditional mathematical programming algorithms.

Evolutionary algorithms (EAs), including genetic algorithms (GAs), are search heuristics for optimization problems which generate candidate solutions to improve (evolve) initial solutions according to some objective(s). Generally, such algorithms terminate after a predetermined number of evolutions or when the value of the objective(s) is no longer improving. EAs have been developed, in large part, to overcome the difficulties associated with solving nonlinear optimization problems. For the design and dispatch problem, these algorithms can be used to determine the lowest cost system while realistically capturing the nonlinearities in the operation of the technologies. Unfortunately, this class of algorithms provides no guarantee of obtaining a globally optimal, or even locally optimal, solution. Because EAs do not include methods for bounding the optimal objective function value, there is no way of determining whether the solution which results from the algorithm is close to optimal.

More traditional optimization algorithms focus on obtaining solutions with the guarantee of global optimality. Linear programming (LP) problems that include only continuous-valued variables are solved with algorithms such as the simplex and interior point methods. These algorithms take advantage of the convex structure of linear, continuous problems in order to guarantee that any locally optimal solution is also a globally optimal solution. Mixed-integer, linear programming (MILP) problems are solved using the branch-and-bound algorithm. This algorithm solves continuous versions of the integer problem at each iteration by relaxing integrality restrictions to obtain upper and lower bounds on the optimal objective function value. When the upper and lower bounds converge, the algorithm obtains a guaranteed globally

optimal solution. When applied to the design and dispatch problem, the branch-and-bound method determines the mix, capacity, and operational schedule of DG technologies which meet the demands of a building at the globally minimum cost. However, these traditional algorithms are not capable of solving nonlinear problems. Solution criteria, such as Kuhn-Tucker optimality conditions, and techniques, such as Lagrangian relaxation, for nonlinearly constrained problems do exist. However, depending on the problem structure, there may be no guarantee of global optimality with these approaches. Accordingly, much of the work applied to the design and dispatch problem avoids the inherent nonlinearities in the system by developing simpler, linear formulations which can be solved with algorithms that guarantee global optimality. The next section presents applications of simulation models, evolutionary algorithms, and traditional algorithms.

1.2 Applications

Research regarding DG focuses on various aspects of the design and dispatch problem. Some studies address the optimal design of an individual DG technology, rather than the design of an integrated system of technologies. Braun [5] presents a techno-economic design model for a solid oxide fuel cell (SOFC) CHP system to determine operating parameters and capacities which maximize the life-cycle savings or minimize the life-cycle cost. Sayyaadi [6], Toffolo and Lazzaretto [7] develop a multi-objective EA to determine the pressure, temperature, and efficiency parameters for a gas turbine which minimize the levelized cost of investment, operation, and emissions while maximizing efficiency. Azhdari et al. [8] solve a linear program to determine the optimal distribution of available steam to turbines in order to maximize power output. Each of these studies presents the optimal design for an individual technology, but does not resolve the system-level problem of sizing, integrating, and operating multiple technologies together.

Many studies address the operation of an existing system, but do not consider the system design. Boait et al. [9] address DG system operation with a simulation model that evaluates the energy costs for various building sizes based on stochastic demand and disparate levels of occupancy. Mago and Hueffed [10] also simulate the operation of an existing system and test the impact of multiple operational strategies on cost, energy consumption from the grid, and carbon emissions. Nosrat and Pearce [11] simulate the operation of a hybrid PV-CHP system in order to determine the impact on dispatch strategy of accounting for building cooling loads. Subbaraj et al. [12] solve a nonlinear model of DG system operation using a GA to minimize the total fuel cost required to meet heat and power demand by choosing the dispatch levels from integrated power-only, heat-only, and CHP generators. Similarly, Kong and Wang [13] minimize the total cost of fuel and electricity to operate a DG system to meet power, heat, and cooling loads by selecting the optimal load fraction for a gas turbine and distribution of exhaust to a chiller and boiler. Ishida et al. [14] also model a gas turbine-based system, but derive Kuhn-Tucker optimality conditions to determine system operating levels that meet demand in a single time period at minimum operating cost. Firestone et al. [15] present a mixed-integer linear program with stochastic scenarios for load demand, generator availability, and solar capacity that determines the optimal dispatch of renewable and non-renewable generation in each hour in order to minimize the expected monthly operational cost. Though these studies examine the potential cost savings from operating a specific DG system, they do not address the design of the system itself.

Several existing studies consider both system design and dispatch, but apply dissimilar solution techniques, objectives, and technologies. Medrano et al. [16] simulate a small set of possible system designs, consisting of fuel cells, microturbines, photovoltaic (PV) cells, and absorption chillers, for four commercial building types, in order to compare annual costs and emissions to those of conventional systems. Though this

work does evaluate the savings associated with DG integration, the authors do not consider energy storage, and the system configuration, sizing, and operational strategy are determined a priori. When enumerating only a subset of possible system designs, there is no means to determine whether one of the few designs under consideration leads to globally minimum costs and emissions. The Hybrid Optimization Model for Electric Renewables (HOMER), developed by the National Renewable Energy Laboratory (NREL), is a simulation model which enumerates *all* possible configurations of a variety of user-specified DG technologies, including storage. HOMER calculates the hourly operation of the system configurations that can feasibly meet the annual demand of the building(s) of interest and rank orders the systems based on life-cycle cost (see [17], [18], [19], and [20]). Although these simulation models investigate feasible system configurations to determine which of the system designs under consideration provides the lowest cost, the system dispatch strategy is pre-specified by the user, rather than determined by the model. The inability to optimally select the system dispatch is particularly troublesome when the system design includes storage, because the model cannot consider the demand in future time periods when choosing the dispatch in the current time period. Thus, as with any simulation model, the results are inherently *descriptive* rather than *prescriptive*.

In contrast to simulation models, many studies prescribe the system design and dispatch with EAs. Burer et al. [21] combine simulation and EAs by initially simulating feasible system designs consisting of a combined-cycle fuel cell and gas turbine, a heat pump, and a chiller, and then using an EA to determine the optimal dispatch for each design. The optimal dispatch is based on either the minimum total annual cost or minimum carbon dioxide emissions. The authors apply the model to a cluster of residential buildings, which exhibits a very different load profile compared to a single commercial building, and do not consider storage or renewable sources of generation. Xu et al. [22] consider *only* storage and renewable generation by design-

ing a stand-alone wind-PV-battery power system for a small residence using a GA to simultaneously minimize the capital cost of the acquired technologies and maximize the reliability of the system. While this model addresses only the capital cost of a stand-alone renewable system, a hybrid renewable-nonrenewable, grid-connected system must also consider the operational cost of fuel and power from the utilities. Kayo and Ooka [23] minimize the consumption of fuel and power from the utilities using a GA to design and dispatch a DG system for a large commercial building that includes a gas-fed co-generation unit, a heat pump, a chiller, and PV cells. The system is designed by selecting from a list of capacity options for each technology and dispatched for three representative days throughout the year; however, the authors do not address the capital cost of designing the system.

Although these models are capable of prescribing a system design and dispatch schedule, the EA approach is fundamentally different than that of traditional mathematical programming algorithms. In general, search heuristics such as EAs do not include methods for bounding the optimal objective function value and terminate based solely on decreased improvement in the objective. Thus, there is often no way of determining whether the solution which results from the algorithm is close to globally (or even locally) optimal. By contrast, traditional algorithms apply global upper and lower bounding techniques which provide a provable measure of the quality of design and dispatch solutions. The work described next leverages provable global optimization techniques, such as the simplex and branch-and-bound algorithms, to determine the optimal system design and dispatch.

Weber et al. [24] combine EAs and the simplex algorithm by first determining the system design with a multi-objective EA aimed at minimizing the cost (capital and operational) and carbon emissions of the selected technologies, and then determining the system dispatch by solving a linear program that minimizes the cost of utility-purchased electricity and fuel. In this model, fuel cells are integrated with

heat exchangers, thermal storage tanks, and absorption chillers to meet the power, heating, and cooling demands of an office building for 12 representative days of the year. The authors do not consider net-metering, renewable generation, or electricity storage. Beihong and Weiding [25] and Oh et al. [26] present similar mixed-integer programs for optimally sizing and operating a DG system consisting of a gas turbine, a waste heat recovery boiler, and an absorption chiller, for a large commercial building. These models apply branch-and-bound algorithms to minimize the capital and operational costs of the system, subject to the power, heating, and cooling demands of the building and the minimum and maximum capacities of the technologies that are operating in a given representative time period. The authors do not consider renewable generation, energy storage, or the cost of emissions. Siddiqui et al. [27] and Ren and Gao [28] formulate similar MILPs for the optimal design and dispatch of a DG system that includes renewable generation, energy storage (thermal and electric), and the cost of carbon emissions. The Siddiqui et al. model, developed by researchers at Lawrence Berkeley National Laboratory (LBNL), is referred to as the Distributed Energy Resources Customer Adoption Model (DER-CAM). Instances of DER-CAM are solved using the branch-and-bound algorithm to determine the number of DG technologies to acquire, along with their operating levels over time, to meet the power, heating, and cooling demands of various building types at minimum capital, operational, and environmental (i.e., emissions) cost (see also [29] and [30]).

In contrast to other research, DER-CAM addresses both the design and dispatch of a DG system, applies a provable global optimization approach, includes both economic and environmental costs in its objective, and considers the generation and storage of both power and heat using renewable and nonrenewable technologies. Given all of these attributes, DER-CAM is the most flexible of the design and dispatch models in the existing literature. But, DER-CAM fails to consider many performance characteristics that constrain the dynamic (i.e., off-design) operation of DG technologies.

These characteristics can be critical to accurately modeling the operation of the DG system. Thus, (\mathcal{P}) contributes to the DG literature by providing a model that determines the globally minimum economic and environmental cost CHP system design and dispatch, while still considering the dynamic performance characteristics of the technologies.

CHAPTER 2

MODEL

In this chapter, we present a global optimization model that determines the minimum cost mix, capacity, and operational schedule of DG technologies that meet the hourly power and heating demands of an existing commercial building for an entire year. The characteristics of such a model can largely depend on the technologies under consideration. Thus, we begin the chapter by presenting the specific DG system considered in our research and by discussing the performance characteristics of the individual technologies in that system. We then provide a general description of the parameters, variables, objective, and constraints in the system model. We conclude the chapter by presenting the detailed mathematical formulation of (\mathcal{P}).

2.1 System Technologies

The specific system addressed in this research is depicted in Figure 2.1. We consider the retrofit of an existing commercial building with a CHP DG system. If no DG technologies are acquired, then the building receives all of its electricity from the power utility (i.e., macrogrid) and all of its heat from a natural gas-fired boiler. The cooling demand is met by existing vapor-compression air conditioning units and is included as part of the power demand. The heating demand includes space and water heating, both of which are met with hot water (i.e., space heat is provided by hot water radiators). Our model considers the acquisition of a DG system which generates power with fixed-tilt PV cells and/or natural gas-fed solid oxide fuel cells (SOFCs) which, according to Greene and Hammerschlag [31], provide lower carbon emissions than other DG-scale generators. The CHP SOFCs are integrated with heat exchangers and a water tank, which allow for the storage of thermal energy in the

form of hot water. The system also includes the option for electric storage using lead-acid batteries. We do not consider other non-renewable generators, wind turbines, solar thermal, or absorption chillers. However, our model can be adapted to include these technologies.

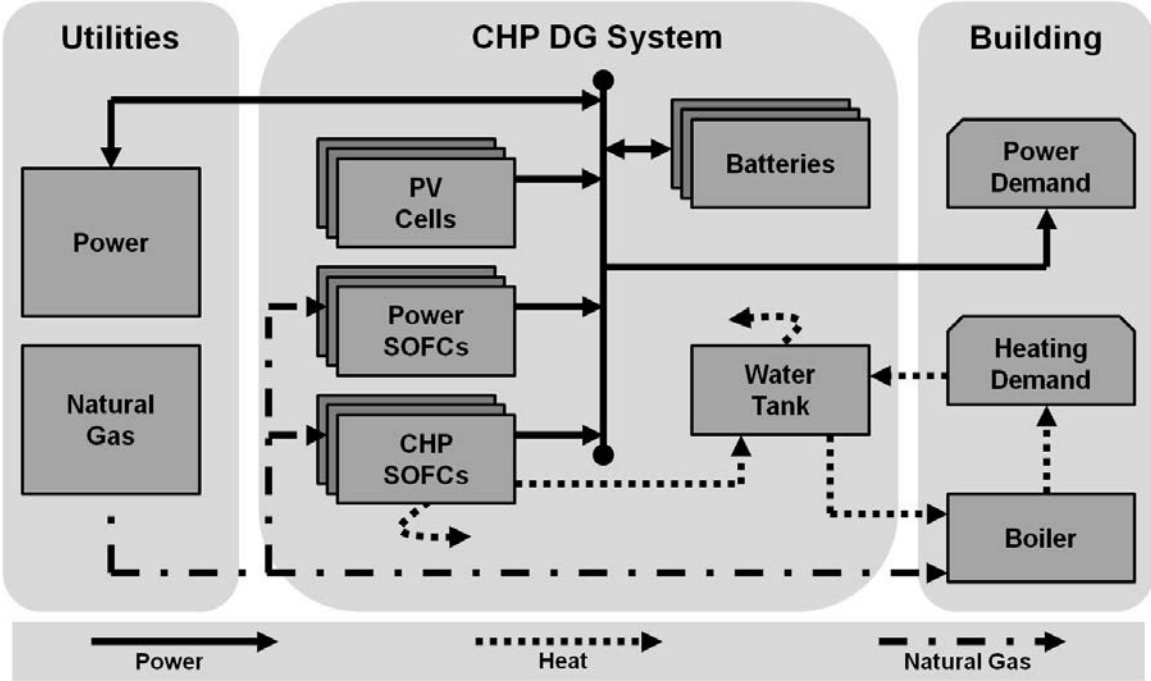


Figure 2.1: Combined heat and power (CHP), distributed generation (DG) system consisting of photovoltaic (PV) cells, power-only and CHP solid-oxide fuel cells (SOFCs), lead-acid batteries, and a hot water storage tank.

PV cells provide power by converting solar radiation into electricity. Individual PV panels or larger arrays can be installed on buildings or on the ground in fixed positions or with the ability to track the sun. Given that solar radiation is reduced during cloudy and night-time periods, only a fraction of a PV cell’s nameplate power capacity is available in any given hour. This restriction on PV availability is modeled in (\mathcal{P}) . Despite their limited ability to produce power, PV cells could prove economically viable in the commercial building market, particularly when integrated with electric storage technologies. See Price and Margolis [32] for further details on specific PV technologies.

Existing electric storage devices include many different types of battery, flywheel, and pumped hydro technologies. The applicability of these technologies depends on the amount of storage capacity required and the discharge rate at which it must be delivered. In general, the rate at which energy can be added to or removed from a battery is limited by its energy capacity. The charge-discharge process, which is captured in (\mathcal{P}) , also suffers from losses due to inefficiencies in the conversion between electrical and chemical energy. Thus, greater power output is achieved by acquiring larger, or more, batteries. Considering these performance characteristics, lead-acid batteries are particularly well-suited for DG applications given their discharge capabilities, and their commercial market availability and maturity. See Schoenung and Hassenzahl [33] for further details on specific battery technologies.

Fuel cells convert the chemical energy of a fuel, such as natural gas, directly into electrical energy through electrochemical reactions. In this way, the performance and technological characteristics of fuel cells resemble those of batteries more than those of conventional, fossil fuel-based combustion generators. However, unlike batteries, fuel cells do not require charging and can continue to produce power as long as they are supplied with reactants (such as fuel and air). The materials of construction employed by SOFCs, in particular, demand high operating temperatures to achieve practical power generating efficiencies. Because SOFCs require a significant amount of time to reach operating temperature (i.e., maximum turn-down), their ability to depart standby mode (i.e., start up) and change power output between time periods (i.e., ramp) is limited. Additionally, the ratio of their electric energy output to fuel energy input (i.e., electric efficiency) decreases as power output increases. Thus, power is generated with greater efficiency at part load (i.e., below maximum power output) than at rated capacity. Maximum turn-down, start-up fuel consumption, power ramping, and part-load electric efficiency are all performance characteristics of off-design SOFC power generation that are modeled in (\mathcal{P}) . See Stambouli and

Traversa [34], Braun et al. [35], and Hawkes et al. [36] for further details regarding SOFC technology.

SOFCs can also be integrated with waste heat recovery and storage to form a CHP system. For instance, the high-temperature exhaust gases from the SOFCs could flow through heat exchangers in a water tank to store thermal energy in the form of hot water. The flowrate of exhaust gas from SOFCs depends on their power output and electric efficiency. As power output increases, electric efficiency decreases, and the flowrate of exhaust gas increases. However, the heat that can be applied to the tank depends not only on the flowrate of exhaust gas, but also on the temperature difference between the gas and the tank water. Thus, the time-varying temperature of the water stored in the tank, which is modeled in (\mathcal{P}) , impacts the effective thermal efficiency of the SOFCs. See Braun [5] for further details on SOFC CHP building applications.

2.2 Model Description

Our model includes parameters for the time fidelity and horizon being considered, the heat and power demands of the building, the pricing and carbon emissions rates of the utilities, and the capital and operational costs, carbon emissions rates, and performance characteristics of all the technologies in the system. All of these parameters are treated as deterministic.

The model includes two types of variables: design and dispatch. The design variables establish the configuration and capacity of the DG system. In other words, these variables determine how many of each DG technology in Figure 2.1 to acquire. Since generators and batteries can only be purchased in discrete sizes, their associated design variables are restricted to integer values. However, the acquisition of CHP SOFCs includes a hot water storage tank, the volume of which can be increased by a continuous number of gallons. If none of the DG technologies is acquired, then the system is reduced to the existing configuration, which consists of only the macrogrid

and the boiler.

The dispatch variables prescribe the distribution of energy across the system in each time period. In other words, these variables determine the flow of power, heat, and natural gas along the arrows depicted in Figure 2.1. If none of the DG technologies is acquired, the system dispatch consists of supplying all of the power demand with the macrogrid and all of the heat demand with the boiler. However, if some DG technologies are acquired, then our model determines the share of demand supplied by these technologies.

The objective of our model is to determine the DG system design and dispatch which minimizes the total cost incurred by the building owner to meet demand over the time horizon of interest. We assume the building owner and system owner are the same entity. The total cost includes the capital and operational costs of the acquired technologies, as well as the operational costs from the macrogrid and boiler. The operational costs include operations and maintenance (O&M) costs, the cost of purchased natural gas and electricity, and the taxes paid for the carbon emissions from both the on-site system and the macrogrid's centralized generation. The cost of purchased electricity is a net cost, which considers the sale of electricity (i.e., net-metering) back to the macrogrid.

Our model includes constraints on the power and heat demands of the building, restrictions imposed by the utilities, and limits on the performance of the technologies. The power demand must be supplied in each time period by the macrogrid and/or by any acquired DG technologies. According to typical net-generation regulations imposed by the utility, the total DG-generated power which is sold to the macrogrid in each billing period cannot exceed the total power purchased from the macrogrid. The heat demand must be supplied by the boiler and/or by the water storage tank. In supplying power and heat, the DG system is constrained by the minimum and maximum capacities of all the acquired technologies. The SOFCs are additionally constrained

by their operating status and by their ability to ramp power output between time periods. The model also limits increases and decreases to the inventories of electric and thermal energy for the batteries and water storage tank, respectively. Finally, we include a number of constraints to control the complex interactions between the technologies which are acquired and operated within the system.

2.3 Mathematical Formulation (\mathcal{P})

We now present the mathematical formulation of our problem, (\mathcal{P}), using the sets, parameters, and variables defined in the nomenclature. To avoid verbosity, we define the elements of the set \mathcal{J} numerically as 1=Battery, 2=PV, 3=Power SOFC, 4=CHP SOFC, 5=Water Tank, 6=Boiler. Detailed descriptions of the objective and constraints of (\mathcal{P}) are provided in Sections 2.3.1 through 2.3.12.

Problem (\mathcal{P})

(see §2.3.1 Minimum Total Cost)

Minimize

$$\sum_{i \in \mathcal{I}} C_i \quad (2.1)$$

subject to

(see §2.3.2 Power and Heating Demand)

$$(\eta_1^{\max} P_{1t}^{\text{out}} - P_{1t}^{\text{in}}) + \sum_{j=2..4} P_{jt}^{\text{out}} + (U_t^{\text{out}} - U_t^{\text{in}}) = d_t^P \quad \forall t \in \mathcal{T} \quad (2.2a)$$

$$h_5(\tau_6^{\text{out}} - \tau_5^{\text{in}})F_{5t}^{\text{out}} \left[\left(1 - \left[1 - \frac{\tau_6^{\text{out}} - \tau_{\min}}{T_{5t} - \tau_{\min}} \right] B_{5t}^{\text{out}} \right)^{-1} \right] = d_t^Q \quad \forall t \in \mathcal{T} \quad (2.2b)$$

(see §2.3.3 Utility Restrictions)

$$U_n^{\max} \geq U_t^{\text{out}} \quad \forall n \in \mathcal{N}, t \in \mathcal{T}_n \quad (2.3a)$$

$$\sum_{t \in \mathcal{T}_n} U_t^{\text{in}} \leq \sum_{t \in \mathcal{T}_n} U_t^{\text{out}} \quad \forall n \in \mathcal{N} \quad (2.3b)$$

(see §2.3.4 Power Capacity)

$$P_{1t}^{\text{out}} \leq k_1^{\text{out}} A_1 \quad \forall t \in \mathcal{T} \quad (2.4a)$$

$$P_{1t}^{\text{in}} \leq k_1^{\text{in}} A_1 \quad \forall t \in \mathcal{T} \quad (2.4b)$$

$$P_{2t}^{\text{out}} \leq a_{2t} k_2^{\text{out}} A_2 \quad \forall t \in \mathcal{T} \quad (2.4c)$$

$$\mu_j k_j^{\text{out}} N_{jt} \leq P_{jt}^{\text{out}} \leq k_j^{\text{out}} N_{jt} \quad \forall j = 3, 4, t \in \mathcal{T} \quad (2.4d)$$

$$N_{jt} \leq A_j \quad \forall j = 3, 4, t \in \mathcal{T} \quad (2.4e)$$

(see §2.3.5 Electric Efficiency)

$$E_{jt} = \left(\frac{\eta_j^{\max} - \mu_j \eta_j^{\min}}{1 - \mu_j} \right) - \left(\frac{\eta_j^{\max} - \eta_j^{\min}}{k_j^{\text{out}} (1 - \mu_j)} \right) \left(\frac{P_{jt}^{\text{out}}}{N_{jt}} \right) \quad \forall j = 3, 4, t \in \mathcal{T} \quad (2.5a)$$

(see §2.3.6 Natural Gas Consumption)

$$G_{jt} = \frac{P_{jt}^{\text{out}}}{E_{jt}} \quad \forall j = 3, 4, t \in \mathcal{T} \quad (2.6a)$$

$$G_{6t} = \frac{h_5 F_{5t}^{\text{out}} (\tau_6^{\text{out}} - T_{5t}) (1 - B_{5t}^{\text{out}})}{\eta_6^Q} \quad \forall t \in \mathcal{T} \quad (2.6b)$$

(see §2.3.7 Start Up and Ramping)

$$N_{j,t+1} - N_{jt} \leq \dot{N}_{j,t+1} \quad \forall j = 3, 4, t < |\mathcal{T}| \quad (2.7a)$$

$$-\delta r_j^{\text{down}} N_{jt} \leq P_{j,t+1}^{\text{out}} - P_{jt}^{\text{out}} \leq \delta r_j^{\text{up}} N_{j,t+1} \quad \forall j = 3, 4, t < |\mathcal{T}| \quad (2.7b)$$

(see §2.3.8 Power Storage)

$$S_{1,t+1} - S_{1t} = \delta (\eta_1^{\max} P_{1t}^{\text{in}} - P_{1t}^{\text{out}}) \quad \forall t < |\mathcal{T}| \quad (2.8a)$$

$$s_1^{\min} A_1 \leq S_{1t} \leq s_1^{\max} A_1 \quad \forall t \in \mathcal{T} \quad (2.8b)$$

$$S_{1,1} = S_{1,|\mathcal{T}|} \quad (2.8c)$$

(see §2.3.9 Heat Capacity)

$$F_{5t}^{\text{in}} \leq \gamma_4 G_{4t} \quad \forall t \in \mathcal{T} \quad (2.9a)$$

(see §2.3.10 Heat Storage)

$$T_{5,t+1} - (1 - \alpha_5 B_{5t}^{\text{in}})T_{5t} = \frac{\delta \eta_5^Q h_4 F_{5t}^{\text{in}} (\tau_4^{\text{out}} - T_{5t}) - \delta h_5 F_{5t}^{\text{out}} (T_{5t} - \tau_5^{\text{in}})}{h_5 V_5} \quad \forall t < |\mathcal{T}| \quad (2.10a)$$

$$T_{5t} - \tau_5^{\text{in}} \leq (\tau^{\text{max}} - \tau_5^{\text{in}}) A_5 \quad \forall t \in \mathcal{T} \quad (2.10b)$$

$$\varepsilon B_{5t}^{\text{in}} \leq T_{5t} - \tau_5^{\text{in}} \leq \varepsilon + (\tau^{\text{max}} - \tau_5^{\text{in}} - \varepsilon) B_{5t}^{\text{in}} \quad \forall t \in \mathcal{T} \quad (2.10c)$$

$$(\tau_5^{\text{in}} - \tau_6^{\text{out}})(1 - B_{5t}^{\text{out}}) \leq T_{5t} - \tau_6^{\text{out}} \leq (\tau^{\text{max}} - \tau_6^{\text{out}}) B_{5t}^{\text{out}} \quad \forall t \in \mathcal{T} \quad (2.10d)$$

$$T_{5,1} = T_{5,|\mathcal{T}|} \quad (2.10e)$$

(see §2.3.11 Heat Storage Acquisition)

$$A_5 \leq A_4 \leq \left\lceil \frac{\max_{t \in \mathcal{T}} \{d_t^P\}}{k_4^{\text{out}}} \right\rceil A_5 \quad (2.11a)$$

$$v_5^{\text{min}} \leq V_5 \leq v_5^{\text{max}} \quad (2.11b)$$

(see §2.3.12 Non-negativity and Integrality)

$$P_{jt}^{\text{out}}, P_{jt}^{\text{in}}, S_{jt}, \dot{N}_{jt}, E_{jt}, G_{jt}, F_{jt}^{\text{out}}, F_{jt}^{\text{in}}, T_{jt}, V_j \geq 0 \quad \forall j \in \mathcal{J}, t \in \mathcal{T} \quad (2.12a)$$

$$U_t^{\text{out}}, U_t^{\text{in}}, U_n^{\text{max}} \geq 0 \quad \forall n \in \mathcal{N}, t \in \mathcal{T} \quad (2.12b)$$

$$A_j, N_{jt} \geq 0, \text{ integer} \quad \forall j \neq 5, t \in \mathcal{T} \quad (2.12c)$$

$$A_j, B_{jt}^{\text{in}}, B_{jt}^{\text{out}} \text{ binary} \quad \forall j = 5, t \in \mathcal{T} \quad (2.12d)$$

2.3.1 Minimum Total Cost

The objective is to minimize the total cost over the entire time horizon. The total cost expressed in the objective function (2.1) includes the capital and operational costs of the acquired technologies, as well as the existing operational costs resulting from demand met by the macrogrid and boiler.

The fixed capital cost, C_1 , consists of the total amortized cost of all the DG technologies that are acquired:

$$C_1 = c_1 s_1^{\max} A_1 + \sum_{j=2..4} c_j k_j^{\text{out}} A_j + c_5 (V_5 - v_5^{\min}).$$

The capital cost of the CHP SOFCs is greater than that of the power-only SOFCs in order to account for the acquisition of the water storage tank and heat exchangers. The water tank's initial size (v_5^{\min}) is based on the building heating load. However, the tank size can be increased for an additional cost per gallon.

The initial capital cost for each of the technologies can be amortized in a number of different ways. One method of amortization uses the parameters and general equation that follow:

ρ = interest rate [% (fraction) per time horizon]

λ_j = average lifetime of technology j [number of time horizons]

κ_j = initial capital cost of technology j [\$/kWh, \$/kW, or \$/gal]

$$c_j = \frac{\kappa_j e^{\rho \lambda_j}}{\lambda_j}. \quad (2.13)$$

The numerator of equation (2.13) calculates what κ_j is worth after investment at interest rate ρ over the average lifetime λ_j of technology j (see [37]). Thus, the numerator represents the lifetime opportunity cost of acquiring the technology rather than investing the initial capital cost at the current rate of return. The lifetime opportunity cost is then divided by λ_j to determine the opportunity cost per time horizon, which we call the amortized capital cost c_j . Ultimately, the primary focus of this research is not on the method of amortization. Rather, the final amortized cost (c_j) is the value of interest. Equation (2.13) is just one method for calculating that cost, without loss of generality.

The variable operational costs of the DG system consist of O&M costs for the PV cells and SOFCs, the cost of natural gas to fuel the SOFCs, the cost of the carbon emissions associated with the combustion of natural gas, and the negative cost (i.e.,

revenue) from the sale of power to the macrogrid. The O&M costs, C_2 , for the PV cells and SOFCs increase with the energy output:

$$C_2 = \sum_{j=2..4} \sum_{t \in \mathcal{T}} m_j \delta P_{jt}^{\text{out}}.$$

The O&M cost for the CHP SOFCs, which accounts for the additional operational costs of the water tank and heat exchangers, is greater than that for the power-only SOFCs. Due to the limited need for variable maintenance on lead-acid battery systems, the O&M costs for the batteries are assumed fixed and are treated as part of the capital cost. The parameter δ is included to appropriately convert units of power (kW) to units of energy (kWh).

Fuel and emissions costs, C_3 , are incurred both to start up the SOFCs (i.e., to reach operating temperature) and to operate them within their performance limits. These costs depend on the price (g_t) of natural gas from the local utility, the price (zz^g) of carbon emissions, as determined by the tax rate and the emissions rate, and the total amount of gas required for start up and operation:

$$C_3 = \sum_{j=3..4} \sum_{t \in \mathcal{T}} (g_t + zz^g) \left[\frac{\sigma_j \mu_j k_j}{2\eta_j^{\text{min}}} \dot{N}_{jt} + \delta G_{jt} \right].$$

Our formulation assumes a carbon tax exists where the building is located and that the tax is paid by the building owner. We further assume that the SOFCs consume natural gas with the same fixed electric efficiency during start up as at maximum power output. Thus, the amount of gas required for a single SOFC to reach operating temperature is treated as a fixed value. The variable \dot{N}_{jt} determines how many SOFCs start up in a given time period, which allows for the calculation of the total amount of gas required. Once a SOFC reaches operating temperature, the amount of natural gas (G_{jt}) consumed depends on the power output and the electric efficiency as defined in constraint (2.6a).

The final operational cost for the DG technologies is the negative cost, C_4 , associated with the sale of power to the macrogrid:

$$C_4 = - \sum_{t \in \mathcal{T}} \nu_t p_t \delta U_t^{\text{in}}.$$

We assume that net-metering is available with the local power utility and that the utility can purchase power from the building owner in any hour at a fraction of, or possibly full, market price. However, the total power purchased by the utility in each billing cycle is subject to the restrictions imposed by constraint (2.3b).

In addition to the capital and operational costs of the acquired DG technologies, the system incurs the cost of electricity purchased from the macrogrid and the operational costs for the boiler. If DG technologies are not acquired, then the macrogrid and boiler costs are the only costs. The macrogrid charges both hourly and peak monthly rates, which determine the total electricity cost, C_5 :

$$C_5 = \sum_{t \in \mathcal{T}} (p_t + z z^p) \delta U_t^{\text{out}} + \sum_{n \in \mathcal{N}} p_n^{\text{max}} U_n^{\text{max}}.$$

Depending on the rate schedule dictated by the power utility for the building and location of interest, the charges p_t and p_n^{max} could vary by time-of-day and/or season. We must also consider the cost of the carbon emitted by the generation sources employed by the macrogrid. Our formulation applies an average carbon emissions rate (z^p) for all of the macrogrid's generation sources and assumes that the building owner is taxed for the emissions associated with the purchased electricity. For both natural gas and power utilities, the fixed monthly customer charge for service is not included in the formulation since this cost is constant and therefore does not impact the optimal solution.

Finally, the total cost includes the O&M, fuel, and emissions costs, C_6 , for the existing boiler:

$$C_6 = \sum_{t \in \mathcal{T}} (\eta_6^Q m_6 + g_t + z z^g) \delta G_{6t}.$$

Similar to the operational costs of the SOFCs, the fuel and emissions costs of the boiler depend on the price of natural gas and the price of carbon emissions. In contrast to the SOFCs, the rated thermal efficiency (η_6^Q) of the boiler is treated as fixed. The amount of natural gas (G_{6t}) consumed depends on whether the temperature of the water flowing to the boiler is above or below the required delivery temperature. The relationship between the water temperature and the amount of natural gas consumed by the boiler is defined in constraint (2.6b).

2.3.2 Power and Heating Demand

Constraint (2.2a) ensures that the hourly demand for power is met by the net discharge of the batteries (after accounting for the discharge efficiency η_1^{\max}), the PV cells, the power-only and CHP SOFCs, and the net supply from the macrogrid. Constraint (2.2b) dictates that the hourly demand for heat must be met by a mix of hot and cold water flow. The demanded hot water, which is heated by the CHP SOFC exhaust and/or by the boiler, must be delivered at a fixed temperature (τ_6^{out}). If the temperature of the hot water is above delivery temperature (i.e., $B_{5t}^{\text{out}} = 1$), then the hot water must be mixed with cold water at the main supply temperature (τ^{min}). As the temperature of the tank water increases, the required flow of cold water for mixing increases, and the required flow of hot water from the tank decreases.

In the actual application of the model (see Appendix A), we use an algebraically equivalent version of constraint (2.2b) with no fractional term. The elimination of the fractional term avoids the possibility of division by zero when $(T_{5t} - \tau^{\text{min}}) = 0$. The presentation of constraint (2.2b) in this formulation is strictly to ease the interpretation by the reader.

2.3.3 Utility Restrictions

Constraint (2.3a) establishes the peak power load supplied by the macrogrid in each monthly billing cycle as the largest hourly load supplied by the macrogrid each month. Constraint (2.3b) dictates that the DG system cannot be a “net-generator” of power in each monthly billing cycle. Accordingly, the total power sold to the macrogrid each month cannot exceed the total power purchased from the macrogrid each month.

2.3.4 Power Capacity

Constraints (2.4a) and (2.4b) limit the rate at which power is discharged from and charged to, respectively, all of the acquired batteries. If batteries are not acquired, then the charge and discharge rates are set equal to zero. Constraint (2.4c) ensures that only a fraction (a_{2t}) of the nameplate power capacity of the acquired PV cells is available in each hour, based on the prevailing weather conditions. Because the solar radiation is often low enough that the available power from PV cells is zero (e.g., during the night), there is no minimum power output enforced for PV cells. Constraint (2.4d) limits the maximum *and* minimum power output of all operating SOFCs in a given hour. The maximum turn-down (μ_j) results from the minimum operating temperature necessary for the SOFCs to produce power. Constraint (2.4e) dictates that the number of SOFCs operating in a given hour cannot exceed the number acquired. Power supplied by the macrogrid in each hour is unconstrained in this formulation.

2.3.5 Electric Efficiency

Constraint (2.5a) demonstrates that the average electric efficiency across all SOFCs is a function of the number (N_{jt}) of SOFCs operating and the total power (P_{jt}^{out}) they produce. Our formulation assumes that each operating SOFC provides an equal share of the total power produced in a given hour. Using the maximum (η_j^{max}) and mini-

mum (η_j^{\min}) electric efficiencies as endpoints, we treat the average electric efficiency of all SOFCs as a decreasing linear function of the share of total power provided by a single SOFC.

In the actual application of the model (see Appendix A), we use an algebraically equivalent version of constraint (2.5a) that eliminates the fractional-variable term. This alternate version of the constraint avoids the possibility of division by zero when $N_{jt} = 0$. The presentation of constraint (2.5a) in this formulation is strictly to ease the interpretation by the reader.

2.3.6 Natural Gas Consumption

Constraint (2.6a) dictates that the total amount of natural gas consumed by all of the operating power-only or CHP SOFCs in each hour is the quotient of their total power output and their average electric efficiency. In the actual application of the model, we use an algebraically equivalent version of this constraint that eliminates the fractional-variable term by multiplying both sides of the equation by E_{jt} .

Constraint (2.6b) calculates the amount of natural gas consumed by the boiler in each hour as the quotient of its heat output and its rated thermal efficiency. The amount of heat the boiler must provide depends on the temperature (T_{5t}) of the water from the storage tank, if one is acquired. We assume the hot water must be delivered to the building's faucets and radiators at a fixed temperature (τ_6^{out}). If the temperature of the water from the storage tank is below τ_6^{out} in a given hour (i.e., $B_{5t}^{\text{out}} = 0$), then the boiler must provide the additional heat to increase the water temperature to τ_6^{out} . In this case, the amount of heat is calculated as the product of the specific heat of the tank water (h_5), the flowrate of the tank water (F_{5t}^{out}), and the difference ($\tau_6^{\text{out}} - T_{5t}$) between the delivery temperature and the tank water temperature. If the temperature of the water from the storage tank is at or above τ_6^{out} in a given hour (i.e., $B_{5t}^{\text{out}} = 1$), then no additional heating from the boiler is required. If a storage tank is not acquired, then the boiler must provide all of the heat

demand, which entails heating all of the water from the average return temperature (τ_5^{in}) up to delivery temperature (τ_6^{out}).

2.3.7 Start Up and Ramping

Constraint (2.7a) establishes the number of SOFCs that start up between time periods t and $t + 1$. If there is an increase in the number of operating SOFCs between time periods (i.e., $N_{j,t+1} > N_{jt}$), then a positive number ($\dot{N}_{j,t+1}$) of SOFCs incur the cost of fuel for start up. The cost-minimizing objective induces any solution to set $\dot{N}_{j,t+1}$ to the smallest value allowable, given the constraints. Thus, in each hour t , $\dot{N}_{j,t+1}$ is set *equal* to $N_{j,t+1} - N_{jt}$ when $N_{j,t+1} > N_{jt}$ and zero otherwise (i.e., $\dot{N}_{j,t+1} = \max\{N_{j,t+1} - N_{jt}, 0\}$). Given the integrality restrictions on N_{jt} , we obtain integer values for \dot{N}_{jt} without including such a constraint in the model.

According to constraint (2.7b), if SOFC power output increases from hour t to hour $t + 1$ (i.e., $P_{j,t+1}^{\text{out}} > P_{jt}^{\text{out}}$), then it cannot increase by more than the total ramp-up capacity of all the SOFCs that are operating in hour $t + 1$. Similarly, if SOFC power output decreases between consecutive hours (i.e., $P_{j,t+1}^{\text{out}} < P_{jt}^{\text{out}}$), then it cannot decrease by more than the total ramp-down capacity of the SOFCs operating in hour t . The parameter δ is included to properly convert units from kW/hr to kW.

2.3.8 Power Storage

Constraint (2.8a) demonstrates that the change in the inventory of energy in the acquired batteries from the start of hour t to the start of hour $t + 1$ is determined by the net power added to the batteries in hour t (after accounting for the charge efficiency η_1^{max}). The parameter δ is included to convert units from kW to kWh. According to constraint (2.8b), the energy in all of the acquired batteries at the start of any hour must remain within the total minimum and maximum state-of-charge. If batteries are not acquired, then the total state-of-charge is set equal to zero in all hours. Constraint (2.8c) requires the batteries to attain the same state-of-charge in

the final time period as in the initial time period.

2.3.9 Heat Capacity

The water in the storage tank is heated with the exhaust gas from the CHP SOFCs. Thus, constraint (2.9a) limits the maximum flowrate of hot exhaust gas into the water tank in each hour to the exhaust gas output by the CHP SOFCs. The exhaust gas output depends on the flow of natural gas into the CHP SOFCs, which is calculated in constraint (2.6a). For time periods in which the use of *all* of the available exhaust gas would cause the tank water temperature to exceed its maximum, we assume the excess exhaust gas is vented. We further assume that the boiler is sized to meet the peak heat load of the building. Thus, the maximum capacity of the boiler is unconstrained in our formulation.

2.3.10 Heat Storage

Constraint (2.10a) demonstrates that the change in the temperature of the tank water from the start of hour t to the start of hour $t + 1$ (after accounting for heat loss to the ambient) is determined by the net thermal energy added to the water in hour t and the heat capacity of the water. Though in reality the ambient heat loss is a function of the temperature difference between the tank water and the ambient, we apply a fixed heat loss factor (α_5) for simplicity. However, the ambient heat loss factor only applies if the tank water temperature is above the average temperature of the water upon return to the tank (i.e., $B_{5t}^{\text{in}} = 1$). The thermal energy added to the tank is the product of the time increment (δ), the heat exchanger efficiency (η_5^Q), the specific heat (h_4) and flowrate (F_{5t}^{in}) of the CHP SOFC exhaust gas, and the temperature difference ($\tau_4^{\text{out}} - T_{5t}$) between the exhaust gas and the tank water. The thermal energy removed from the tank is the product of the time increment (δ), the specific heat (h_5) and flowrate (F_{5t}^{out}) of the tank water, and the temperature difference ($T_{5t} - \tau_5^{\text{in}}$) between the tank water and the return water. The net thermal

energy added to the water is divided by the heat capacity (h_5V_5) of the volume of water to determine the net temperature change. In the actual application of the model (see Appendix A), we eliminate the fractional term on the right-hand side of constraint (2.10a) by multiplying both sides of the equation by h_5V_5 .

Constraint (2.10b) demonstrates the impact of not acquiring a storage tank. If a tank is not acquired (i.e., $A_5 = 0$), then the “tank” water is reduced to the temperature of the return water in every hour. As a result, all of the water must be heated to delivery temperature by the boiler. If a tank is acquired, then the water in the tank is limited to the maximum temperature (τ^{\max}) in all hours. Constraint (2.10c) determines whether the tank water temperature is arbitrarily close (within ε) to the return water temperature. This constraint establishes the value of the binary variable (B_{5t}^{in}) which controls the temperature decay due to heat loss to the ambient. Constraint (2.10d) determines whether the tank water is above or below the hot water delivery temperature. This constraint establishes the value of the binary variable (B_{5t}^{out}) which controls the need for additional heating from the boiler or for mixing with cold water. Constraint (2.10e) requires the tank water to attain the same temperature in the final time period as in the initial time period.

2.3.11 Heat Storage Acquisition

Constraint (2.11a) ensures that a water tank is acquired if and only if at least one CHP SOFC is acquired. We use a conservative upper bound on the number of CHP SOFCs acquired to control this if-and-only-if relationship between the binary variable A_5 and the integer variable A_4 . Constraint (2.11b) bounds the selected capacity for the water storage tank based on the heat demands of the building of interest. The lower bound on the tank size is the initial capacity, the cost of which is included in the acquisition of CHP SOFCs.

2.3.12 Non-negativity and Integrality

Finally, constraints (2.12a) - (2.12d) ensure all of the variables in our formulation assume non-negative values. In addition to non-negativity restrictions, constraints (2.12c) and (2.12d) establish the integrality of the appropriate variables.

CHAPTER 3

SOLUTION TECHNIQUES

The algorithms capable of solving large, nonconvex MINLPs, such as (\mathcal{P}) , are limited and dependent on the problem structure. A branch-and-bound algorithm requires methods to obtain global lower and upper bounds on the objective value at each node in order to converge at the optimal solution. For a mixed-integer linear minimization problem, lower bounds are generally provided by solutions to the continuous relaxation of the integer problem and upper bounds are provided by integer-feasible solutions. However, continuous relaxations may not return valid lower bounds for nonconvex problems, and integer-feasible solutions can be difficult to obtain for large problems. Thus, we develop problem-specific convex underestimation techniques to obtain global lower bounds on the objective value of (\mathcal{P}) . We also develop a linearization heuristic to obtain integer-feasible solutions, and thus global upper bounds, for (\mathcal{P}) . These bounding techniques can be applied as part of a nonlinear branch-and-bound algorithm to solve large instances of (\mathcal{P}) to global optimality.

In this chapter, we discuss the mathematical structure of (\mathcal{P}) , which motivates the requirement for specialized solution techniques. We then present the lower-bounding problem, (\mathcal{U}) , and upper-bounding problem, (\mathcal{H}) , that we use to bound and solve instances of (\mathcal{P}) . We conclude the chapter by contrasting our solution techniques with those of existing MINLP solvers.

3.1 Mathematical Structure

The size of a particular instance of (\mathcal{P}) is determined by the selected time fidelity, δ , and time horizon, $|\mathcal{T}|$. The time horizon also determines the number of months, $|\mathcal{N}|$, under consideration in a given instance. (\mathcal{P}) has a linear objective, $22|\mathcal{T}| + |\mathcal{N}| + 6$ variables ($2|\mathcal{T}| + 4$ general integer, $2|\mathcal{T}| + 1$ binary), and $33|\mathcal{T}| + |\mathcal{N}| - 2$ constraints

($7|\mathcal{T}| - 1$ nonlinear), not including non-negativity and integrality restrictions. Table 3.1 lists the number of variables and constraints contained in (\mathcal{P}) for various time horizons at the hourly ($\delta = 1$) level of fidelity, culminating in the one-year ($|\mathcal{T}| = 8,760$) time horizon. In order to capture short-term fluctuations in demand

Table 3.1: Size of (\mathcal{P}) instances for time horizons of interest.

Time Horizon (Hours)	Number of Variables (Integer/Binary)	Number of Constraints (Nonlinear)
One Day (24)	533 (52/49)	791 (167)
Two Days (48)	1,061 (100/97)	1,583 (335)
Four Days (96)	2,117 (196/193)	3,167 (671)
One Week (168)	3,701 (340/337)	5,543 (1,175)
One Month (744)	16,373 (1,492/1,489)	24,551 (5,207)
One Year (8,760)	192,736 (17,524/17,521)	289,090 (61,319)

and support long-term capital investment decisions, we wish to determine a DG system design and dispatch that meets the *hourly* demands of a building for a typical *year* at the globally minimum total cost.

One might consider a smaller time increment (i.e., $\delta < 1$) in order to capture the greater demand volatility that exists at the sub-hourly level of fidelity. However, smaller time increments increase the size of problem instances, even for the same time horizon. For example, 15-minute time increments ($\delta = 0.25$) increase the size ($|\mathcal{T}| = 35,040$) of one-year instances significantly. Similarly, a longer time horizon increases the size of problem instances, even for the same time increment. One might consider a time horizon of greater than one year (i.e., $|\mathcal{T}| > 8,760$), at the hourly fidelity, in order to account for the variability in demand over multiple years. However, a four-year time horizon, for example, produces the same significant increase in the size ($|\mathcal{T}| = 35,040$) of problem instances. We believe the hourly-increment ($\delta = 1$), one-year ($|\mathcal{T}| = 8,760$) instance is the appropriate balance between fidelity and horizon. The difficulty associated with solving larger (i.e., greater fidelity or horizon) problem

instances is primarily due to the nonlinearities in (\mathcal{P}) .

Upon expanding and rearranging nonlinear constraints (2.2b), (2.5a), (2.6a), (2.6b), and (2.10a), and suppressing the linear terms, we find that all of the nonlinearities in (\mathcal{P}) consist of bilinear and trilinear terms in equality constraints (see below). Thus, the constraint set is nonconvex.

$$\begin{aligned}
\text{Linear} + h_5(\tau_6^{\text{out}} - \tau_5^{\text{in}})F_{5t}^{\text{out}}T_{5t} + d_t^Q T_{5t}B_{5t}^{\text{out}} &= 0 \\
\text{Linear} + N_{jt}E_{jt} &= 0 \\
\text{Linear} + G_{jt}E_{jt} &= 0 \\
\text{Linear} + (h_5/\eta_6^Q)(\tau_6^{\text{out}}F_{5t}^{\text{out}}B_{5t}^{\text{out}} + F_{5t}^{\text{out}}T_{5t} - F_{5t}^{\text{out}}T_{5t}B_{5t}^{\text{out}}) &= 0 \\
\text{Linear} + h_5(V_5T_{5,t+1} - V_5T_{5t} + \alpha_5V_5T_{5t}B_{5t}^{\text{in}} + \delta F_{5t}^{\text{out}}T_{5t}) + \delta\eta_5^Q h_4F_{5t}^{\text{in}}T_{5t} &= 0
\end{aligned}$$

The algorithms suitable for solving nonconvex MINLPs are limited. The application of a nonlinear branch-and-bound algorithm to solve (\mathcal{P}) requires methods for determining global upper and lower bounds on the objective value. When applied to an integer-restricted minimization problem, branch-and-bound generates a non-increasing sequence of global upper bounds on the objective value and a non-decreasing sequence of global lower bounds on the objective value which eventually converge (within some tolerance) to provide the optimal solution. In general, global upper bounds are provided by integer-feasible solutions obtained with local solvers and global lower bounds are provided by solutions to continuous relaxations of the integer problem. Both types of bounds can be difficult to obtain for large, nonconvex MINLPs. Our testing indicates few existing MINLP solvers are capable of finding solutions to one-day instances of (\mathcal{P}) , and none of those tested can provide solutions for time horizons of one week or greater. Additionally, the nonconvex nature of (\mathcal{P}) dictates that solutions to continuous relaxations do not necessarily provide global lower bounds. Accordingly, the next two sections discuss our techniques to obtain lower and upper bounds which can be applied in a nonlinear branch-and-bound algorithm.

3.2 Lower Bounding: Convex Underestimation (\mathcal{U})

A lower bound for a mixed-integer *linear* programming (MILP) minimization problem is obtained by relaxing the integrality restrictions and solving the resulting continuous problem. A lower bound for an MINLP minimization problem can also be obtained in this manner as long as the problem is convex. However, nonconvex problems provide no guarantee of obtaining a global lower bound when solving the NLP relaxation. Thus, we formulate a convex underestimation problem, henceforth referred to as (\mathcal{U}), to obtain a global lower bound on (\mathcal{P}).

Convex underestimation methods similar to those suggested by McCormick [38] still appear in the literature today. According to equations (3) and (4) of Adjiman and Floudas [39], bilinear and trilinear terms, respectively, are underestimated by their convex envelope. The convex envelopes are constructed by replacing each of the nonlinear terms with a new variable and adding linear inequality constraints that bound the new variable. Bilinear terms require four constraints on the new variable while trilinear terms require eight constraints. Considering some of our nonlinear terms are repeated across constraints, (\mathcal{P}) contains $9|\mathcal{T}| - 1$ distinct bilinear terms and $2|\mathcal{T}| - 1$ distinct trilinear terms that must be replaced with new variables. Accordingly, the (\mathcal{U}) formulation is identical to (\mathcal{P}) with the exceptions of adding $11|\mathcal{T}| - 2$ new continuous variables, replacing each of the bilinear and trilinear terms with the appropriate new continuous variable, and adding $52|\mathcal{T}| - 12$ new linear constraints. Hence, (\mathcal{U}) is an MILP, the solution to which provides a global lower bound on the optimal solution to (\mathcal{P}).

The formulation of the convex envelopes in (\mathcal{U}) requires the following upper and lower bounds on each of the original variables in the bilinear and trilinear terms:

Variable bounds applied in (\mathcal{U})

$$\begin{aligned}
0 \leq N_{jt} &\leq \left\lceil \frac{\max_{t \in \mathcal{T}} \{d_t^P\}}{k_j^{\text{out}}} \right\rceil \\
0 \leq G_{jt} &\leq \left(\frac{k_j^{\text{out}}}{\eta_j^{\text{min}}} \right) \left\lceil \frac{\max_{t \in \mathcal{T}} \{d_t^P\}}{k_j^{\text{out}}} \right\rceil \\
0 \leq F_{5t}^{\text{in}} &\leq \gamma_4 \left(\frac{k_4^{\text{out}}}{\eta_4^{\text{min}}} \right) \left\lceil \frac{\max_{t \in \mathcal{T}} \{d_t^P\}}{k_4^{\text{out}}} \right\rceil \\
\eta_j^{\text{min}} &\leq E_{jt} \leq \eta_j^{\text{max}} \\
\left(\frac{\tau_6^{\text{out}} - \tau^{\text{min}}}{\tau^{\text{max}} - \tau^{\text{min}}} \right) \left(\frac{d_t^Q}{h_5(\tau_6^{\text{out}} - \tau_5^{\text{in}})} \right) &\leq F_{5t}^{\text{out}} \leq \left(\frac{d_t^Q}{h_5(\tau_6^{\text{out}} - \tau_5^{\text{in}})} \right) \\
\tau_5^{\text{in}} &\leq T_{5t} \leq \tau^{\text{max}} \\
0 &\leq B_{5t}^{\text{in}} \leq 1 \\
0 &\leq B_{5t}^{\text{out}} \leq 1 \\
v_5^{\text{min}} &\leq V_5 \leq v_5^{\text{max}}.
\end{aligned} \tag{3.1}$$

The number of SOFCs operating (N_{jt}) in any hour is bounded above by the number of SOFCs acquired, according to constraint (2.4e). We apply a conservative upper bound on the number of SOFCs acquired by assuming the building owner never buys more SOFCs than what is required to supply the peak power load without assistance from the macrogrid. This upper bound on the number of SOFCs acquired also limits the maximum amount of natural gas (G_{jt}) fed to the SOFCs in any hour, according to constraints (2.4d), (2.5a), and (2.6a), and the maximum flowrate (F_{5t}^{in}) of CHP SOFC exhaust heat into the water tank, according to constraint (2.9a). The electric efficiency (E_{jt}) of the SOFCs is bounded above and below by the maximum and minimum efficiencies, respectively, according to constraint (2.5a). The flowrate (F_{5t}^{out}) of heated water out of the tank is bounded above by the demand flowrate with no cold water mixing and bounded below by the demand flowrate with the maximum cold water mixing, according to constraints (2.2b) and (2.10d). The temperature (T_{5t}) of the water in the tank is bounded above and below by the maximum and

return temperatures, respectively, according to constraint (2.10d), while the binary temperature variables (B_{5t}^{in} and B_{5t}^{out}) are bounded by zero and one. Finally, the capacity (V_5) of the water tank is bounded by the same limits dictated in constraint (2.11b).

We next attempt to tighten the variable bounds in (3.1) using an optimization-based approach (see [39] or [40]). With this approach, each of the variables in (3.1) is maximized or minimized subject to the constraints in (\mathcal{U}) in order to obtain tighter upper or lower bounds, respectively. After executing bound tightening on all of the variable bounds in (3.1) for various small (i.e., one-day) instances of the problem, we find that only the upper bound on T_{5t} , the upper bound on B_{5t}^{out} , and the lower bound on F_{5t}^{out} benefit from the bound tightening. The fact that these three bounds can be tightened logically follows from the relationships dictated by constraints (2.2b), (2.10a), and (2.10d). In certain time periods, the maximum possible inflow of heat from the CHP SOFCs and the minimum required outflow of heat to meet demand could make it impossible for the tank water temperature (T_{5t}) to reach its upper bound (τ^{max}), or even delivery temperature (τ_6^{out}), in the following time period, according to constraint (2.10a). If the tank water temperature is below the delivery temperature, then the indicator variable (B_{5t}^{out}) must be set to its lower bound (zero), according to constraint (2.10d), and the flow of hot water (F_{5t}^{out}) must be set to its upper bound, according to constraint (2.2b). Based on this information, we expedite the bound tightening procedure for larger (i.e., two-day and greater) instances of the problem by only applying the optimization-based approach to obtain the tight upper bound on T_{5t} (referred to as \hat{T}_{5t}) and subsequently directly calculating the tight upper bound on B_{5t}^{out} (referred to as $\hat{B}_{5t}^{\text{out}}$) and the tight lower bound on F_{5t}^{out} (referred to as $\check{F}_{5t}^{\text{out}}$). To further speed the bound tightening, we relax integrality in (\mathcal{U}) as part of the following algorithm:

Bound Tightening Algorithm

1. Set $\hat{T}_{5t} = \tau^{\max}$, $\hat{B}_{5t}^{\text{out}} = 1$, $\check{F}_{5t}^{\text{out}} = \left(\frac{\tau_6^{\text{out}} - \tau^{\min}}{\tau^{\max} - \tau^{\min}} \right) \left(\frac{d_t^Q}{h_5(\tau_6^{\text{out}} - \tau_5^{\text{in}})} \right) \forall t$.
2. Loop $\forall t \in \mathcal{T}$.
 - (a) Maximize T_{5t} subject to (\mathcal{U}) with integrality relaxed.
 - (b) Set \hat{T}_{5t} equal to the objective value resulting from (a).
 - (c) Set $\hat{B}_{5t}^{\text{out}} = 1$ if $\hat{T}_{5t} > \tau_6^{\text{out}}$ and 0 otherwise.
 - (d) Set $\check{F}_{5t}^{\text{out}} = \left(1 - \left[1 - \frac{\tau_6^{\text{out}} - \tau^{\min}}{\hat{T}_{5t} - \tau^{\min}} \right] \hat{B}_{5t}^{\text{out}} \right) \left(\frac{d_t^Q}{h_5(\tau_6^{\text{out}} - \tau_5^{\text{in}})} \right)$.

This algorithm can be repeated multiple times to try and achieve even tighter bounds. However, empirical evidence suggests the majority of the improvement in the bounds occurs within the first two to three iterations. We also find the algorithm results in the greatest improvement in the bounds on T_{5t} , B_{5t}^{out} , and F_{5t}^{out} in hours that follow large spikes in the heating demand. These tighter bounds are then applied in (\mathcal{U}) , with the original objective function and integrality once again enforced, to obtain an improved (i.e., greater) global lower bound on the optimal objective value for (\mathcal{P}) . For the six instances of varying size presented in Section 3.4, the bound tightening algorithm increases the global lower bound on (\mathcal{P}) by an average of 1.6%. We next present techniques for obtaining a global upper bound on the optimal objective value for (\mathcal{P}) .

3.3 Upper Bounding: Linearization Heuristic (\mathcal{H})

An upper bound for an MI(N)LP minimization problem is provided by any integer-feasible solution. One integer-feasible solution to (\mathcal{P}) is to acquire no DG technologies and meet all of the building's demand with the macrogrid and boiler. The cost of this “no DG” solution can be directly calculated, without solving (\mathcal{P}) , using the C_5 and C_6 portions of the objective function and setting $U_t^{\text{out}} = d_t^P \forall t$, $U_n^{\max} = \max_{t \in \mathcal{T}_n} \{d_t^P\} \forall n$, and

$G_{6t} = d_t^Q / \eta_6^Q \forall t$. However, the “no DG” solution provides a weak upper bound on the total cost for the optimal solution to (\mathcal{P}) if DG technologies are economically viable. Thus, we wish to find an integer-feasible solution, if one exists, that includes some DG technologies *and* provides a lower total cost, and therefore a tighter upper bound, than the “no DG” solution. Integer-feasible solutions can be obtained by solving (\mathcal{P}) with existing MINLP solvers for small problem instances. However, based on our testing, larger problem instances (i.e., one week and greater) cannot be solved with the currently available solvers. Accordingly, we next present a linearization heuristic, henceforth referred to as (\mathcal{H}) , for determining integer-feasible solutions to (\mathcal{P}) that can be applied to the large instances.

The intuition behind (\mathcal{H}) is the observation that fixing the electric efficiency of the SOFCs (E_{3t}, E_{4t}) and the tank water temperature (T_{5t}) renders (\mathcal{P}) linear. Simpler models in the literature similarly fix the efficiencies of generators and fix, or ignore, the temperature of thermal storage devices to avoid nonlinearity (e.g., [41]). When E_{3t} and E_{4t} are fixed, constraint (2.5a) is linearized by clearing the denominator on the right-hand side of the equation and constraint (2.6a) is linear without modification. When T_{5t} is fixed, constraints (2.10c) and (2.10d) fix the values of B_{5t}^{in} and B_{5t}^{out} , respectively. With $T_{5t}, B_{5t}^{\text{in}}$, and B_{5t}^{out} all fixed, constraints (2.2b) and (2.6b) are linear without modification and constraint (2.10a) is linearized by clearing the denominator on the right-hand side of the equation. Thus, the (\mathcal{H}) formulation is identical to (\mathcal{P}) with the exception of fixing $3|\mathcal{T}|$ continuous variable values (E_{3t}, E_{4t} , and T_{5t}) and $2|\mathcal{T}|$ binary variable values (B_{5t}^{in} and B_{5t}^{out}). Consequently, any feasible solution to the MILP (\mathcal{H}) is feasible for the MINLP (\mathcal{P}) .

Although we obtain (\mathcal{P}) -feasible solutions from (\mathcal{H}) -feasible solutions, the fixed values for $E_{3t}, E_{4t}, T_{5t}, B_{5t}^{\text{in}}$, and B_{5t}^{out} must be carefully selected in order to achieve (\mathcal{H}) -feasibility. Additionally, not every (\mathcal{P}) -feasible solution produces a total cost less than the “no DG” solution. In general, the fixed variable values used in (\mathcal{H}) will

produce lower cost (\mathcal{P})-feasible solutions if those fixed values are tailored to the power and heating demands of the building of interest. Hence, we next present techniques for selecting the fixed variable values used in (\mathcal{H}) with the goal of obtaining (\mathcal{P})-feasible solutions that incur a lower total cost than the “no DG” solution. In presenting these techniques, we distinguish between two types of system design solutions: DG systems with only power generation and storage (referred to as “power DG”) and DG systems with both power and heat generation and storage (referred to as “CHP DG”). Depending on the particular problem instance, one of these system design types may produce a lower cost solution than the other.

For a “power DG” system, the selection of fixed values for E_{4t} , T_{5t} , B_{5t}^{in} , and B_{5t}^{out} is trivial. Because there is no SOFC exhaust heat capture in this case, CHP SOFCs are never acquired and the associated electric efficiency can simply be set to its minimum. Also, because there is no water storage tank, the water enters the boiler at return temperature in every hour and must be fully heated to delivery temperature. Less trivial, however, is the selection of the fixed values for the power-only SOFC electric efficiency (E_{3t}). One might ignore the specific power demands of the building and simply fix the efficiency to the same value (e.g., the minimum, average, or maximum efficiency) in all hours. However, this approach forces the SOFCs to operate at the same power output for all hours in which they are utilized (see constraint (2.5a)) and, therefore, is unlikely to produce a (\mathcal{P})-feasible solution with a total cost as low as that produced by efficiency values which are tailored to the power demands. We can obtain these tailored fixed values for E_{3t} from the solution to (\mathcal{U}). Given the underestimation of constraint (2.5a) in (\mathcal{U}), we cannot directly apply the values for E_{3t} from the solution to (\mathcal{U}). However, the solution to (\mathcal{U}) provides valid values for P_{3t}^{out} and N_{3t} , referred to as $\check{P}_{3t}^{\text{out}}$ and \check{N}_{3t} , that we use along with constraint (2.5a) to derive \check{E}_{3t} . The fixed efficiency and temperature values are applied in (\mathcal{H}) as part of the following algorithm to obtain a (\mathcal{P})-feasible solution:

“Power DG” (\mathcal{P})-feasible Solution Algorithm

1. Solve (\mathcal{U}) and store resulting values for $\check{P}_{3t}^{\text{out}}$ and $\check{N}_{3t} \forall t$.
2. Set $T_{5t} = \tau_5^{\text{in}}$, $B_{5t}^{\text{in}} = 0$, $B_{5t}^{\text{out}} = 0$, and $E_{4t} = \eta_4^{\text{min}} \forall t$.
3. Set $E_{3t} = \check{E}_{3t} = \left(\frac{\eta_3^{\text{max}} - \mu_3 \eta_3^{\text{min}}}{1 - \mu_3} \right) - \left(\frac{\eta_3^{\text{max}} - \eta_3^{\text{min}}}{k_3^{\text{out}}(1 - \mu_3)} \right) (\check{P}_{3t}^{\text{out}} / \check{N}_{3t})$ if $\check{N}_{3t} > 0$, η_3^{min} otherwise $\forall t$.
4. Solve (\mathcal{H}) and return its solution.

For “CHP DG” systems, the fixed values for E_{3t} and E_{4t} are both determined from the solution to (\mathcal{U}), as with \check{E}_{3t} for “Power DG” systems. However, it may no longer be advisable, in terms of the efficient use of the available thermal energy, to trivially fix the values for T_{5t} , B_{5t}^{in} , and B_{5t}^{out} to their minima. Fixing these variables to their minimum values prevents the storage of heat across time periods (see constraint (2.10a)) and likely wastes a large portion of the available exhaust heat from the CHP SOFCs. We would prefer to use as much of the exhaust heat as possible to keep the tank water as hot as possible and to reduce the heat provided by the boiler. Hence, the fixed values for T_{5t} , B_{5t}^{in} , and B_{5t}^{out} should be tailored to the heat supplied to the water tank by the CHP SOFCs and the heat demanded from the water tank by the building.

Any fixed values selected for T_{5t} , B_{5t}^{in} , and B_{5t}^{out} must satisfy constraints (2.10a) through (2.10e) to be (\mathcal{H})-feasible. In order to derive fixed values for T_{5t} that satisfy constraint (2.10a), we require values for the flowrate of heat from the CHP SOFCs (F_{5t}^{in}), the flowrate of hot water from the tank (F_{5t}^{out}), and the tank size (V_5). The values for F_{5t}^{in} and V_5 are determined from the solution to (\mathcal{U}). Given $\check{P}_{4t}^{\text{out}}$ and \check{E}_{4t} , along with constraints (2.6a) and (2.9a), we calculate the maximum flowrate of exhaust gas from the CHP SOFCs in each hour and use this as the value for F_{5t}^{in} . The value for V_5 is taken directly from the solution to (\mathcal{U}). With a fixed inflow of heat

and fixed tank size, we can iteratively calculate values for T_{5t} that satisfy constraint (2.10a), values for B_{5t}^{in} that satisfy constraint (2.10c), and values for B_{5t}^{out} that satisfy constraint (2.10d). As part of the algorithm, we also calculate values for F_{5t}^{out} that satisfy constraint (2.2b); however, these values are not fixed in (\mathcal{H}) . Finally, in order to ensure the satisfaction of constraint (2.10e), we set the tank temperature in the initial time period ($T_{5,1}$) equal to the temperature in the terminal time period ($T_{5,|\mathcal{T}|}$) after the first execution of the algorithm. We then continue executing the algorithm until the terminal tank temperature is equal to the initial tank temperature. Empirically, we find that the terminal temperature is so insensitive to the initial temperature that only two repetitions total of the algorithm are necessary. The fixed efficiency and temperature values are applied in (\mathcal{H}) as part of the following algorithm to obtain a ‘‘CHP DG’’ (\mathcal{P}) -feasible solution:

‘‘CHP DG’’ (\mathcal{P}) -feasible Solution Algorithm

1. Solve (\mathcal{U}) and store resulting values for $\check{P}_{jt}^{\text{out}}, \check{N}_{jt} \forall j, t$, and \check{V}_5 .
2. Set $E_{jt} = \check{E}_{jt} \forall j, t$, $F_{5t}^{\text{in}} = \gamma_4(\check{P}_{4t}^{\text{out}}/\check{E}_{4t}) \forall t$, $V_5 = \check{V}_5$, and $T_{5,1} = \tau^{\text{max}}$.
3. Loop $\forall t \in \mathcal{T}$.
 - (a) Set $B_{5t}^{\text{in}} = 1$ if $T_{5t} > (\tau_5^{\text{in}} + \varepsilon)$, 0 otherwise.
 - (b) Set $B_{5t}^{\text{out}} = 1$ if $T_{5t} > \tau_6^{\text{out}}$, 0 otherwise.
 - (c) Let $F_{5t}^{\text{out}} = \left(1 - \left[1 - \frac{\tau_6^{\text{out}} - \tau_5^{\text{min}}}{T_{5t} - \tau_5^{\text{min}}}\right] B_{5t}^{\text{out}}\right) \left(\frac{d_t^{\text{Q}}}{h_5(\tau_6^{\text{out}} - \tau_5^{\text{in}})}\right)$.
 - (d) Set $T_{5,t+1} = \max\left\{\tau_5^{\text{in}}, \min\left\{\tau^{\text{max}}, (1 - \alpha_5 B_{5t}^{\text{in}})T_{5t} + \frac{\delta\eta_5^{\text{Q}} h_4 F_{5t}^{\text{in}} (\tau_4^{\text{out}} - T_{5t}) - \delta h_5 F_{5t}^{\text{out}} (T_{5t} - \tau_5^{\text{in}})}{h_5 V_5}\right\}\right\}$.
4. If $T_{5,|\mathcal{T}|} = T_{5,1}$ then go to Step 5. Otherwise, set $T_{5,1} = T_{5,|\mathcal{T}|}$ and return to Step 3.
5. Solve (\mathcal{H}) and return its solution.

Upon obtaining the “no DG,” “power DG,” and “CHP DG” (\mathcal{P})-feasible solutions for a given problem instance, we choose the solution with the lowest cost to provide the tightest upper bound on the optimal solution to (\mathcal{P}).

3.4 Comparison with Existing Solvers

In this section, we provide solutions from (\mathcal{U}) and (\mathcal{H}) for a six-story, 122,000 square foot hotel located in Los Angeles, California. We then compare our solutions to those provided by existing solvers. The hourly electricity and heating demands for the hotel are simulated using a benchmark building model in EnergyPlus (see [42]). The electricity demand includes lighting, equipment, and cooling, while the heating demand includes both space and water heating. The hotel’s hourly power and heat demands on a summer weekday and winter weekday are depicted in Figure 3.1.

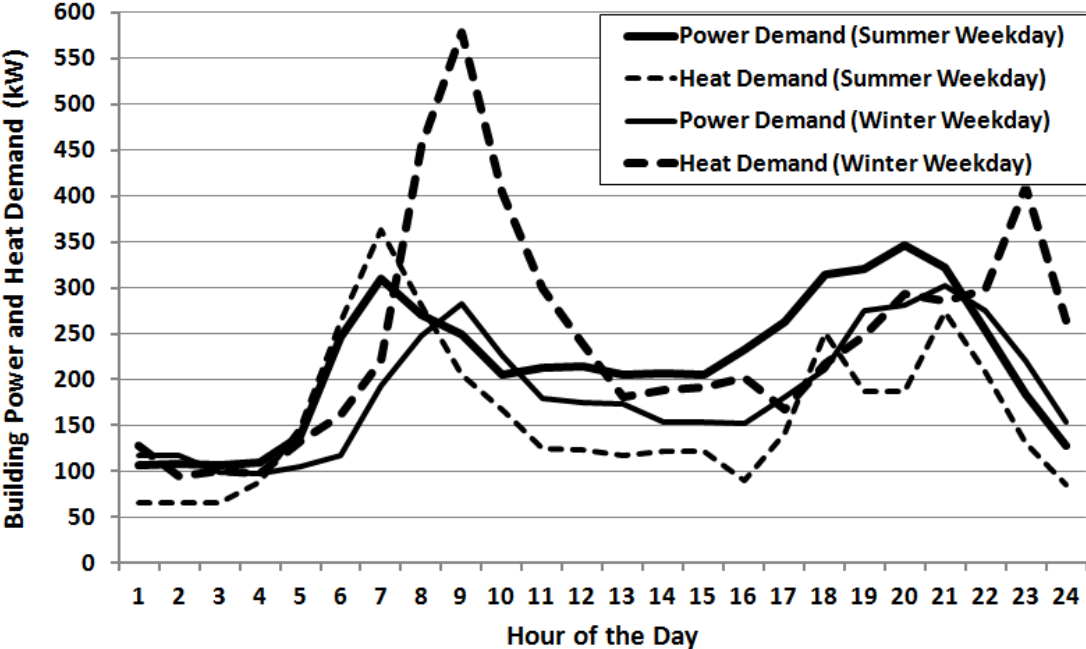


Figure 3.1: Power and heating demands for a large hotel located in Los Angeles, California.

Electricity prices are based on Southern California Edison’s rate schedule for commercial customers (see [43]), while natural gas prices are based on Southern California

Gas Company’s rate schedule for core commercial service (see [44]). The energy prices from each utility on a summer weekday and winter weekday are provided in Figure 3.2. According to Kaffine et al. [45], the average carbon emissions rate for power plants in the California Independent System Operator (CAISO) territory, which serves Los Angeles, is 0.15 kg/kWh (\approx 0.16 tons/MWh). This relatively low rate is due to the lack of coal-fired plants and the prevalence of wind power and natural gas-fired plants. We use a carbon tax of \$0.02 per kg (\approx \$20 per ton) and assume the building owner is taxed for the generation of the purchased power.

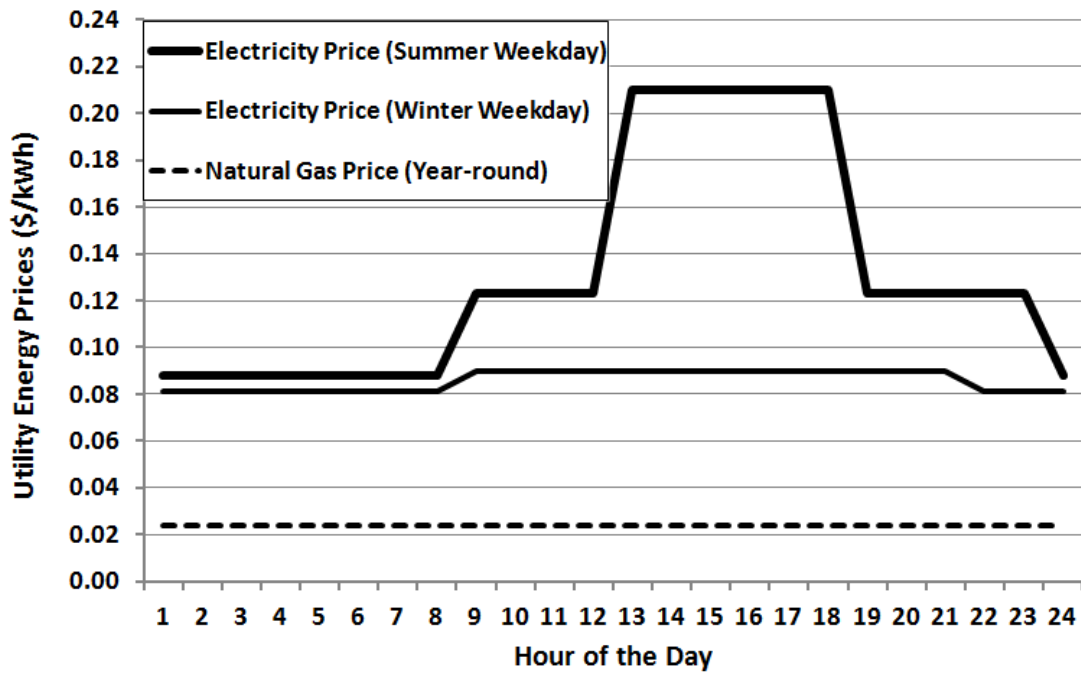


Figure 3.2: Electricity and natural gas prices for commercial customers in southern California.

For our DG system, the generators available for acquisition are power-only SOFCs, CHP SOFCs, and fixed-tilt PV cells with the costs and performance characteristics provided in Table 3.2. The average hourly availability of the PV cells, given the prevailing weather, is determined by the PVWATTS Performance Calculator developed by the National Renewable Energy Laboratory (see [46]). The amortized capital costs

of all of the technologies are calculated according to equation (2.13) based on the initial capital costs and average lifetimes in Table 3.2, along with a 5% annual interest rate. The initial capital costs applied here are lower than those typically found in other research. However, we find that higher capital costs result in the “no DG” solution for most instances, which limits the ability to demonstrate our bounding techniques.

Table 3.2: Generator cost and performance parameter values.

Parameter	Power SOFC	CHP SOFC	PV Cell
Initial Capital Cost [\$/kW]	2,800	3,360	2,800
O&M Cost [\$/kWh]	0.02	0.024	0.04
Nameplate Power Rating [kW]	10	10	10
Avg. Availability [%]	100	100	PVWATTS
Max Turn-Down [%]	20	20	0
Start-up Time [hours]	0.5	0.5	N/A
Max Ramp Rate [kW/h]	16	16	N/A
Max (Min) Electric Efficiency [%]	57 (41)	57 (41)	N/A
Exhaust Output [kg/kWh]	N/A	2.05	N/A
Avg. Exhaust Temperature [°C]	N/A	365	N/A
Avg. Lifetime [years]	15	15	15

The storage technologies available for acquisition are lead-acid batteries (electric) and a hot water tank (thermal), with the costs and performance characteristics listed in Table 3.3. For simplicity, we assume that there is no additional capital cost to increase the size of the water tank beyond its minimum. Thus, the increased capital cost for the CHP SOFC option is assumed to account for the cost of the water tank, regardless of its size. The temperature of the water in the tank is assumed to decrease by 1% per hour due to ambient heat loss. The values for the specific heat of SOFC exhaust and tank water are 0.0003 kWh/(kg °C) and 0.0044 kWh/(gal °C), respectively. The average return and maximum temperatures for the water in the tank are 16 °C and 85 °C, respectively, and we assume the hot water must be delivered to all faucets and radiators at 60 °C.

Table 3.3: Storage cost and performance parameter values.

Parameter	Lead-acid Battery	Water Tank
Initial Capital and O&M Cost	\$140/kWh	\$0/gal
Nameplate Capacity	10 kWh	500-1,000 gal
Min State-of-Charge or Temperature	30%	15°C
Max Charge (Discharge) Rate	1 (2.5) kW	N/A
Charge-Discharge or Thermal Efficiency	90%	80%
Avg. Lifetime	5 years	15 years

The boiler has an average thermal efficiency of 75% and O&M costs of \$0.01 per kWh of heat supplied. We use a carbon emissions rate of 0.18 kg/kWh for the combustion of natural gas (see [47]). Thus, the carbon emissions from the SOFCs and boiler are determined by multiplying this emissions rate by the amount of natural gas consumed.

We next solve (\mathcal{U}) and (\mathcal{H}) for instances with time horizons ranging from one day to one year (see Table 3.1), and compare our solutions with those provided by solving (\mathcal{P}) directly using existing MINLP solvers. As we demonstrate in Appendix A, (\mathcal{U}) , (\mathcal{H}) , and (\mathcal{P}) are all coded in AMPL Version 20090327 (see [48]). (\mathcal{U}) and (\mathcal{H}) are solved with CPLEX 12.2 (see [48]) on a 64-bit workstation under the Linux operating system with four Intel processors running at 2.27 GHz and with 12 GB of RAM. MINLP solvers which accept models (e.g., (\mathcal{P})) coded in AMPL include MINOTAUR, BONMIN, Couenne, FilMINT, and MINLP-B&B. MINOTAUR (see [49]) resides on our 64-bit workstation, while the other four solvers are publicly available on the NEOS Server for Optimization (see [50] and [51]). In all instances, we provide the solvers the “no DG” solution as an initial feasible solution, set an optimality gap of 1%, and enforce a time limit of 36,000 seconds.

Of the five MINLP solvers we tested, MINOTAUR demonstrates the greatest success in solving instances of (\mathcal{P}) . MINOTAUR solves up to the four-day instance, but is unable to find an integer solution for the instances of one week or greater.

BONMIN solves the one-day instance and obtains the same objective function value as MINOTAUR, but is unable to find an integer solution for the instances of two days or greater. Couenne is unable to converge on an optimal solution for the one-day instance and terminates with a best integer solution worse (i.e., greater) than that found by (\mathcal{H}) . FilMINT and MINLP-B&B terminate immediately for the one-day instance with error messages stating “no feasible solution” and “ran out of memory,” respectively. By contrast, (\mathcal{U}) and (\mathcal{H}) provide global lower bounds and integer solutions, respectively, for (\mathcal{P}) instances of up to one year. We compare the solutions provided by (\mathcal{U}) and (\mathcal{H}) with those provided by MINOTAUR in Table 3.4. In all instances, the solutions are expressed as a fraction of the total cost for the “no DG” solution.

Table 3.4: (\mathcal{P}) -feasible solutions provided by our techniques and by MINOTAUR for time horizons of one day to one year. *In these instances, (\mathcal{U}) reaches the 36,000 second time limit prior to achieving a 1% optimality gap. The time beyond 36,000 seconds is the solve time for (\mathcal{H}) . †In these instances, we use the best lower bound on (\mathcal{U}) at the point of termination as the global lower bound on (\mathcal{P}) . ‡In these instances, an optimality gap of <1% is reported by MINOTAUR using the best continuous relaxation solution as the lower bound. Given the nonconvex nature of (\mathcal{P}) , these gaps are not an indication of the proximity to *global* optimality.

Time Horizon (hours)	(\mathcal{U}) and (\mathcal{H})			MINOTAUR		
	Best Integer Solution (% of “no DG”)	Solve Time (sec)	Opt. Gap (%)	Best Integer Solution (% of “no DG”)	Solve Time (sec)	Opt. Gap (%)
24	85.92	4	8.97	85.16	38	‡
48	96.79	15	8.41	97.22	1,905	‡
96	96.82	629	8.34	96.98	6,127	‡
168	91.46	36,002*	9.42†	∞	36,000	∞
744	91.66	36,007*	11.34†	∞	36,000	∞
8,760	100.00	36,027*	12.07†	∞	36,000	∞

For each of the six instances, we solve (\mathcal{U}) to obtain a global lower bound on (\mathcal{P}) . We then use variable values from the solution to (\mathcal{U}) to solve (\mathcal{H}) and obtain an integer solution (upper bound) for (\mathcal{P}) . For the three largest instances, (\mathcal{U}) terminates at

the 36,000 second time limit prior to achieving the optimality gap of 1%. In these instances, we use the best lower bound on (\mathcal{U}) at the point of termination as the global lower bound on (\mathcal{P}) . Thus, the optimality gaps reported in the table are based on the difference between the optimal objective function value of (\mathcal{H}) and the appropriate global lower bound provided by (\mathcal{U}) . By contrast, the optimality gaps reported for MINOTAUR are based on the solver’s best integer solution (upper bound) and best continuous relaxation solution (lower bound). Given the nonconvex nature of (\mathcal{P}) , solutions from continuous relaxations of the problem may not provide valid global lower bounds. Hence, MINOTAUR’s optimality gaps do *not* indicate the proximity of the integer solutions to *global* optimality.

Our techniques and MINOTAUR are both capable of obtaining (\mathcal{P}) -feasible solutions for instances with time horizons of up to four days (96 hours). For these small instances, our solutions are close to those obtained by MINOTAUR and require a significantly shorter solve time. Additionally, only (\mathcal{U}) and (\mathcal{H}) provide the possibility of solving instances with time horizons of one week and greater. For these instances, MINOTAUR terminates at the time limit without an integer-feasible solution. Though (\mathcal{U}) terminates at the time limit without convergence for these larger instances, we still obtain a global lower bound on (\mathcal{P}) and information that can be used in solving (\mathcal{H}) to obtain an integer solution to (\mathcal{P}) . Therefore, our bounding techniques provide two critical advantages over existing MINLP solvers: the capacity to solve large instances of (\mathcal{P}) and an indication of the proximity of those solutions to *global* optimality.

CHAPTER 4

SHORTFALLS IN SIMPLER MODELS

Prominent among the global optimization models in the DG literature is the Distributed Energy Resources Customer Adoption Model (DER-CAM) (see [27], [29], [41], and [30]). DER-CAM is a mixed-integer linear programming (MILP) model that is solved using the branch-and-bound algorithm to determine the number of DG technologies to acquire, along with their operating levels over time, to meet the power and heating demands of a building at minimum capital, operational, and environmental (i.e., emissions) cost. In contrast to other existing research, DER-CAM addresses both the design and dispatch of a DG system, applies a provable global optimization approach, includes both economic and environmental costs in its objective, and considers the generation and storage of both power and heat using renewable and nonrenewable technologies. Given all of these attributes, DER-CAM is the most flexible of the design and dispatch models in the existing literature. But, DER-CAM fails to consider many performance characteristics that constrain the dynamic (i.e., off-design) operation of DG technologies.

(\mathcal{P}) addresses this shortcoming by prescribing a globally minimum cost system design and dispatch while considering the maximum turn-down, start-up fuel consumption, ramping capability, and part-load electric efficiency of power generation technologies, and the time-varying temperature of thermal storage technologies. The consideration of these dynamic performance characteristics can be particularly important when the technologies are operated in a load-following, rather than base-load, manner. In some applications, the DG system configuration and capacity, the building's energy demands, and/or the local utility's rates, policies, and procedures may require a load-following dispatch from the DG technologies. In these instances, (\mathcal{P})

captures the real-world operation of the technologies more accurately than models which simplify or ignore dynamic performance characteristics.

We begin this chapter by discussing system operating strategies and identifying applications that may require a particular strategy. We then present a representative MILP formulation of the design and dispatch problem, called (\mathcal{S}) , and qualitatively compare this linear approach to the nonlinear approach (\mathcal{P}) . We conclude the chapter with a case study that reveals the quantitative impact of ignoring system dynamics in (\mathcal{S}) .

4.1 System Operating Strategies

For the DG systems examined in this research, we consider SOFCs as the primary source of on-site power generation. Thus, one of the goals of solving specific instances of (\mathcal{P}) is to determine the appropriate operating strategy (e.g., baseload versus load-following) for the SOFCs. Accurately modeling the operation of CHP technologies, such as SOFCs, can require the consideration of numerous dynamic performance characteristics. The implications for failing to model the dynamic aspects of power and heat generation depend largely on how the SOFCs are operated. Accordingly, we next discuss the performance limitations of SOFC power and heat dispatch in the context of two operating strategies: baseload and load-following.

Baseload Strategy

A DG system with multiple sources of electricity import and export, such as that in Figure 2.1, provides flexibility in how the SOFCs are operated. For instance, Figure 4.1 depicts an operating strategy for which the SOFCs baseload at their rated (i.e., maximum) capacity. In the region labeled (i), the SOFC power output falls short of the building demand. Consequently, the remaining power demand must be supplied by the PV cells, battery discharge, and/or the grid. The complementary case is demonstrated in the region labeled (ii), where the SOFC power output exceeds the building demand. In (ii), the surplus power generated by the SOFCs must be charged

to the batteries or exported to the grid. Thus, a DG system with the technological means to address shortages (i) and surpluses (ii) in power supply permits SOFCs the flexibility to operate according to a variety of strategies, including baseloading.

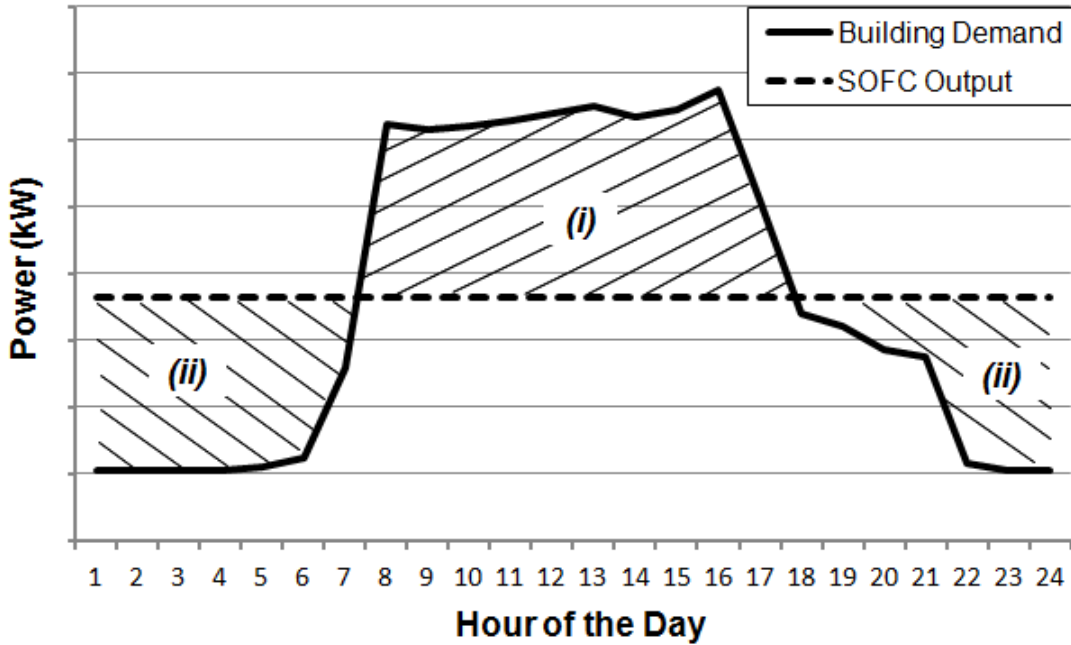


Figure 4.1: SOFC power output given a baseload operating strategy. The SOFC output falls short of the building load in periods of high demand (i) and exceeds the building load in periods of low demand (ii).

If the SOFCs baseload, then limitations on dynamic performance may be of little concern. When baseloading at rated capacity, the SOFCs are never turned down to part load or standby, and do not change power or exhaust gas output between time periods. With a fixed exhaust gas input to the storage tank, the heating demand of the building is the only time-varying factor affecting the temperature of the tank water. In this case, the rated power output and efficiency may be the only characteristics required to accurately model the operation of the SOFCs. Thus, in applications for which it is physically possible and economically beneficial to operate the SOFCs in a baseload manner, the system design and dispatch solutions prescribed by (\mathcal{P}) may be similar to, if not the same as, solutions prescribed by simpler models that ignore

dynamic performance limitations. However, certain conditions for the DG system and energy market might prevent or discourage baseloading.

Load-following Strategy

Both physical and economic conditions could dictate a decrease in design options compared to the system in Figure 2.1. Renewable sources of power, such as PV cells, could have prohibitive capital costs and unpredictable supply. Similarly, high capital costs and charge-discharge inefficiencies could render electricity storage technologies unavailable or unattractive. Finally, local utility net-metering policies or interconnection procedures could discourage or prevent excess power from being exported to the grid. Under these conditions, the DG system has no means of disposing of excess SOFC power and relies solely on the grid to address power shortages. Figure 4.2 depicts a system for which PV cells, batteries, and exportation of power to the grid are not viable, and for which, consequently, SOFC baseloading may not be an option.

With a more limited DG system, such as that in Figure 4.2, there is far less flexibility in how the SOFCs are operated. This is particularly true when the rated SOFC capacity is greater than the minimum power load of the building, and the effective price of electricity from the SOFCs is less than that of the utility. In this case, the preferred operating strategy is that depicted in Figure 4.3, wherein SOFC power output follows the building load (i.e., load-follows) in all hours for which the demand is less than the rated capacity. In the region labeled (iii), where the building demand exceeds the rated capacity of the SOFCs, the remaining power is provided by the grid. Thus, a DG system with no technological means to address surplus power and only limited means to address power shortages (iii), may force SOFCs to load-follow.

Because load-following requires the SOFCs to operate at off-design power levels, it can be important to consider dynamic performance characteristics like maximum

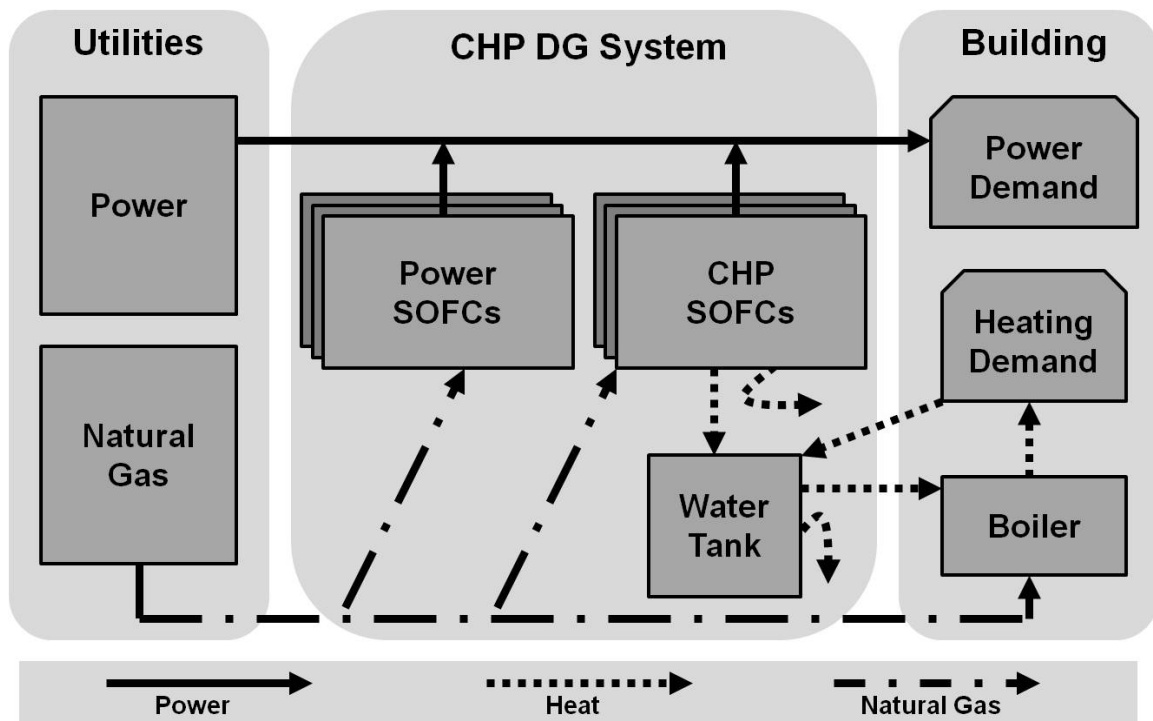


Figure 4.2: Combined heat and power (CHP), distributed generation (DG) system consisting of solid-oxide fuel cells (SOFCs) and a hot water storage tank.

turn-down, start up, ramping, and part-load electric efficiency and exhaust gas output in order to avoid prescribing an unrealistic system dispatch. When SOFCs operate at part load, it is possible that some of the SOFCs could be forced into standby mode and, therefore, must later start back up when the required power output increases above the maximum turn-down. Also, large increases and decreases in power output throughout the day are constrained to the ramping capability of the SOFCs. As the power output of the SOFCs changes over time, so too do their electric efficiency, their rate of natural gas consumption, and their rate of exhaust gas production. Thus, with load-following, the temperature of the water in the storage tank is determined by both time-varying heat input and output.

The aspects of dynamic SOFC operation described above can be critical to realistically modeling the operation of a CHP system in applications that require load-following. However, existing global optimization models of the design and dispatch

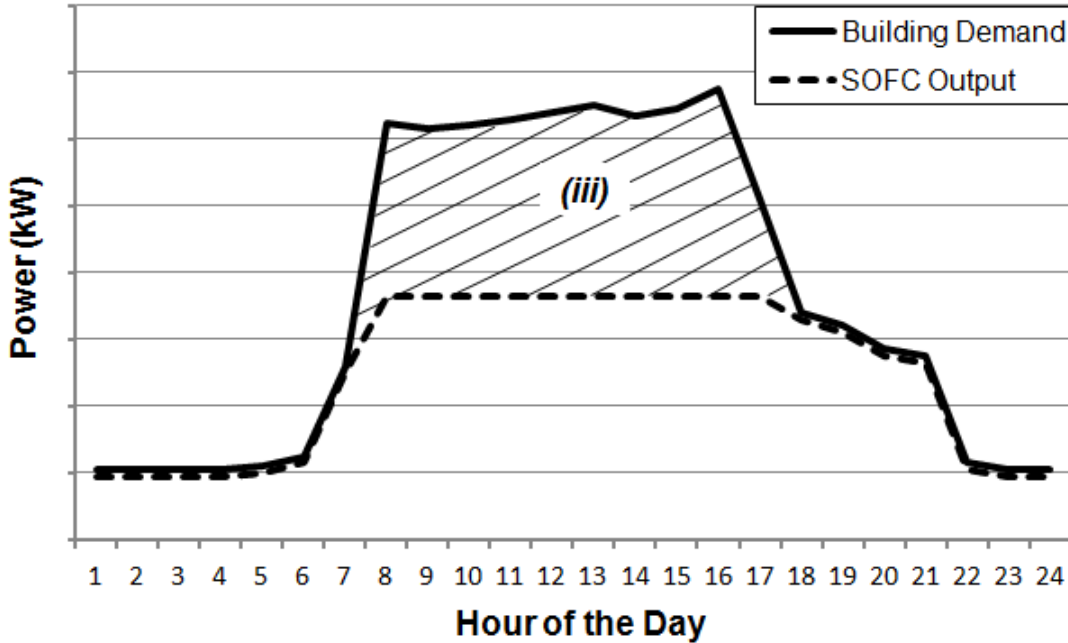


Figure 4.3: SOFC power output given a load-following operating strategy. The SOFC output falls short of the building load only in the periods of high demand (iii).

problem fail to consider the maximum turn-down, start-up fuel consumption, ramping capability, and/or part-load electric efficiency of power generators, and/or do not include the quality (i.e., temperature) of stored thermal energy. Ignoring these aspects of system operation allows for a linear formulation of the problem with fewer variables and constraints, but might lead to the prescription of a suboptimal or unrealistic system design and dispatch.

4.2 Simplified Formulation (\mathcal{S})

In this section, we present a simplified design and dispatch model, called (\mathcal{S}), that does not include maximum turn-down, start up, ramping, or part-load efficiency, and that models thermal storage in terms of energy inventory rather than temperature. The formulation of (\mathcal{S}) as a representative model that ignores system dynamics permits both qualitative and quantitative comparisons with (\mathcal{P}). By making these comparisons, we are able to highlight the scenarios for which a more detailed model,

such as (\mathcal{P}) , is preferable to a simpler model, such as (\mathcal{S}) .

The (\mathcal{S}) formulation presented here models the reduced DG system depicted in Figure 4.2, rather than the more robust system in Figure 2.1. We examine the reduced system, which does not include PV cells, batteries, or electricity export to the grid, in order to focus on the modeling aspects that differ between (\mathcal{P}) and (\mathcal{S}) . Thus, for purposes of comparison with (\mathcal{S}) in this chapter, (\mathcal{P}) objective component C_1 does not include the capital costs for PV cells or batteries, objective component C_4 is removed, constraint (2.2a) includes only SOFC and utility-generated power, and constraints (2.3b), (2.4a), (2.4b), (2.4c), (2.8a), (2.8b), and (2.8c) are removed. The reduced version of (\mathcal{P}) has $5|\mathcal{T}| + 2$ fewer variables and $6|\mathcal{T}| + |\mathcal{N}|$ fewer constraints than the formulation presented in Chapter 2. However, the solution methodology remains the same as that presented in Chapter 3.

We now present the mathematical formulation of (\mathcal{S}) using the sets, parameters, and variables defined in the nomenclature. The most significant difference in nomenclature between (\mathcal{P}) and (\mathcal{S}) regards the representation of heat. In (\mathcal{S}) , heat is represented directly by the variables Q_{jt}^{out} and Q_{jt}^{in} , rather than by the product of specific heat capacity, flow, and temperature, as in (\mathcal{P}) .

Problem (\mathcal{S})

Minimum Total Cost

Minimize

$$\sum_{j=3,4} c_j k_j^{\text{out}} A_j + \sum_{j=3,4} \sum_{t \in \mathcal{T}} m_j \delta P_{jt}^{\text{out}} + \sum_{j=3,4} \sum_{t \in \mathcal{T}} (g_t + z z^g) \delta G_{jt} \quad (4.1a)$$

$$+ \sum_{t \in \mathcal{T}} (p_t + z z^p) \delta U_t^{\text{out}} + \sum_{n \in \mathcal{N}} p_n^{\text{max}} U_n^{\text{max}} + \sum_{t \in \mathcal{T}} (\eta_6^Q m_6 + g_t + z z^g) \delta G_{6t} \quad (4.1b)$$

subject to

Power and Heating Demand

$$\sum_{j=3,4} P_{jt}^{\text{out}} + U_t^{\text{out}} = d_t^P \quad \forall t \in \mathcal{T} \quad (4.2a)$$

$$U_n^{\text{max}} \geq U_t^{\text{out}} \quad \forall n \in \mathcal{N}, t \in \mathcal{T}_n \quad (4.2b)$$

$$Q_{5t}^{\text{out}} + Q_{6t}^{\text{out}} = d_t^Q \quad \forall t \in \mathcal{T} \quad (4.2c)$$

Power Capacity

$$P_{jt}^{\text{out}} \leq k_j^{\text{out}} A_j \quad \forall j = 3, 4, t \in \mathcal{T} \quad (4.3a)$$

Natural Gas Consumption

$$\eta_j^P G_{jt} = P_{jt}^{\text{out}} \quad \forall j = 3, 4, t \in \mathcal{T} \quad (4.4a)$$

$$\eta_6^Q G_{6t} = Q_{6t}^{\text{out}} \quad \forall t \in \mathcal{T} \quad (4.4b)$$

Heat Capacity

$$Q_{5t}^{\text{in}} \leq \eta_4^Q G_{4t} \quad \forall t \in \mathcal{T} \quad (4.5a)$$

Heat Storage

$$Q_{5,t+1} - (1 - \alpha_5)Q_{5t} = \delta(\eta_5^Q Q_{5t}^{\text{in}} - Q_{5t}^{\text{out}}) \quad \forall t < |\mathcal{T}| \quad (4.6a)$$

$$Q_{5t} \leq s_5^{\text{max}} A_5 \quad \forall t \in \mathcal{T} \quad (4.6b)$$

$$Q_{5,1} = Q_{5,|\mathcal{T}|} \quad (4.6c)$$

Heat Storage Acquisition

$$A_5 \leq A_4 \leq \left\lceil \frac{\max_{t \in \mathcal{T}} \{d_t^P\}}{k_4^{\text{out}}} \right\rceil A_5 \quad (4.7a)$$

Non-negativity and Integrality

$$U_t^{\text{out}}, P_{jt}^{\text{out}}, G_{jt}, Q_{jt}, Q_{jt}^{\text{out}}, Q_{jt}^{\text{in}} \geq 0 \quad \forall j \in \mathcal{J}, t \in \mathcal{T} \quad (4.8a)$$

$$U_n^{\text{max}} \geq 0 \quad \forall n \in \mathcal{N} \quad (4.8b)$$

$$A_j \geq 0, \text{ integer} \quad \forall j = 3, 4 \quad (4.8c)$$

$$A_j \text{ binary} \quad \forall j = 5 \quad (4.8d)$$

The (\mathcal{S}) formulation includes $7|\mathcal{T}| + 1$ fewer variables and $16|\mathcal{T}| - 4$ fewer constraints than the reduced version of (\mathcal{P}) . Additionally, (\mathcal{S}) contains only two general integer variables, one binary variable, and is comprised of only linear constraints. With so few integer variables and a convex constraint set, instances of (\mathcal{S}) are much simpler to solve than those of (\mathcal{P}) .

4.3 Qualitative Differences Between (\mathcal{P}) and (\mathcal{S})

Qualitatively, (\mathcal{P}) and (\mathcal{S}) differ in how they model the generation of power and heat by the SOFCs, and the storage of heat in the water tank. In this section, we provide a detailed discussion of these qualitative differences. We then examine the quantitative impact of the modeling differences in Section 4.4.

Power Generation

An examination of SOFC natural gas consumption at various power output levels highlights the differences in how (\mathcal{P}) and (\mathcal{S}) model power generation. Figure 4.4 depicts the hourly natural gas consumption of a representative SOFC as a function of its power output.

In (\mathcal{P}) , the left-hand side of constraint (2.4d) enforces a minimum power output for the SOFCs that are operating (i.e., not in standby mode) in a given time period. Given the minimum operating temperature required for power generation, SOFCs cannot operate at power levels below this maximum turn-down. Thus, the range of power output levels below the maximum turn-down (i.e., between zero and minimum power output) is appropriately restricted in (\mathcal{P}) . However, because constraint (4.3a) in (\mathcal{S}) ignores the operational status and maximum turn-down of the SOFCs, power

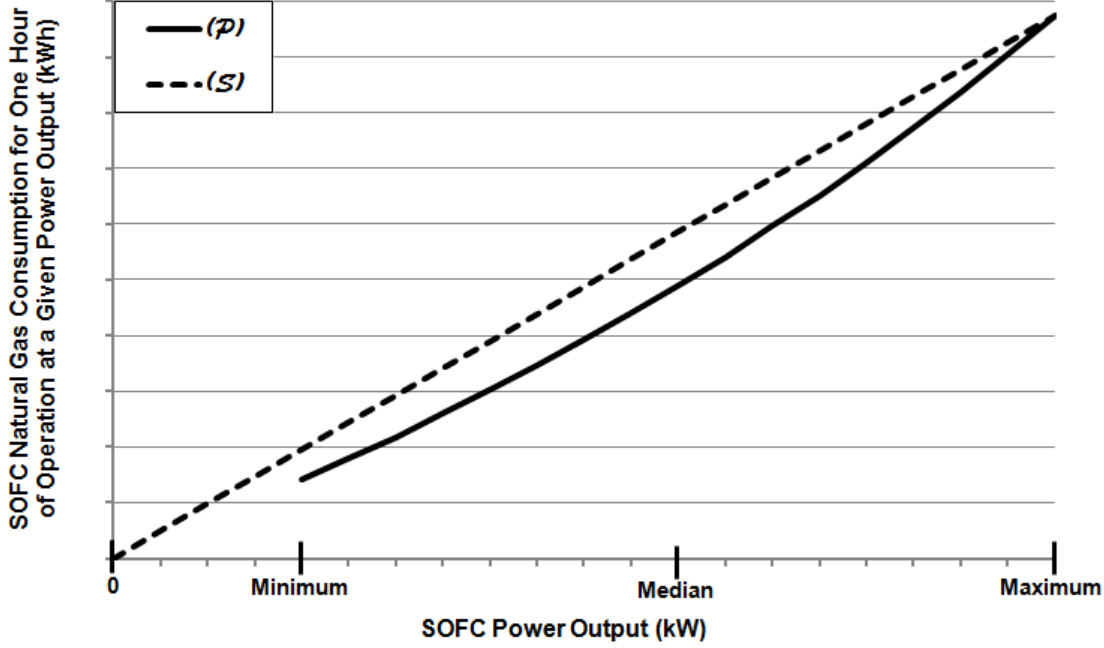


Figure 4.4: Comparison of SOFC natural gas consumption at minimum, median, and maximum power output as modeled in (\mathcal{P}) versus (\mathcal{S}) .

dispatch solutions (i.e., prescribed values for P_{jt}^{out}) are permitted to select output levels below the maximum turn-down (as depicted in Figure 4.4). Such solutions cannot be implemented in reality.

Constraints (2.4d) and (2.4e) in (\mathcal{P}) and constraint (4.3a) in (\mathcal{S}) similarly limit the maximum aggregate power output of the SOFCs to the total nameplate power rating of the SOFCs that are acquired. Furthermore, because (\mathcal{S}) fixes the electric efficiency of the SOFCs to the rated efficiency (i.e., the efficiency at maximum power output), the natural gas consumption at maximum power output is the same as in (\mathcal{P}) . However, the natural gas consumption of the SOFCs at part-load differs between the two formulations. In (\mathcal{P}) , constraints (2.5a) and (2.6a) dictate that natural gas consumption decreases nonlinearly as power output decreases. By contrast, constraint (4.4a) in (\mathcal{S}) indicates that natural gas consumption decreases linearly as power output decreases. The result of these differences is that (\mathcal{S}) overestimates the fuel consumption

whenever the SOFCs operate at part-load (as depicted in Figure 4.4). Thus, when SOFCs load-follow, the time-varying electric efficiency captured in (\mathcal{P}) allows for a more accurate calculation of fuel consumption.

The overestimation of SOFC fuel consumption in (\mathcal{S}) is partially offset in time periods in which a positive number of SOFCs start up. In (\mathcal{P}) , the variable \dot{N}_{jt} found in objective component C_3 and constraint (2.7a) enforces a fuel requirement for the SOFCs to depart standby mode and achieve operating temperature. If a SOFC's operational status changes from “standby” to “on” between successive time periods in constraint (2.7a), then objective component C_3 accounts for the cost associated with the natural gas consumed by the SOFC to achieve the maximum turn-down. We calculate the gas required for start up by assuming a SOFC requires σ_j hours to increase power from zero to $\mu_j k_j^{\text{out}}$, and that fuel is consumed during start up with the same efficiency η_j^{min} as at rated power output. However, objective component (4.1a) in (\mathcal{S}) does not account for the fuel required for SOFC start up, nor do any constraints. Thus, in (\mathcal{S}) , the underestimation of start-up fuel consumption partially offsets the overestimation of steady-state fuel consumption in any hour in which SOFCs start up.

Another key difference in how (\mathcal{P}) and (\mathcal{S}) model power generation pertains to the ramping capability of the SOFCs. In (\mathcal{P}) , ramping is explicitly limited in constraint (2.7b), which we restate here:

$$-\delta r_j^{\text{down}} N_{jt} \leq P_{j,t+1}^{\text{out}} - P_{jt}^{\text{out}} \leq \delta r_j^{\text{up}} N_{j,t+1} \quad \forall j = 3, 4, t < |\mathcal{T}|.$$

On the other hand, (\mathcal{S}) only implicitly restricts changes in SOFC power output. Based on constraints (4.3a) and (4.8a), we can derive the following ramping restrictions:

$$-k_j^{\text{out}} A_j \leq P_{j,t+1}^{\text{out}} - P_{jt}^{\text{out}} \leq k_j^{\text{out}} A_j \quad \forall j = 3, 4, t < |\mathcal{T}|. \quad (4.9)$$

Equation (4.9) indicates that, in (\mathcal{S}) , SOFC power output is permitted to increase or decrease by the aggregate nameplate power rating of the SOFCs that are acquired. However, depending on the demand time increment and the number of operational SOFCs, a ramp (i.e., $P_{j,t+1}^{\text{out}} - P_{jt}^{\text{out}}$) of this magnitude may not be achievable. Constraint (2.7b) in (\mathcal{P}) accounts for this ramping limitation. If $-\delta r_j^{\text{down}} N_{jt} > -k_j^{\text{out}} A_j$ or $\delta r_j^{\text{up}} N_{j,t+1} < k_j^{\text{out}} A_j$ in a given time period, then (\mathcal{P}) provides *tighter* restrictions on SOFC ramping than (\mathcal{S}) does. Given typical SOFC ramp rates, it is unlikely that (\mathcal{P}) provides tighter ramping restrictions in instances which consider hourly power demand (i.e., $\delta = 1$) and for which it is beneficial to operate all of the acquired SOFCs (i.e., $N_{jt} = A_j$) in all time periods. However, the consideration of sub-hourly power demand (i.e., $\delta < 1$) and SOFC standby mode (i.e., $N_{jt} < A_j$) increase the likelihood that (\mathcal{S}) overestimates the ramping capacity. This situation could result in (\mathcal{S}) prescribing dispatch schedules that cannot be implemented in reality.

Heat Generation and Storage

In addition to the differences in modeling power generation, (\mathcal{P}) and (\mathcal{S}) differ in how they account for the generation and storage of heat. The most fundamental difference is how heat itself is represented in the two formulations. In (\mathcal{S}) , the flow of heat is represented directly by the variables Q_{jt}^{out} and Q_{jt}^{in} , and the amount of thermal energy stored is represented by Q_{jt} . In (\mathcal{P}) , however, heat (or thermal energy) is determined as the product of a fluid's specific heat capacity, flowrate (or volume), and temperature change. This alternative representation of heat and thermal energy permits the consideration of more detailed performance characteristics of thermal systems. Specifically, the heat charged to and discharged from the storage tank can be modeled as a function of the flowrate and temperature of the exhaust gas supplied by the SOFCs and the hot water demanded by the building.

Figure 4.5 depicts the maximum thermal energy that can be charged to the storage tank in an hour by the exhaust gas from a representative SOFC operating at mini-

num, median, and maximum power output. In (\mathcal{S}) , the thermal energy that can be

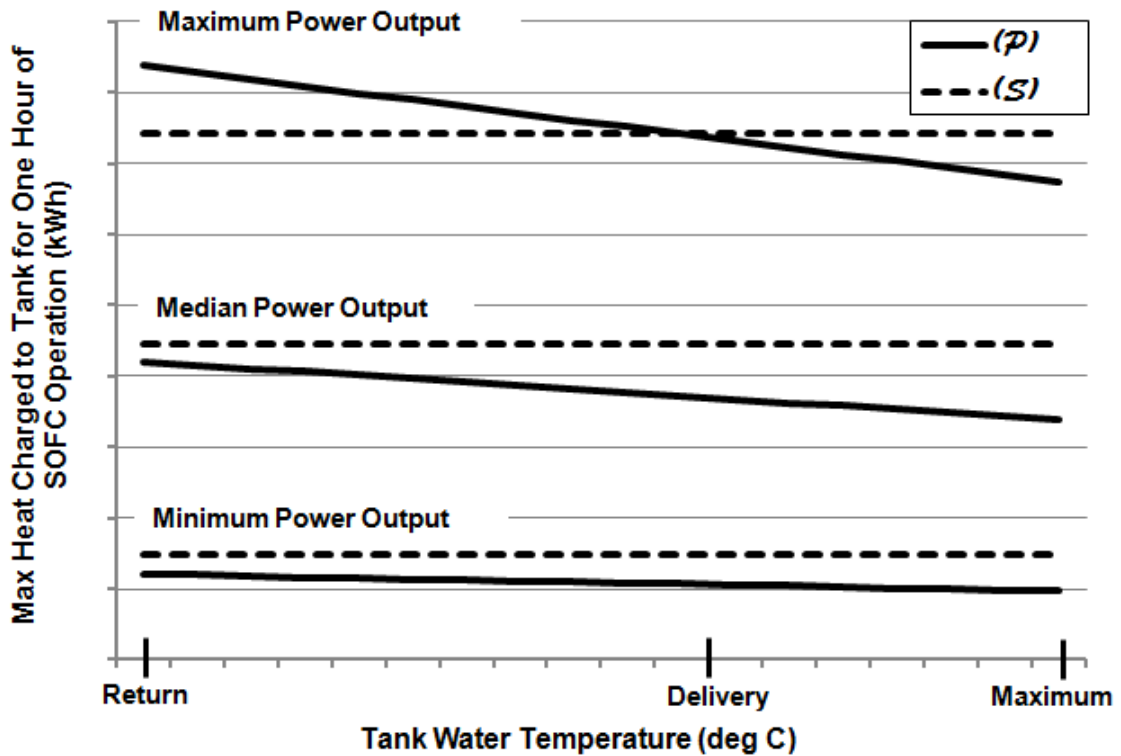


Figure 4.5: Comparison of heat charged to storage tank for SOFC operating at minimum, median, and maximum power output as modeled in (\mathcal{P}) versus (\mathcal{S}) .

added to the storage tank by SOFC exhaust gas is independent of the temperature of the water in the tank, and is based solely on the rated thermal efficiency of the SOFC (see constraints (4.5a) and (4.6a)). As a result, the maximum thermal energy that can be charged to the tank is fixed for a given SOFC power output (as demonstrated in Figure 4.5). Conversely, in (\mathcal{P}) , the thermal energy that can be added to the tank is directly determined by the temperature of the tank water (see constraints (2.9a) and (2.10a)). The greater the temperature differential between the SOFC exhaust gas and the tank water, the greater the heat that can be applied to the tank. Consequently, the maximum thermal energy that can be added to the tank decreases as the water temperature increases (as demonstrated in Figure 4.5). In general, these differences between the two formulations result in (\mathcal{S}) overestimating the amount of heat that

can be charged to the storage tank. However, when the tank water is below delivery temperature and SOFC power output is at or near its maximum, (\mathcal{S}) underestimates the available heat.

Accounting for water temperature also leads to differences in how (\mathcal{P}) and (\mathcal{S}) model the tank discharge. Figure 4.6 presents the minimum thermal energy that must be discharged from the storage tank in an hour to meet representative minimum, median, and maximum demands. In (\mathcal{S}) , there is no minimum requirement

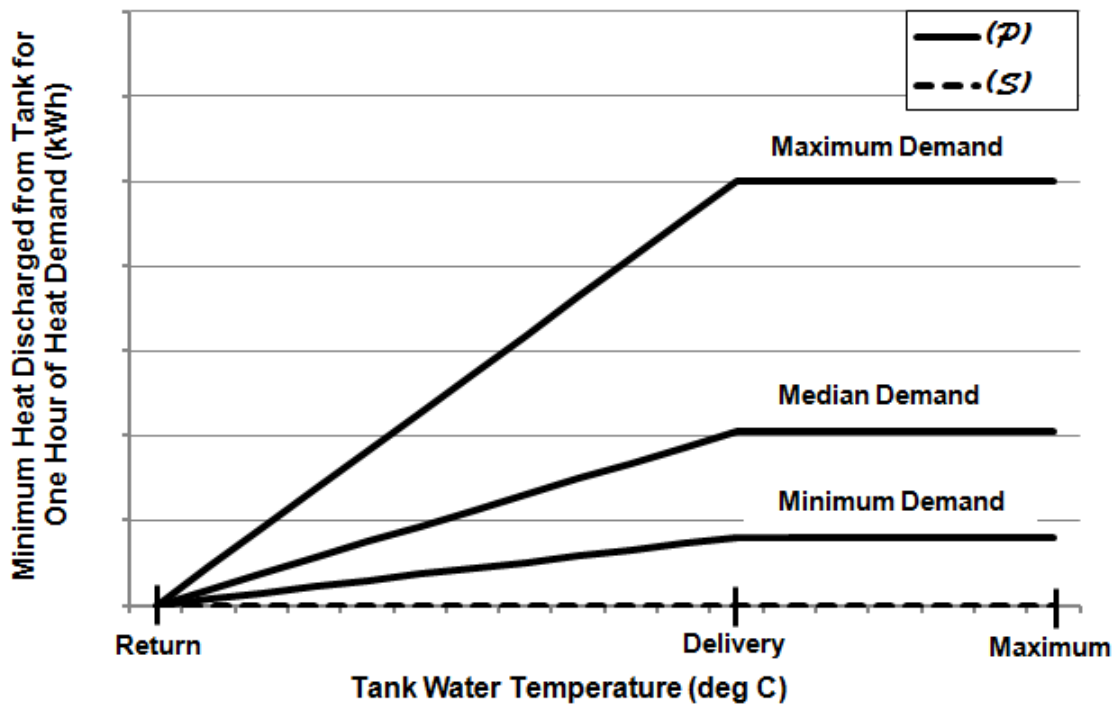


Figure 4.6: Comparison of heat discharged from storage tank to meet minimum, median, and maximum demands as modeled in (\mathcal{P}) versus (\mathcal{S}) .

on the portion of heating demand that must be met by the storage tank (see constraints (4.2c) and (4.6a)). Thus, the tank is permitted to provide as little as zero kilowatt-hours of thermal energy (as depicted in Figure 4.6) or as much as the full inventory of stored energy in the tank, regardless of the water temperature. By contrast, constraints (2.2b) and (2.10a) in (\mathcal{P}) enforce a minimum provision of heat by

the storage tank whenever the tank water temperature is above the average return temperature. For hours in which the tank water is between the return and delivery temperatures (as determined by constraints (2.10c) and (2.10d)), the storage tank provides a positive flow of hot water (and thus heat), with the boiler providing the remaining heat required to deliver the water (see constraint (2.6b)). As the tank water temperature increases, the portion of heating demand met by the storage tank increases (as depicted in Figure 4.6), and the portion met by the boiler decreases. For hours in which the tank water is at or above delivery temperature, *all* of the heating demand is met by the storage tank. In this case, no additional heating is required by the boiler. Thus, for hours in which both the tank water temperature and heating demand are high, (\mathcal{S}) likely underestimates the portion of demand met by the storage tank. However, in periods of lower heating demand and water temperature, it is possible for (\mathcal{S}) to overestimate the tank heat discharge.

For the representative cases demonstrated in Figure 4.5 and Figure 4.6, the net result of the limitations on tank heat charge and discharge is that the time-varying inventory of stored thermal energy is more accurately modeled in (\mathcal{P}) versus (\mathcal{S}). This is particularly true when the SOFC power output and building heating demand are high. When SOFC power output is at its maximum, the slope of the (\mathcal{P})-line in Figure 4.5 is at its greatest (in absolute value). The same is true of the slope of the (\mathcal{P})-line in Figure 4.6 when the heating demand is at its maximum. Due to the steep slopes of these lines, the thermal energy charged to or discharged from the storage tank is more sensitive to changes in the water temperature compared to when SOFC power output and heating demand are low. This sensitivity can lead to wild fluctuations in the thermal energy available from the tank. Because the limits on maximum charge and minimum discharge in (\mathcal{S}) are independent of the tank water temperature, (\mathcal{S}) is less capable of capturing these fluctuations in available thermal energy. As a result, there exist instances for which (\mathcal{S}) inaccurately represents the

real-world operation of the tank.

The final difference between (\mathcal{P}) and (\mathcal{S}) concerns the way in which the two formulations model the capacity of the thermal storage device. In (\mathcal{S}) , the maximum allowable inventory of thermal energy in the storage tank (i.e., the tank size) is a fixed parameter s_5^{\max} (see constraint 4.6b), the value of which is selected by the user a priori. Alternatively, (\mathcal{P}) models the tank size as a variable V_5 (see constraint 2.11b), the value of which is optimally selected by the algorithm. When modeling the temperature and flowrate of fluids into and out of the tank, the size of the tank determines the increase or decrease in stored thermal energy. Thus, (\mathcal{P}) optimally sizes the storage device based on the heat supplied by the SOFCs and the heat demanded by the building.

4.4 Quantitative Differences Between (\mathcal{P}) and (\mathcal{S})

In this section, we contrast solutions from (\mathcal{P}) and (\mathcal{S}) for a six-story, 122,000 square foot hotel located in southern Wisconsin. The power and heating loads for this building type, and the local utility rates, policies, and procedures, encourage the load-following behavior by the SOFCs previously discussed in Section 4.1. Hence, this scenario highlights the deficiencies exhibited by (\mathcal{S}) in modeling dynamic performance. We first present the building, utility, and technology parameter values applied in the case study, and then provide the results from solving (\mathcal{P}) and (\mathcal{S}) .

The hourly ($\delta = 1$) power and heating demands (d_t^P and d_t^Q) for the building are simulated using a benchmark building model in EnergyPlus (see DOE [42]). The power demand includes lighting, equipment, and cooling, while the heating demand includes both space and water heating. Annual power and heating demand statistics for the hotel are provided in Table 4.1, while the hotel’s hourly demands on the peak power day of the year are depicted in Figure 4.7.

The average electricity and natural gas prices listed in the top portion of Table 4.2 are based on Wisconsin Electric Power Company’s rate schedule for general commer-

Table 4.1: Annual power and heating demand statistics for a large hotel located in southern Wisconsin.

Statistic	Power Demand	Heating Demand
Maximum [kW]	264	1,086
Minimum [kW]	52	50
Average [kW]	142	256
Total [MWh]	1,244	2,245

cial service (see [52]) and Wisconsin Electric-Gas Operations’ rate schedule for firm sales service (see [53]). These energy charges are also consistent with statistics reported by the Energy Information Administration (EIA) for the state of Wisconsin (see [54] and [55]). The aforementioned EIA reports additionally provide the basis for our calculation of the Wisconsin electric industry’s average rate of carbon emissions (see Appendix B).

According to the Network for New Energy Choices (NNEC), the state of Wisconsin’s net-metering policies and interconnection procedures discourage customer-sited DG (see [56]). The NNEC cites Wisconsin Public Service Commission standards which limit DG system capacity, restrict customer energy credits, require excessive customer insurance, and include hidden interconnection fees. The limitation with the greatest impact for our case study is a 20 kW maximum system capacity. As we demonstrate in the numerical results, the optimal DG system capacity for the large hotel is much greater than 20 kW. Because the DG system exceeds the allowable capacity, net-metering is not permitted, and the SOFCs have no means to dispose of excess power.

The costs and performance characteristics of the SOFCs and water tank are listed in the bottom portion of Table 4.2. The annualized capital costs for the SOFCs applied here are lower than those typically reported in the current literature. However, we find that larger capital costs result in both (\mathcal{P}) and (\mathcal{S}) choosing the grid-only

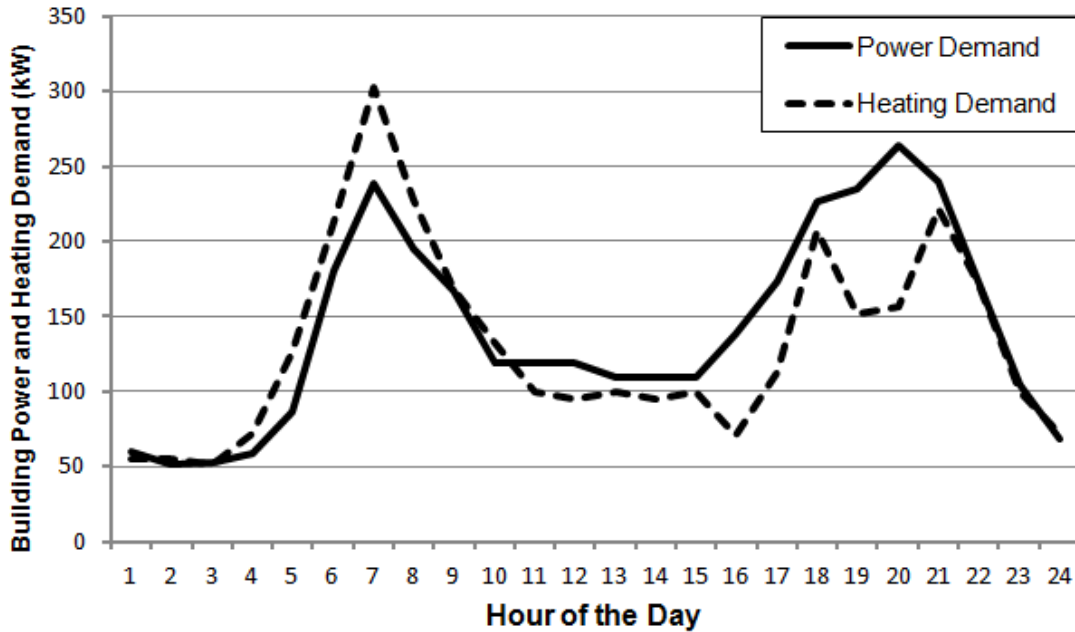


Figure 4.7: Power and heating demands on the peak power day for a large hotel located in southern Wisconsin.

solution (i.e., no SOFCs acquired). The initial acquisition and installation cost used for the SOFCs is \$1,600/kW. The cost increase for CHP integration, including the water tank, is 20%. The initial capital costs are continuously compounded at 5% interest over a 15-year system lifetime to obtain a lifetime opportunity cost, which is then divided by the 15 years to determine the annual costs reported in Table 4.2. We assume these reduced capital costs in order to induce DG acquisition according to both (\mathcal{P}) and (\mathcal{S}) , thereby providing a means to contrast the system design and dispatch selected by the two formulations.

Each of the performance characteristics of the SOFCs and water tank listed in the table are captured in (\mathcal{P}) . On the other hand, (\mathcal{S}) ignores the maximum turn-down, start up, ramping, and part-load efficiency of the SOFCs, and ignores the temperature of the water in the storage tank. Given these exclusions, (\mathcal{S}) simply models the operation of the SOFCs with the maximum power output (k_j^{out}), and fixed electric and thermal efficiencies (η_j^P, η_j^Q) of 0.41 and 0.19, respectively. These

Table 4.2: Cost, emissions, and technology parameter values.

Parameter	Value	Units
$p_t, g_t \quad \forall t$	0.10, 0.03	\$/kWh
$p_n^{\max} \quad \forall n$	6.00	\$/kW/month
z	0.02	\$/kg
z^p, z^g	0.74, 0.18	kg/kWh
c_3, c_4	226, 271	\$/kW/year
m_3, m_4, m_6	0.020, 0.024, 0.010	\$/kWh
$k_3^{\text{out}}, k_4^{\text{out}}$	10, 10	kW
σ_3, σ_4	2, 2	hours
μ_3, μ_4	0.2, 0.2	n/a
$r_3^{\text{up}}, r_4^{\text{up}}, r_3^{\text{down}}, r_4^{\text{down}}$	4, 4, 4, 4	kW/hour
$\eta_3^{\max}, \eta_4^{\max}, \eta_3^{\min}, \eta_4^{\min}$	0.57, 0.57, 0.41, 0.41	n/a
v_5^{\max}, v_5^{\min}	4200, 1000	gallons
η_5^Q, η_6^Q	0.80, 0.75	n/a
α_5	0.01	n/a
γ_4	2.05	kg/kWh
h_4	0.0003	kWh/(kg °C)
h_5	0.004	kWh/(gal °C)
$\tau_4^{\text{out}}, \tau_5^{\text{in}}, \tau_6^{\text{out}}$	365, 20, 60	°C
τ^{\max}, τ^{\min}	85, 15	°C

efficiencies are consistent with the SOFCs operating at maximum power output and the exhaust heat transferring to tank water at delivery temperature. In (\mathcal{S}) , the fixed storage capacity (s_5^{\max}) of the tank is expressed in terms of thermal energy, rather than water volume, and is set to a value equivalent to the maximum hourly heating load (1,086 kWh) for the year. This capacity is consistent with the upper bound on tank volume in (\mathcal{P}) , given the maximum allowable temperature of the water.

Next, we present the optimal system design and dispatch prescribed by (\mathcal{P}) and (\mathcal{S}) for the hotel, based on a typical year's hourly demand (8,760 hours). Both formulations are coded in AMPL Version 20090327 and solved with CPLEX 12.3 (see IBM [48]) on a 64-bit workstation under the Linux operating system with four Intel processors running at 2.27 GHz and with 12 GB of RAM. We apply the heuristic linearization and convex underestimation techniques presented in Chapter 3 to solve

(\mathcal{P}).

The optimal system design determined by (\mathcal{P}) includes 130 kW of on-site capacity (13 CHP SOFCs) and a 3,900 gallon water storage tank. Based on the maximum allowable water temperature of 85 °C and the average return temperature of 20 °C, the 3,900 gallon tank has a maximum thermal energy capacity of roughly 1,014 kWh. By contrast, (\mathcal{S}) chooses only 110 kW of capacity (11 CHP SOFCs) and the pre-determined 1,086 kWh tank. Both of the system designs prescribed by the two formulations afford a total annual cost less than that incurred by the grid and boiler alone. However, the total annual cost (including capital *and* operational costs) for the 13-SOFC system determined by (\mathcal{P}) is *less* than the total annual cost of the 11-SOFC system determined by (\mathcal{S}). Thus, according to (\mathcal{S}), a DG system with 20 kW *smaller* on-site capacity costs *more* to acquire and operate than the larger system selected by (\mathcal{P}). The suboptimal system design determined by (\mathcal{S}) results from its failure to consider the dynamic performance of the SOFCs and water tank. We demonstrate this by fixing the system design in (\mathcal{S}) to the 13-SOFC system, resolving (\mathcal{S}), and comparing the system dispatch results with those of (\mathcal{P}) for the peak power day of the year (hours 5,137 through 5,160).

Figure 4.8 demonstrates that (\mathcal{P}) and (\mathcal{S}) select the same aggregate power dispatch for the 13 SOFCs over the 24-hour period. Namely, the optimal aggregate SOFC power output is the minimum of the aggregate nameplate power capacity and the power demand (i.e., $P_{4t}^{\text{out}} = \min(130, d_t^P)$). However, the natural gas consumed by the SOFCs to generate that power differs between the two formulations. As previously predicted in Figure 4.4, (\mathcal{S}) overestimates the natural gas consumption in any hour in which the SOFCs operate below maximum power output. In fact, in the early hours of the day, (\mathcal{S}) overestimates the SOFC gas consumption by as much as 29% compared to (\mathcal{P}). The more hours the SOFCs operate at part-load, the more (\mathcal{S}) overestimates the fuel requirements for the SOFCs.

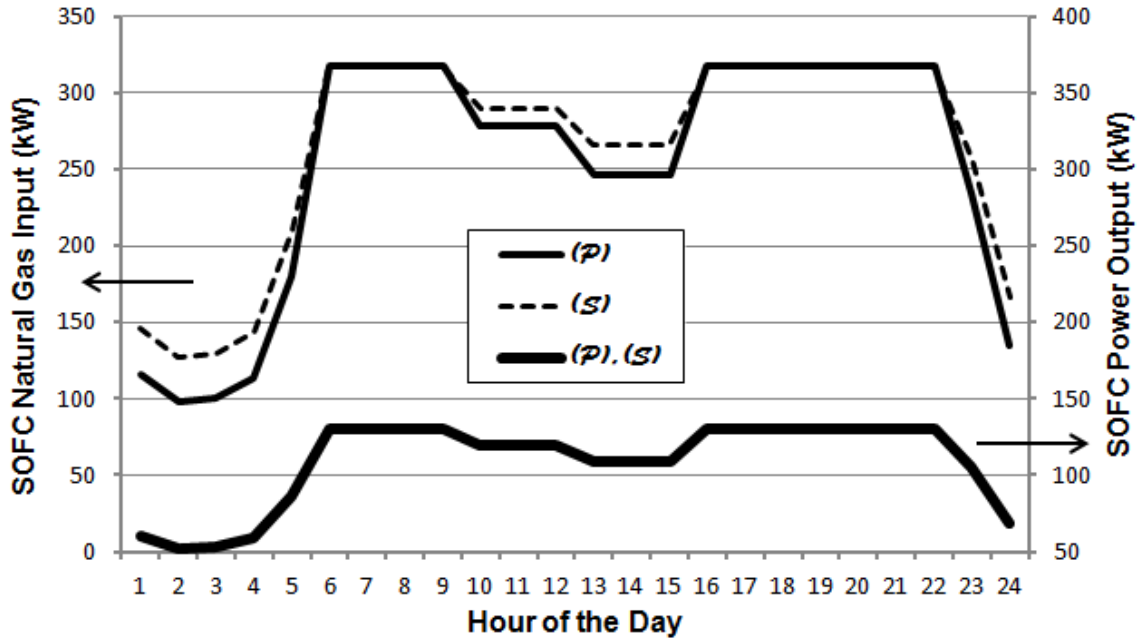


Figure 4.8: Optimal SOFC power output and natural gas consumption as determined by (\mathcal{P}) versus (\mathcal{S}) .

For this particular building power load, the aggregate power output of the SOFCs never reaches the maximum turn-down. With 130 kW of rated capacity and a 20% maximum turn-down, the aggregate power output must decrease below 26 kW before any number of SOFCs is forced into standby mode. Because the minimum hourly power load for the year is 52 kW, this particular system does not demonstrate SOFC standby mode or, consequently, SOFC start-up. However, for other simulated load profiles (or in the real-world application of the system) the power demand could fall below the 26 kW threshold. In these cases, the ability to model the effects of SOFC standby and start-up is important.

As we discuss in Section 4.3, the ramping constraints on the SOFCs are not likely to bind at the hourly level of fidelity. The largest hourly ramp up (44 kW) and ramp down (37 kW) on the peak power day are within the 52 kW total hourly ramping capacity of the 13 SOFCs. However, the consideration of a 30-minute, or less, demand time increment (i.e., $\delta < 0.5$) would tighten the ramping constraints

in (\mathcal{P}) , and potentially impact the feasibility of the hourly fidelity solution. With a maximum ramp rate of 4 kW/hr, the 30-minute ramping capability of each SOFC is only 2 kW (assuming an equal distribution over the hour). Thus, with 13 SOFCs operating, the total 30-minute ramping capability is only 26 kW. If we were to solve both (\mathcal{P}) and (\mathcal{S}) to determine the system dispatch at the 30-minute level of fidelity, (\mathcal{P}) would appropriately limit the power ramping capabilities of the SOFCs to 26 kW. However, for large increases or decreases in power demand, (\mathcal{S}) might allow infeasible increases or decreases in SOFC power output that exceed the 26 kW limitation.

The overestimation of SOFC fuel requirements by (\mathcal{S}) also contributes to differences in the thermal dispatch prescribed by the two formulations. Figure 4.9 depicts the optimal exhaust heat dispatch from the SOFCs to the water tank as determined by (\mathcal{P}) versus (\mathcal{S}) . (\mathcal{S}) overestimates the heat charged to the tank at low SOFC power

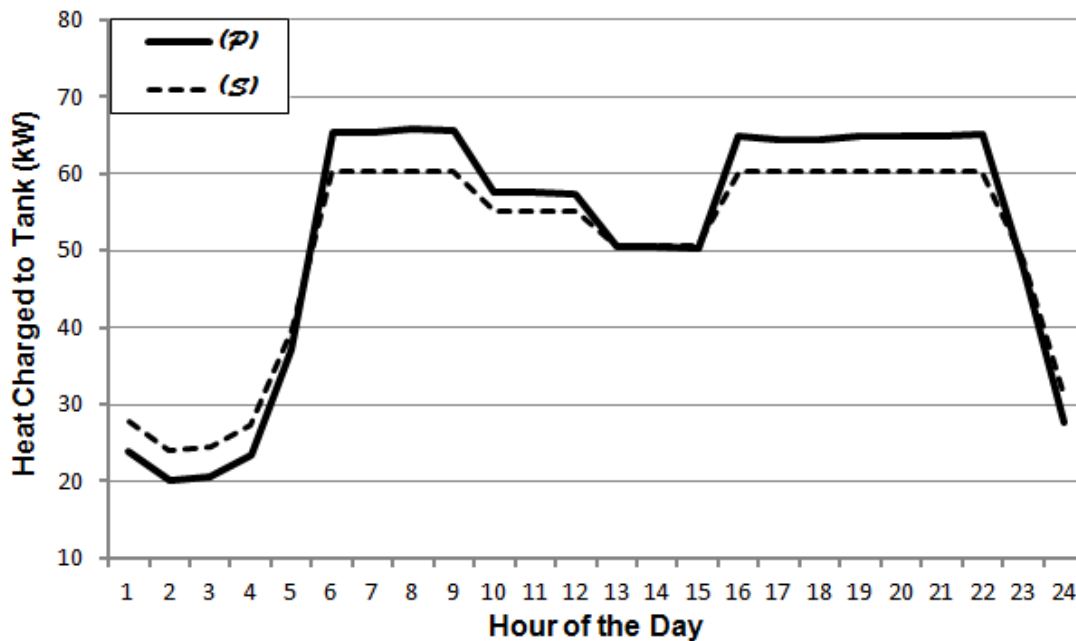


Figure 4.9: Optimal SOFC exhaust heat transferred to storage tank as determined by (\mathcal{P}) versus (\mathcal{S}) .

output and underestimates it at high SOFC power output (as previously shown in Figure 4.5). In the early hours of the day, when SOFC power output is low, (\mathcal{S}) over-

estimates the exhaust heat charged to the storage tank by as much as 20%. During the two peak power demand periods of the day, when SOFC power output is at or near maximum, (\mathcal{S}) underestimates the exhaust heat charged to the tank by as much as 8%. The more hours the SOFCs operate at or near rated capacity, the more (\mathcal{S}) underestimates the heat that can be generated by the SOFCs.

In the description of Figure 4.6, we stated that (\mathcal{S}) likely underestimates the heat discharged from the storage tank in periods of high heating demand and/or high tank water temperature, and likely overestimates the heat discharge in periods of low heating demand and/or low tank water temperature. Figure 4.10 depicts the flowrate and temperature of the tank water on the peak power day, as determined by (\mathcal{P}). The

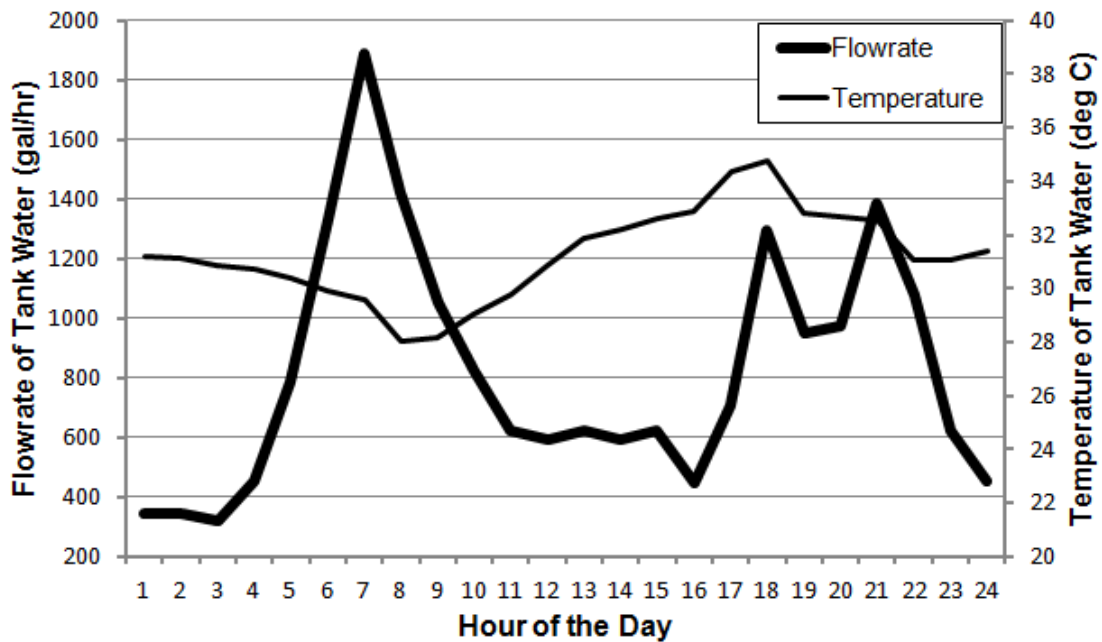


Figure 4.10: Optimal storage tank water flowrate and temperature as determined by (\mathcal{P}).

flowrate of the tank water closely follows the heating demand of the building, while the tank water temperature increases during periods of low demand and decreases during periods of high demand. Figure 4.11 demonstrates the impact of the water flowrate and temperature on the tank heat discharge, as determined by (\mathcal{P}), and

contrasts the prescribed heat discharge with that of (\mathcal{S}). During the two peak heating

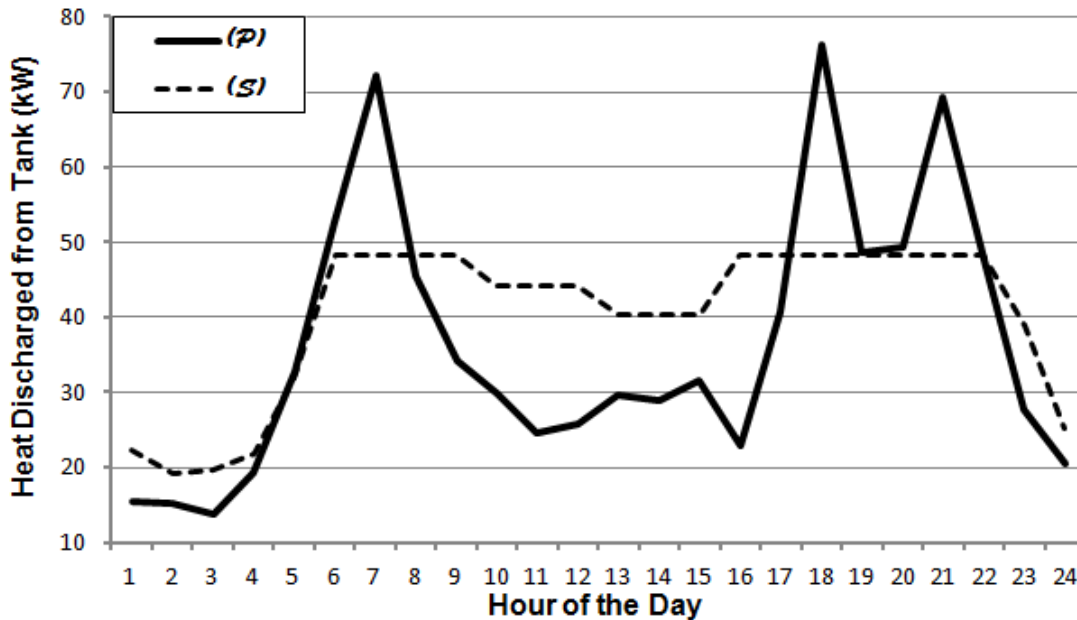


Figure 4.11: Optimal storage tank heat dispatch as determined by (\mathcal{P}) versus (\mathcal{S}).

demand periods of the day, (\mathcal{S}) underestimates the tank heat discharge by as much as 37%. However, in the middle of the day, when the heating demand is relatively low and the tank water is still well below delivery temperature, (\mathcal{S}) overestimates the tank heat discharge by as much as 111% when compared to (\mathcal{P}). Any hour in which (\mathcal{S}) overestimates the heat provided by the storage tank, it underestimates the additional heat that must be provided by the boiler, and thus underestimates the fuel requirements for the boiler.

The cumulative effects of the hourly dispatch differences between (\mathcal{P}) and (\mathcal{S}), over the entire year, are summarized in Table 4.3. (\mathcal{S}) overestimates the total natural gas energy required for the SOFCs by 5%, underestimates the total thermal energy provided by the SOFCs by 4%, overestimates the total thermal energy provided by the storage tank by 7%, and underestimates the total natural gas energy required for the boiler by 1%. These miscalculations of the system’s energy requirements cause

Table 4.3: Summary of solution differences between (\mathcal{P}) and (\mathcal{S}) for the annual instance of the case study when the system design in (\mathcal{S}) is fixed to the same system design as that selected by (\mathcal{P}) .

Statistic	(\mathcal{P})	(\mathcal{S})	Difference
Total SOFC Gas Input [MWh]	2,222	2,327	+5%
Total SOFC Heat Output [MWh]	461	442	-4%
Total Tank Heat Output [MWh]	332	354	+7%
Total Boiler Gas Input [MWh]	2,552	2,522	-1%
Total Annual Cost [\$]	276,683	278,975	+1%

(\mathcal{S}) to overestimate the total annual operational costs of the system by 1%. Although the difference in operational costs between (\mathcal{P}) and (\mathcal{S}) may appear relatively small, the overestimation of cost is enough to cause (\mathcal{S}) to favor the smaller (110 kW) system capacity when the larger (130 kW) system is not fixed. Thus, the failure to consider the off-design performance characteristics of the DG technologies causes (\mathcal{S}) to undersize the system capacity by 15% compared to (\mathcal{P}) .

Simpler, linear models of the design and dispatch problem, such as DER-CAM, offer the possibility of solving large problem instances with relative ease. Even one-year instances of the linear formulation can be solved directly with existing commercial solvers and require significantly shorter solve times than those of equivalent instances of (\mathcal{P}) . However, a linear formulation of the design and dispatch problem cannot capture many of the critical, off-design performance characteristics of generation and storage technologies. As we demonstrate in this chapter, for certain instances, the failure to consider these characteristics can result in the prescription of an infeasible system dispatch and a suboptimal system design. Therefore, although the added complexity of (\mathcal{P}) leads to longer solve times, compared to models like DER-CAM, it also leads to a more realistic system design and dispatch.

CHAPTER 5

ECONOMIC SCREENING CRITERIA

Chapter 4 demonstrates the advantages of realistically modeling the design and dispatch of a DG system with (\mathcal{P}) . Given its greater level of detail compared to existing models, (\mathcal{P}) provides a novel means of conducting sensitivity analyses to evaluate the economic viability of DG. These sensitivity analyses can be accomplished by varying the parameter values for demand, pricing, and performance to create an array of problem instances, and then solving those instances of (\mathcal{P}) to determine which combinations of parameter values result in DG acquisition. However, large instances of (\mathcal{P}) can be time consuming and computationally expensive to solve. In Section 3.4, we present a one-year time horizon, hourly fidelity instance of (\mathcal{P}) which has nearly 200,000 variables and 300,000 constraints, and which requires more than 10 hours to reach a solution that is within 12% of global optimality. Additionally, for many instances, the combination of energy market, building type, and DG technology under consideration results in an optimal design and dispatch solution that does *not* include the acquisition of DG. In Sections 3.4 and 4.4, we are forced to use dramatically reduced capital and installation costs in order to witness DG acquisition. Thus, a great deal of time and computing power can be expended solving various building-market-technology instances of (\mathcal{P}) in order to discover a combination for which DG is economically viable. For this reason, it would be beneficial to identify which combinations are likely to be economically viable prior to solving (\mathcal{P}) to determine the optimal design and dispatch.

In this chapter, we develop parametric conditions for the economic viability of a CHP DG system based on the objective function of (\mathcal{P}) . This comparative *static* analysis requires the substitution of parameters for the variables in the objective

function. Because the analysis requires fixed parameters, only a single design and dispatch strategy can be tested at one time. Thus, for a given analysis, we must choose a system configuration, capacity, and operational strategy for which we evaluate economic viability. We then derive necessary conditions on the model parameters for the selected design and dispatch to result in operational savings that exceed the capital and installation costs. These conditions provide insight regarding economically attractive building, market, and technology characteristics and afford screening criteria for the instances of (\mathcal{P}) we wish to solve. Armed with a *viable* system design and dispatch, we can solve (\mathcal{P}) to determine the *optimal* design and dispatch.

The specific CHP DG system considered in our comparative static analysis is depicted in Figure 5.1. For this system, if DG is not acquired, then the building

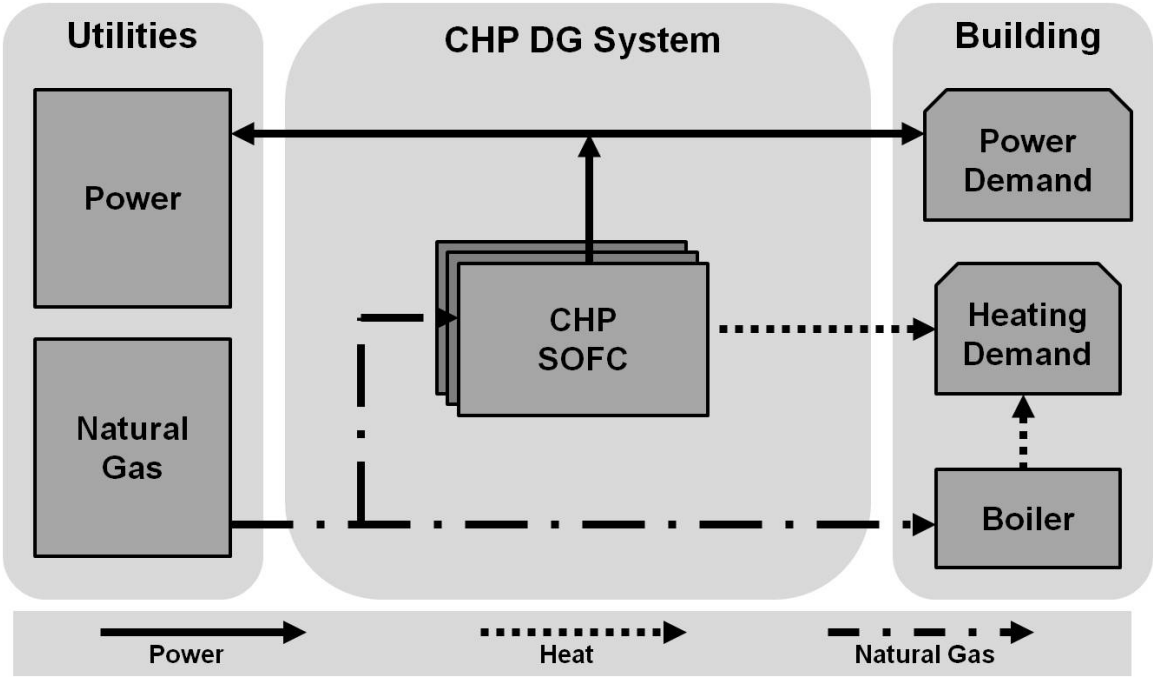


Figure 5.1: Combined heat and power (CHP), distributed generation (DG) system consisting of solid-oxide fuel cells (SOFCs).

has its power demand met by the utility and its heating demand met by an existing natural gas-fed boiler. We wish to consider retrofitting the building with a natural gas-

fed, SOFC system. The system’s primary product is power, which reduces the electric energy that must be imported from the utility, and which provides a source of revenue when electricity can be exported from the SOFCs to the utility. Additionally, when waste heat capture is included in the system, high temperature exhaust gas from the SOFCs is supplied to the building to reduce the thermal energy that must be provided by the boiler. In the next two sections, we derive general conditions for which the operational savings provided by the SOFCs exceed their capital and installation costs. We then demonstrate those conditions numerically with eight real-world scenarios.

5.1 Cost Analysis

In this section, we examine the total cost of supplying the power and heating demands of the building in Figure 5.1, based on the objective function of (\mathcal{P}). Depending on the system design (i.e., whether or not DG is acquired), the total cost may or may not include acquisition and operation costs for the SOFCs. By comparing the total costs of the system with and without the SOFCs, we are able to derive conditions for the economic viability of the technology.

Applying the notation for sets, parameters, and variables defined in the nomenclature, and the previous convention that the elements of the set \mathcal{J} are defined numerically as 4=CHP SOFC and 6=Boiler, the total cost to meet the power and heating demands of the building in Figure 5.1 is calculated according to equation (2.1). However, because we are only examining the viability of CHP SOFCs, the total cost does not include the acquisition and operation costs associated with batteries, PV cells, power-only SOFCs, or water tanks. Thus, the cost function defined in (5.1a) through (5.1d) is the same as that defined in (2.1), with the exception of removing all terms with \mathcal{J} -elements 1=Battery, 2=PV, 3=Power SOFC, and 5=Water Tank.

$$\text{Cost} = c_4 k_4^{\text{out}} A_4 + \sum_{t \in \mathcal{T}} \left[\delta m_4 P_{4t}^{\text{out}} + (g_t + z z^g) \left(\frac{\sigma_4 \mu_4 k_4}{2 \eta_4^{\text{min}}} \dot{N}_{4t} + \delta G_{4t} \right) \right] \quad (5.1a)$$

$$+ \sum_{t \in \mathcal{T}} \delta [(p_t + z z^p) U_t^{\text{out}} - \nu_t p_t U_t^{\text{in}}] \quad (5.1b)$$

$$+ \sum_{n \in \mathcal{N}} p_n^{\text{max}} U_n^{\text{max}} \quad (5.1c)$$

$$+ \sum_{t \in \mathcal{T}} \delta (\eta_6^Q m_6 + g_t + z z^g) G_{6t} \quad (5.1d)$$

Total cost component (5.1a) accounts for the capital and installation, O&M, fuel, and carbon emissions costs for the SOFCs. Component (5.1b) captures the energy and carbon emissions costs for electricity imported from the power utility, as well as the electricity export revenues from the SOFCs. Component (5.1c) calculates the monthly peak demand charges from the power utility. Component (5.1d) determines the O&M, fuel, and carbon emissions costs associated with the thermal energy produced by the boiler.

The power demands of the building in Figure 5.1 must be met by the SOFCs and/or the power utility. The power supply and demand are governed by the following relationships.

$$P_{4t}^{\text{out}} + U_t^{\text{out}} - U_t^{\text{in}} = d_t^P \quad \forall t \in \mathcal{T} \quad (5.2a)$$

$$P_{4t}^{\text{out}} = \eta_{4t}^P G_{4t} \quad \forall t \in \mathcal{T} \quad (5.2b)$$

$$U_t^{\text{out}} = \max\{0, d_t^P - P_{4t}^{\text{out}}\} \quad \forall t \in \mathcal{T} \quad (5.2c)$$

$$-U_t^{\text{in}} = \min\{0, d_t^P - P_{4t}^{\text{out}}\} \quad \forall t \in \mathcal{T} \quad (5.2d)$$

$$U_n^{\text{max}} = \max_{t \in \mathcal{T}_n} \{U_t^{\text{out}}\} \quad \forall n \in \mathcal{N} \quad (5.2e)$$

These same relationships are enforced by the combination of constraints (2.2a), (2.3a), (2.5a), and (2.6a) in (\mathcal{P}) when SOFCs are the only technology under consideration. Equation (5.2a) demonstrates that the power produced by the SOFCs and the net-power from the utility must sum to the building's demand. The power output by the SOFCs equates to the product of their fuel input and electric efficiency, according to

equation (5.2b). In this case, we use the notation η_{4t}^P for the electric efficiency, rather than E_{4t} , to represent the fixed value that results from calculating the efficiency according to constraint (2.5a). Power cannot be both imported from and exported to the utility in the same hour. Thus, if the demand exceeds the SOFC output in a given hour, power is imported from the utility according to equation (5.2c). If the SOFC output exceeds the demand, then power is exported to the utility according to equation (5.2d). Equation (5.2e) determines the peak power imported from the utility in each month.

The heating demands of the building in Figure 5.1 must be met by the SOFCs and/or the boiler. The heating supply and demand are governed by the following relationships.

$$Q_{4t}^{\text{out}} + Q_{6t}^{\text{out}} = d_t^Q \quad \forall t \in \mathcal{T} \quad (5.3a)$$

$$Q_{4t}^{\text{out}} = \eta_4^Q G_{4t} \quad \forall t \in \mathcal{T} \quad (5.3b)$$

$$Q_{6t}^{\text{out}} = \eta_6^Q G_{6t} \quad \forall t \in \mathcal{T} \quad (5.3c)$$

These relationships are similar to those enforced by the combination of constraints (2.2b), (2.6a), (2.6b), (2.9a), and (2.10a) in (\mathcal{P}) . However, because thermal storage is not included in the system depicted in Figure 5.1, the flow of heat is modeled in a different manner. In (\mathcal{P}) , the heat from the SOFCs or boiler is modeled as the product of specific heat capacity, flowrate, and temperature change, in order to account for the time-varying temperature of the thermal storage tank. Without thermal storage, the fluid temperatures throughout the system can be modeled as static. With static temperatures, the heat from the SOFCs or boiler can be modeled directly via the variable Q_{jt}^{out} . Equation (5.3a) shows that the heat produced by the SOFCs and the boiler must sum to the building's heating demand. The heat output by each generator in a given hour is equivalent to the product of its fuel input and rated thermal efficiency, according to equations (5.3b) and (5.3c). In this case, we

assume that the thermal efficiency of the SOFCs includes the efficiency of the heat exchanger.

The power supply and demand relationships established in equations (5.2a) through (5.2e), and the heating supply and demand relationships established in equations (5.3a) through (5.3c), permit the substitution of parameters for variables in total cost function components (5.1a) through (5.1d). For instance, if no SOFCs are acquired (i.e., $A_4 = G_{4t} = P_{4t}^{\text{out}} = \dot{N}_{4t} = U_t^{\text{in}} = 0 \forall t$), then all of the power demand is met by the power utility, according to (5.2a), and all of the heating demand is met by the boiler, according to (5.3a). In this case, total cost component (5.1a) is zero, component (5.1b) does not include U_t^{in} , and we substitute $U_t^{\text{out}} = d_t^P$, $U_n^{\text{max}} = \max_{t \in \mathcal{T}_n} \{d_t^P\}$, and $G_{6t} = d_t^Q / \eta_6^Q$ in components (5.1b) through (5.1d). The resulting total cost calculation does not include DG and is based solely on building and market parameter values.

$$\text{Cost}^{\text{noDG}} = \sum_{t \in \mathcal{T}} \delta(p_t + zz^p) d_t^P \quad (5.4a)$$

$$+ \sum_{n \in \mathcal{N}} p_n^{\text{max}} \max_{t \in \mathcal{T}_n} \{d_t^P\} \quad (5.4b)$$

$$+ \sum_{t \in \mathcal{T}} \delta \left(m_6 + \frac{g_t + zz^g}{\eta_6^Q} \right) d_t^Q \quad (5.4c)$$

Cost component (5.4a) calculates the energy and emissions costs associated with the utility supplying all of the power demand, while component (5.4b) determines the monthly demand charges for the peak power load. Cost component (5.4c) accounts for the O&M, fuel, and emissions costs associated with the boiler providing all of the heating demand. Thus, (5.4a) through (5.4c) calculate the total cost to meet the building's demands with the existing system, based solely on parametric, as opposed to variable, values.

An alternative substitution into (5.1a) through (5.1d) forces DG acquisition. If SOFCs *are* acquired (i.e., $A_4 > 0$) and operated in all hours (i.e., $P_{4t}^{\text{out}} > 0$ and

$\dot{N}_{4t} = 0 \forall t$), then the power and heat provided by the existing system are reduced. In this case, we substitute $G_{4t} = P_{4t}^{\text{out}}/\eta_{4t}^P$ in total cost component (5.1a), substitute $U_t^{\text{out}} = \max\{0, d_t^P - P_{4t}^{\text{out}}\}$ and $-U_t^{\text{in}} = \min\{0, d_t^P - P_{4t}^{\text{out}}\}$ in component (5.1b), substitute $U_n^{\text{max}} = \max_{t \in \mathcal{T}_n}\{\max\{0, d_t^P - P_{4t}^{\text{out}}\}\}$ in component (5.1c), and substitute $G_{6t} = [d_t^Q - \eta_4^Q(P_{4t}^{\text{out}}/\eta_{4t}^P)]/\eta_6^Q$ in component (5.1d). The resulting total cost calculation includes DG and is based not only on building and market parameters, but also on the selected SOFC design (A_4) and dispatch (P_{4t}^{out}).

$$\text{Cost}^{\text{DG}} = c_4 k_4^{\text{out}} A_4 + \sum_{t \in \mathcal{T}} \delta \left(m_4 + \frac{g_t + z z^g}{\eta_{4t}^P} \right) P_{4t}^{\text{out}} \quad (5.5a)$$

$$+ \sum_{t \in \mathcal{T}} \delta [(p_t + z z^p) \max\{0, d_t^P - P_{4t}^{\text{out}}\} + \nu_t p_t \min\{0, d_t^P - P_{4t}^{\text{out}}\}] \quad (5.5b)$$

$$+ \sum_{n \in \mathcal{N}} p_n^{\text{max}} \max_{t \in \mathcal{T}_n} \{\max\{0, d_t^P - P_{4t}^{\text{out}}\}\} \quad (5.5c)$$

$$+ \sum_{t \in \mathcal{T}} \delta \left(m_6 + \frac{g_t + z z^g}{\eta_6^Q} \right) \left(d_t^Q - \left(\frac{\eta_4^Q}{\eta_{4t}^P} \right) P_{4t}^{\text{out}} \right) \quad (5.5d)$$

Cost component (5.5a) determines the capital and operational costs associated with acquiring A_4 SOFCs and operating them at an aggregate power output of P_{4t}^{out} in each hour t . Component (5.5b) calculates the cost of power imported from the utility when the demand exceeds the SOFC power output, and the revenue from power exported to the utility when the demand is less than the SOFC power output. Component (5.5c) determines the cost associated with the peak power load imported from the utility each month, after considering the reduction in peak loads provided by the SOFCs. Component (5.5d) calculates the operational costs for the boiler, after considering the thermal energy provided by the SOFCs.

Once we select a specific SOFC system design and dispatch (i.e., fixed values for A_4 and P_{4t}^{out}), the total cost (Cost^{DG}) with DG is calculated based solely on parametric values. Different instances of acquisition and operation strategy can be examined, and lead to different parameter substitutions for the design and dispatch variables

in (5.1a) through (5.1d). Regardless of instance, fixed values must be substituted for the design (A_4) and dispatch (P_{4t}^{out}) variables in order to conduct a comparative *static* analysis. This static analysis differs from the optimization approach described in Chapters 2 through 4 given that the system design and dispatch are selected a priori rather than optimally determined by (\mathcal{P}). However, the purpose of the static analysis is to determine the economic viability of DG for a particular problem instance *prior* to expending the time and computational effort associated with solving (\mathcal{P}) to determine the optimal design and dispatch. Based on the static representations of total cost with (Cost^{DG}) and without ($\text{Cost}^{\text{noDG}}$) DG, we derive economic and technological conditions for which the optimal solution to (\mathcal{P}) is likely to include SOFC acquisition and, consequently, for which a building owner is likely to invest in a SOFC system.

As a minimum criterion, a building owner should not invest in a SOFC system unless the total cost (including amortized capital and installation costs) to meet the demands of the building is less with the SOFCs than without them. Thus, the economic viability of the SOFCs can be examined by comparing the total cost ($\text{Cost}^{\text{noDG}}$) to meet the building demands with the power utility and boiler alone to the total cost (Cost^{DG}) to meet the building demands with the existing system *and* the SOFCs. If the inequality $\text{Cost}^{\text{DG}} < \text{Cost}^{\text{noDG}}$ is satisfied, then the total cost to meet the building's demands is lower with the SOFC system than without it. Based on the definition of $\text{Cost}^{\text{noDG}}$ in (5.4a) through (5.4c) and the definition of Cost^{DG} in (5.5a) through (5.5d), an algebraically equivalent inequality to $\text{Cost}^{\text{DG}} < \text{Cost}^{\text{noDG}}$ is:

$$c_4 k_4^{\text{out}} A_4 < \text{Savings}^{\text{Energy}} + \text{Savings}^{\text{Emissions}} + \text{Savings}^{\text{O\&M}} + \text{Savings}^{\text{Peak}} \quad (5.6)$$

where the right-hand side of (5.6) represents the energy, carbon emissions, O&M, and peak demand savings, respectively, associated with operating the SOFCs. Thus, the SOFC system is economically viable if the total operational savings (right-hand side

of the inequality in (5.6)) it provides exceed its capital and installation costs (left-hand side of the inequality in (5.6)). The representation of $\text{Cost}^{\text{DG}} < \text{Cost}^{\text{noDG}}$ in (5.6) is obtained by subtracting all of the terms in Cost^{DG} other than $c_4 k_4^{\text{out}} A_4$ from both sides of the inequality, and then appropriately grouping the resulting terms on the right-hand side of the inequality. In the next section, we examine in more detail the four types of operational savings that are revealed by our analysis of total cost function components (5.1a) through (5.1d).

5.2 Savings Analysis

In this section, we discuss the different types of savings that are obtained from acquiring and operating the SOFC system in Figure 5.1. The total savings afforded by the SOFCs is then compared to their capital and installation costs to determine the economic viability of the system.

Energy Savings

The first type of savings from acquiring and operating the SOFC system results from the reduction of electric and thermal energy that must be provided by the existing system. The power generated by the SOFCs reduces the electric energy that must be purchased from the power utility, while the exhaust heat produced by the SOFCs reduces the thermal energy (in the form of natural gas) that must be purchased from the gas utility to fuel the boiler.

The energy savings provided by operating the SOFCs at the selected power output P_{4t}^{out} , over the time horizon of length $|\mathcal{T}|$, are calculated according to equation (5.7).

$$\begin{aligned} \text{Savings}^{\text{Energy}} = & \\ & \delta \sum_{t \in \mathcal{T}} \left[p_t \min\{d_t^P, P_{4t}^{\text{out}}\} + \nu_t p_t \max\{0, P_{4t}^{\text{out}} - d_t^P\} - \left(\frac{g_t}{\eta_{4t}^P}\right) \left(1 - \frac{\eta_4^Q}{\eta_6^Q}\right) P_{4t}^{\text{out}} \right] \end{aligned} \quad (5.7)$$

When deriving the terms on the right-hand side of the inequality in (5.6), we obtain $\text{Savings}^{\text{Energy}}$ by grouping the terms that include the energy market pricing parameters

p_t, ν_t , and g_t . This grouping provides the SOFC savings associated with the reduction of electricity and natural gas purchased from the utilities. Depending on the market pricing in a given hour t , the energy savings available from the SOFCs can be positive or negative. *Positive* hourly energy savings are achieved if:

$$p_t \min\left\{\left(\frac{d_t^P}{P_{4t}^{\text{out}}}\right), 1\right\} + \nu_t p_t \max\left\{0, 1 - \left(\frac{d_t^P}{P_{4t}^{\text{out}}}\right)\right\} > \left(\frac{g_t}{\eta_{4t}^P}\right) \left(1 - \frac{\eta_4^Q}{\eta_6^Q}\right) \quad (5.8)$$

in a given hour t . Condition (5.8) must be satisfied in order for an individual term t of the summation in (5.7) to be positive. The left-hand side of the inequality in (5.8) depends on the magnitude of the building's hourly power demand relative to the strictly positive power output of the SOFCs.

If the building demand is greater than or equal to the selected SOFC power output ($d_t^P / P_{4t}^{\text{out}} \geq 1$) in a given hour, then (5.8) reduces to the condition:

$$p_t > \left(\frac{g_t}{\eta_{4t}^P}\right) \left(1 - \frac{\eta_4^Q}{\eta_6^Q}\right). \quad (5.9)$$

The left-hand side of the inequality in (5.9) is the hourly price of electricity from the utility, while the right-hand side is the effective hourly price of electricity from the SOFCs. The price of electricity from the SOFCs depends on the price of natural gas, on their electric and thermal efficiencies, and includes a “credit” for the exhaust heat which reduces the energy (i.e., natural gas) costs of the boiler. Thus, positive energy savings are obtained in a given hour if the price of electricity from the utility exceeds the effective price of electricity from the SOFCs. As an alternative explanation, positive energy savings are achieved if the power utility costs are decreasing (left-hand side of (5.9)) at a greater rate than the gas utility costs are increasing (right-hand side of (5.9)).

The condition for positive hourly energy savings changes when excess power is available from the SOFCs. If the building demand is less than the selected power

output of the SOFCs ($0 \leq d_t^P/P_{4t}^{\text{out}} < 1$) in a given hour, then (5.8) reduces to:

$$\left[\nu_t + (1 - \nu_t) \left(\frac{d_t^P}{P_{4t}^{\text{out}}} \right) \right] p_t > \left(\frac{g_t}{\eta_{4t}^P} \right) \left(1 - \frac{\eta_4^Q}{\eta_6^Q} \right). \quad (5.10)$$

In this case, the gas utility costs are increasing at the same rate (right-hand side (5.10)) as in (5.9). However, the power utility costs now decrease at a rate (left-hand side (5.10)) that depends on the amount of exported power and the net-metering rate paid by the utility. As the power export increases (i.e., $d_t^P/P_{4t}^{\text{out}} \rightarrow 0$), the rate of decrease in power utility costs approaches the export price $\nu_t p_t$. However, as the net-metering rate increases (i.e., $\nu_t \rightarrow 1$), the rate of decrease in power utility costs approaches the import price p_t . Hence, when power is exported and the export price is less than the import price (i.e., $\nu_t < 1$), positive hourly energy savings are more difficult to obtain since the left-hand side of (5.10) is less than the left-hand side of (5.9).

Emissions Savings

The second type of savings from acquiring and operating the SOFC system results from the reduction of taxed carbon dioxide emitted by the existing system. The SOFCs decrease the electricity that must be purchased from the utility and, consequently, reduce the emissions for which the building owner is taxed. Similarly, the SOFCs reduce the boiler's carbon emissions by decreasing the natural gas combusted by the boiler.

The carbon emissions savings provided by operating the SOFCs at the selected power output P_{4t}^{out} , over the time horizon of length $|\mathcal{T}|$, are calculated according to equation (5.11).

$$\text{Savings}^{\text{Emissions}} = z\delta \sum_{t \in \mathcal{T}} \left[z^P \min\{d_t^P, P_{4t}^{\text{out}}\} - \left(\frac{z^g}{\eta_{4t}^P} \right) \left(1 - \frac{\eta_4^Q}{\eta_6^Q} \right) P_{4t}^{\text{out}} \right] \quad (5.11)$$

When deriving the terms on the right-hand side of the inequality in (5.6), we obtain Savings^{Emissions} by grouping the terms that include the carbon emissions parameters z , z^p , and z^g . This grouping provides the SOFC savings associated with the reduction of taxed carbon emissions from the utility and the boiler. The emissions savings increase (in absolute value) as the carbon tax rate z increases. However, depending on the emissions rate of the utility relative to that of natural gas combustion, the emissions savings could be positive or negative. *Positive* hourly emissions savings are achieved if:

$$z^p \min\left\{\left(\frac{d_t^P}{P_{4t}^{\text{out}}}\right), 1\right\} > \left(\frac{z^g}{\eta_{4t}^P}\right) \left(1 - \frac{\eta_4^Q}{\eta_6^Q}\right) \quad (5.12)$$

in a given hour t . Condition (5.12) must be satisfied in order for an individual term t of the summation in (5.11) to be positive. Similar to energy savings, the left-hand side of the inequality in (5.12) depends on the magnitude of the building's hourly power demand relative to the strictly positive power output of the SOFCs.

If the building demand is greater than or equal to the selected power output of the SOFCs ($d_t^P/P_{4t}^{\text{out}} \geq 1$) in a given hour, then (5.12) reduces to the condition:

$$z^p > \left(\frac{z^g}{\eta_{4t}^P}\right) \left(1 - \frac{\eta_4^Q}{\eta_6^Q}\right). \quad (5.13)$$

The left-hand side of (5.13) is the carbon emissions rate associated with utility-generated power, while the right-hand side is the effective carbon emissions rate for SOFC-generated power. The carbon emissions rate for the SOFCs is based on the combustion of natural gas and includes a “credit” for the reduction in carbon emissions from the boiler. Thus, positive emissions savings are obtained in a given hour if the emissions rate of the utility exceeds the effective emissions rate of the SOFCs. As an alternative explanation, positive emissions savings are achieved if the off-site emissions costs are decreasing (left-hand side of (5.13)) at a greater rate than the

on-site emissions costs are increasing (right-hand side of (5.13)).

If excess power is available from the SOFCs, then the condition for positive hourly emissions savings changes. When the building demand is less than the selected power output of the SOFCs ($0 \leq d_t^P/P_{4t}^{\text{out}} < 1$) in a given hour, (5.12) reduces to:

$$z^p \left(\frac{d_t^P}{P_{4t}^{\text{out}}} \right) > \left(\frac{z^g}{\eta_{4t}^P} \right) \left(1 - \frac{\eta_4^Q}{\eta_6} \right). \quad (5.14)$$

In this case, the on-site emissions costs are increasing at the same rate (right-hand side (5.14)) as in (5.13). However, the off-site emissions costs now decrease at a rate (left-hand side (5.14)) that depends on the amount of exported power. As power export increases (i.e., $d_t^P/P_{4t}^{\text{out}} \rightarrow 0$), the rate of decrease in off-site emissions costs approaches zero. Hence, when power is exported, positive hourly emissions savings are more difficult to obtain since the left-hand side of (5.14) is less than the left-hand side of (5.13).

Operations and Maintenance Savings

The third type of savings from acquiring and operating the SOFC system results from reducing the degradation of the existing system. When captured, waste heat from the SOFCs decreases the thermal energy that must be provided by the boiler and, consequently, reduces the operation and maintenance of the boiler.

The O&M savings provided by operating the SOFCs at the selected power output P_{4t}^{out} , over the time horizon of length $|\mathcal{T}|$, are calculated according to equation (5.15).

$$\text{Savings}^{\text{O\&M}} = \delta \sum_{t \in \mathcal{T}} \left[\left(\frac{\eta_4^Q}{\eta_{4t}^P} \right) m_6 - m_4 \right] P_{4t}^{\text{out}} \quad (5.15)$$

When deriving the terms on the right-hand side of the inequality in (5.6), we obtain $\text{Savings}^{\text{O\&M}}$ by grouping the terms that include the operations and maintenance parameters m_4 and m_6 . This grouping provides the SOFC savings associated with reducing the workload on the boiler. Depending on the O&M costs of the boiler rel-

ative to that of the SOFCs, the O&M savings could be positive or negative. *Positive* hourly O&M savings are achieved if:

$$m_6 > \left(\frac{\eta_{4t}^P}{\eta_4^Q} \right) m_4. \quad (5.16)$$

Condition (5.16) must be satisfied in order for an individual term t of the summation in (5.15) to be positive. The left-hand side of (5.16) is the O&M cost per unit of thermal energy output from the boiler. However, the O&M costs for the SOFCs are charged per unit of electric energy produced. Thus, in order to compare the O&M costs of the boiler and SOFCs, the right-hand side of (5.16) converts the O&M costs of the SOFCs to units of thermal energy output. Positive O&M savings are obtained if the O&M cost per unit of thermal energy output is greater for the boiler than for the SOFCs.

Peak Demand Savings

The final type of savings from acquiring and operating the SOFC system results from reducing the burden on the power utility during the building's peak demand periods. The power generated by the SOFCs decreases the maximum power load that must be imported from the utility each month and, therefore, decreases the monthly peak demand costs.

The peak demand savings provided by operating the SOFC at the selected power output P_{4t}^{out} , over the course of $|\mathcal{N}|$ months, are calculated according to equation (5.17).

$$\text{Savings}^{\text{Peak}} = p_n^{\text{max}} \sum_{n \in \mathcal{N}} \left[\max_{t \in \mathcal{T}_n} \{d_t^P\} - \max_{t \in \mathcal{T}_n} \{\max\{0, d_t^P - P_{4t}^{\text{out}}\}\} \right] \quad (5.17)$$

When deriving the terms on the right-hand side of the inequality in (5.6), we obtain $\text{Savings}^{\text{Peak}}$ by grouping the terms that include the peak demand charge parameter p_n^{max} . This grouping provides the SOFC savings associated with reducing the peak

power load imported from the utility. The peak demand savings increase as the monthly peak demand charge p_n^{\max} increases. Unlike energy, emissions, and O&M savings, the peak demand savings provided by operating the SOFCs are strictly *non-negative*. However, *positive* monthly peak demand savings are only achieved if:

$$\max_{t \in \mathcal{T}_n} \{d_t^P\} > \max_{t \in \mathcal{T}_n} \{\max\{0, d_t^P - P_{4t}^{\text{out}}\}\} \quad (5.18)$$

in a given month n . Condition (5.18) must be satisfied in order for an individual term n of the summation in (5.17) to be positive. If the SOFCs produce no power in the peak demand hour t for month n , then the left-hand and right-hand sides of the inequality in (5.18) are equal and the peak demand savings are zero for that month. However, because the hourly power output of the SOFCs is strictly positive ($P_{4t}^{\text{out}} > 0 \forall t$), the right-hand side of (5.18) is strictly less than the left-hand side and positive monthly peak demand savings are achieved.

Total Savings

By summing the four types of savings delineated in equations (5.7), (5.11), (5.15), and (5.17), we obtain the right-hand side of the inequality in (5.6) and, hence, the total operational savings provided by the SOFC system. Given that some of the savings-types can be negative, the total operational savings could be negative for certain instances. For these instances, the SOFCs are not economically viable, since condition (5.6) would require the capital and installation costs ($c_4 k_4^{\text{out}} A_4$) to be negative. However, if the total savings provided by operating the acquired SOFCs are positive and exceed their capital and installation costs over the time horizon of interest, then the SOFCs are economically viable. Stricter conditions involving the pay-off period of the capital or other economic considerations could be imposed by the building owner (i.e., the investor). However, the bound on $c_4 k_4^{\text{out}} A_4$ determined by (5.6) represents the maximum capital and installation costs for which the building owner would obtain *any* economic benefit from operating the SOFC system.

5.3 Building, Market, and Technology Scenarios

In order to numerically demonstrate the general conditions for economic viability, we develop eight distinct scenarios based on varying the building type, energy market, and technological design and dispatch for the system depicted in Figure 5.1. Using these scenarios, we examine the total operational savings provided by the SOFC system and determine which scenarios are likely to result in savings that exceed the capital and installation cost.

We consider two different building types located in two different energy markets. The buildings are a large-sized hotel and a medium-sized office building. The energy markets are southern California and southern Wisconsin. The hourly demand data for the four building-market combinations is generated in EnergyPlus (see [42]). Building size and energy demand statistics for each building-market combination are provided in Table 5.1. The hourly power demands on the peak power day of the year for each

Table 5.1: Size and demand statistics for a large hotel and medium office located in southern California (CA) and southern Wisconsin (WI).

Statistic	LA Hotel	WI Hotel	LA Office	WI Office
Height [floors]	6	6	3	3
Area [thousand ft ²]	122	122	54	54
Average power demand [kW]	201	142	54	44
Maximum power [kW]	346	264	151	107
Minimum power [kW]	88	52	15	15
Average heating demand [kW]	191	256	4	7
Maximum heat [kW]	578	1,086	105	110
Minimum heat [kW]	60	50	0	0
Average thermal-to-electric ratio	0.94	1.84	0.11	0.17
Maximum thermal-to-electric	2.04	7.21	4.04	4.74
Minimum thermal-to-electric	0.36	0.49	0.00	0.00

building-market combination are depicted in Figure 5.2, while the hourly heating demands on the peak heating day of the year are depicted in Figure 5.3. In general, the power demands for a given building type are higher when the building is located

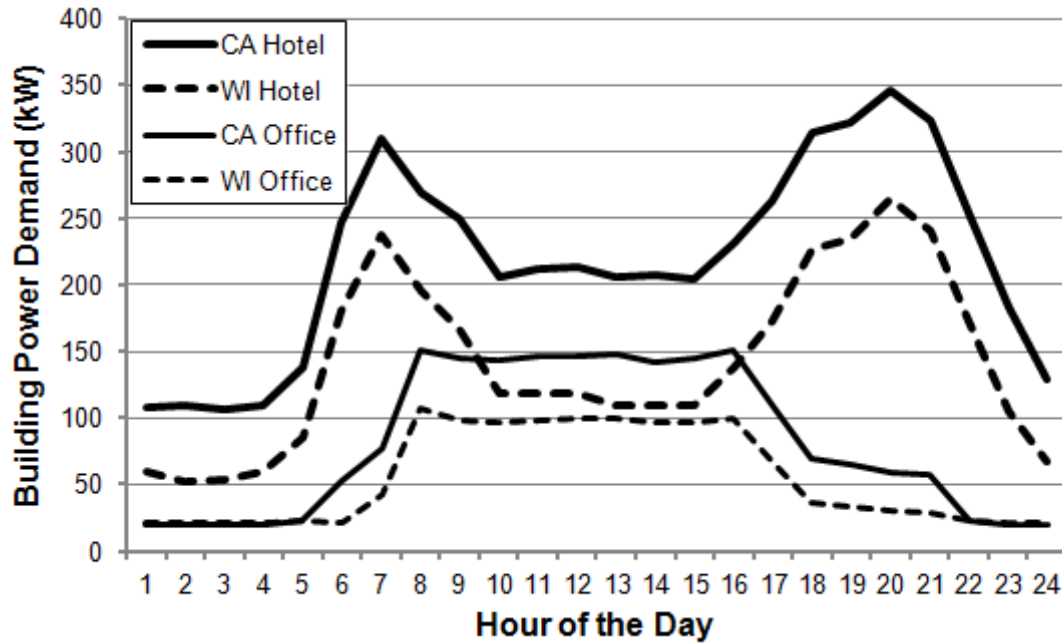


Figure 5.2: Building power demands on the peak power day of the year for a large hotel and medium office located in southern California (CA) and southern Wisconsin (WI).

in southern California versus southern Wisconsin (see Figure 5.2). This is due to the fact that the power demand includes cooling, via vapor-compression air conditioning units, and that the cooling demands are higher in the hotter southern California climate. Conversely, the heating demands for a given building type are higher when the building is located in southern Wisconsin (see Figure 5.3), due to the colder climate.

The electricity and natural gas prices for southern California and southern Wisconsin are based on 2010 commercial rate schedules from Southern California Edison (see [43]), Southern California Gas Company (see [44]), Wisconsin Electric Power Company (see [57]), and Wisconsin Electric-Gas Operations (see [53]), respectively. Figure 5.4 provides the weekday energy prices for each market. In addition to the hourly energy prices for electricity, the utilities charge for the peak power demand each month. Southern California Edison charges \$6.39 per kW per month and Wis-

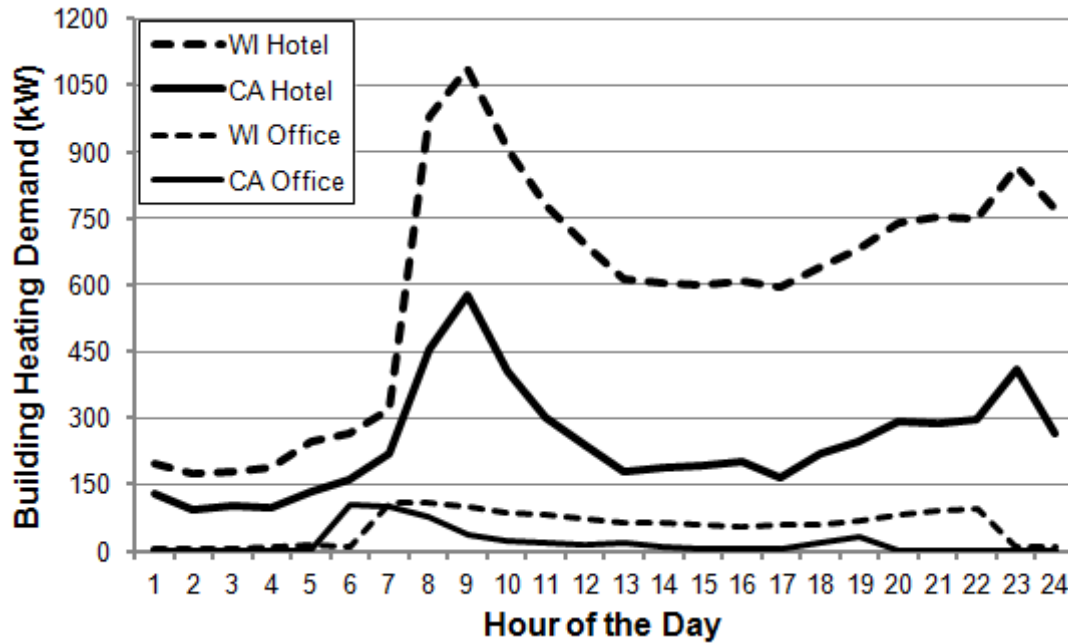


Figure 5.3: Building heating demands on the peak heating day of the year for a large hotel and medium office located in southern California (CA) and southern Wisconsin (WI).

consin Electric Power Company charges \$11.35 per kW per month. The availability of electricity export from the SOFC system to the grid depends on the net-metering policies and interconnection procedures for the market in which the building is located. Based on the 2010 report by the Network for New Energy Choices (see [58]), California is a favorable market for DG net-metering and interconnect, while Wisconsin is not. Thus, for the scenarios demonstrated in this chapter, net-metering is available in southern California, but is not available in southern Wisconsin.

The 2010 reports (see [59] and [60]) by the Energy Information Administration provide the basis for the calculation of the average carbon emissions rate for centralized power generation in California and Wisconsin. The primary fuel source for centralized power generation in California is natural gas. This fuel source, coupled with the prevalence of renewable power generation, results in a relatively low emissions rate of 0.27 kg of carbon per kWh of electricity. By contrast, centralized power gener-

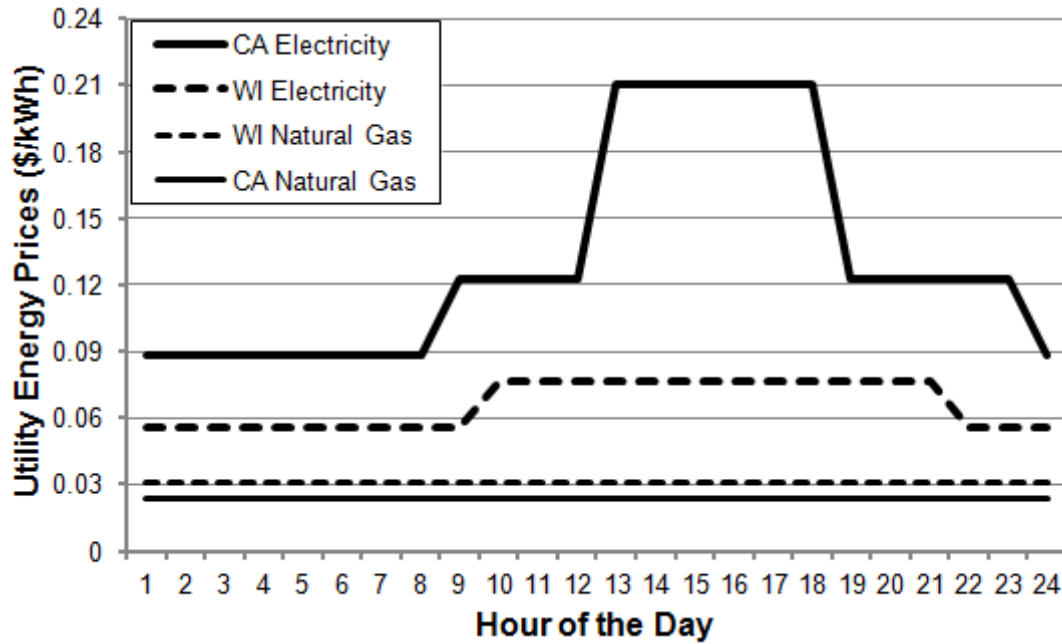


Figure 5.4: Weekday electricity and natural gas prices for commercial service in southern California (CA) and southern Wisconsin (WI).

ation in Wisconsin produces a relatively high carbon emissions rate of 0.74 kg/kWh, given that the primary fuel source is coal.

The aforementioned building type and energy market scenarios provide values for the demand, pricing, and emissions parameters. However, in order to perform a static analysis, we must also choose a design and dispatch strategy (i.e., fixed values for A_4 and P_{4t}^{out}) for the SOFCs. The operational cost and performance data for the SOFC system are derived from Stambouli and Traversa [34], Hawkes et al. [36], and Braun [5]. For the design scenarios tested here, we assume that SOFCs can only be acquired in increments of 50 kW (i.e., $k_4^{\text{out}} = 50$) of power capacity and that the SOFC system is sized as closely as possible to the average power demand of the building. For example, because the hotel in southern Wisconsin has an average power demand of 142 kW, we consider a 150 kW SOFC system (i.e., $A_4 = 3$) for acquisition. Additionally, we include scenarios with and without waste heat capture for the SOFC system in

order to quantify the value of CHP. If heat capture is not included, then the thermal efficiency of the SOFC system is zero (i.e., $\eta_4^Q = 0$). If heat capture is included, via heat exchangers, then we assume a thermal efficiency of 21% for the SOFCs and 80% for the heat exchangers. Thus, the net-thermal efficiency of the SOFC system is 17% (i.e., $\eta_4^Q = 0.17$). The thermal efficiency of the existing boiler is assumed to be 75% (i.e., $\eta_6^Q = 0.75$).

For the dispatch scenarios tested here, we assume that all of the acquired SOFCs are operated at a positive power output in all hours throughout the time horizon (i.e., $\dot{N}_{jt} = 0$ and $P_{4t}^{\text{out}} > 0 \forall t$) and are never forced into standby mode. The feasibility of this simplification is easily confirmed by ensuring the power output of the SOFCs is never forced below the maximum turn-down (see constraint (2.4d)) in a given scenario. For the southern California scenarios, we assume the SOFCs baseload at rated power capacity in all hours (i.e., $P_{4t}^{\text{out}} = k_4^{\text{out}} A_4 \forall t$). Given the availability of net-metering and the relatively high electricity-to-gas price ratio in the California market, the assumption of baseloading is reasonable. For the southern Wisconsin scenarios, we assume the SOFCs load-follow in all hours (i.e., $P_{4t}^{\text{out}} = \min\{d_t^P, k_4^{\text{out}} A_4\} \forall t$). The lack of net-metering and the relatively low electricity-to-gas price ratio make load-following a reasonable assumption in this market.

The carbon emissions rate of the SOFCs is calculated based on their efficiency and the emissions associated with the combustion of natural gas. According to NaturalGas.org [47], the carbon emissions rate from the combustion of natural gas is 0.18 kg per kWh of gas consumed. When the SOFCs baseload at rated capacity, their electric efficiency is fixed at the minimum of 41% (i.e., $\eta_{4t}^P = 0.41 \forall t$). When the SOFCs load-follow, their electric efficiency varies between 41% and 57%, depending on the aggregate power output (see constraint (2.5a)).

Based on varying the building type, energy market, and SOFC system design and dispatch, we develop the eight scenarios listed in Table 5.2. A variety of alternate

Table 5.2: Building, market, and design and dispatch scenarios for which we examine the economic viability of a DG system.

Scenario	Building	Market	System Design (Heat capture?)	System Dispatch (Net-metering?)
1	Hotel	CA	200 kW (No)	Baseload (Yes)
2	Hotel	CA	200 kW (Yes)	Baseload (Yes)
3	Office	CA	50 kW (No)	Baseload (Yes)
4	Office	CA	50 kW (Yes)	Baseload (Yes)
5	Hotel	WI	150 kW (No)	Load-follow (No)
6	Hotel	WI	150 kW (Yes)	Load-follow (No)
7	Office	WI	50 kW (No)	Load-follow (No)
8	Office	WI	50 kW (Yes)	Load-follow (No)

scenarios can be developed to test the economic viability of a SOFC system for certain applications. However, these eight scenarios provide a wide enough range of applications to generally demonstrate the impact on operational savings of varying the building, market, and DG system parameters.

5.4 Scenario Analysis

In this section, we provide two types of sensitivity analyses of the operational savings provided by the SOFC systems in our scenarios. The first type of analysis examines the sensitivity of the operational savings *across* scenarios. In other words, we are interested in how the operational savings in Scenario 1 differ from those of Scenario 2, Scenario 3, and so on. This sensitivity analysis provides insight regarding the general types of buildings, markets, and systems for which DG is economically viable. The second type of analysis examines the sensitivity of the operational savings

within scenarios. In other words, we are interested in how the operational savings for a particular scenario change as the values of certain system and market parameters change. Specifically, we examine the sensitivity of the operational savings to changes in the rated electric efficiency of the SOFCs and the carbon tax enforced in the market of interest. This sensitivity analysis provides insight regarding the specific characteristics of DG systems and energy markets that lead to greater economic viability. The next two sections present a more detailed discussion of the two types of sensitivity analyses.

5.4.1 Savings Sensitivity Across Scenarios

In this section, we calculate and compare the annual energy, emissions, O&M, and peak demand savings provided by the SOFC system in each scenario. Because the system sizes differ across scenarios, we present the savings per unit of system capacity (i.e., \$ per kW) in order to fairly compare scenarios. The total annual savings in each scenario are then compared to the annualized capital and installation cost of the SOFC system to determine its economic viability.

Energy Savings

For Scenarios 1 through 4, because the SOFCs baseload and excess power can be exported to the grid at the market rate ($\nu_t = 1$) in all hours t , conditions (5.9) and (5.10) are equivalent. Thus, for any hour in which the price of electricity from the utility exceeds the effective price of electricity from the SOFCs, the energy savings are positive. Because the SOFCs baseload in Scenarios 1 through 4, the electric efficiency is always the minimum of 41%. The thermal efficiency of the SOFC system is 0% in Scenarios 1 and 3, since heat capture is not included, and 17% in Scenarios 2 and 4. Based on the natural gas price of \$0.024 per kWh, the electric and thermal efficiencies of the SOFC system, and the thermal efficiency of the boiler, the maximum effective price of electricity from the SOFC system is \$0.059 per kWh without heat capture and \$0.045 per kWh with heat capture. Since the minimum price of electricity from

the utility in Scenarios 1 through 4 is \$0.081 per kWh, conditions (5.9) and (5.10) are satisfied and positive energy savings are achieved in *all* hours.

The energy savings may not be positive in *all* hours in Scenarios 5 through 8. For these scenarios, the SOFCs load-follow and power is never exported to the grid (i.e., $d_t^P / P_{4t}^{\text{out}} \geq 1$), so only condition (5.9) applies. Because the SOFCs load-follow, the electric efficiency varies between 41% and 57% depending on the aggregate power output. Given the natural gas price of \$0.031 per kWh, the maximum effective price of electricity from the SOFC system varies between \$0.054-0.074 per kWh without heat capture and between \$0.041-0.058 per kWh with heat capture, depending on the electric efficiency. The minimum price of electricity from the utility in Scenarios 5 through 8 is \$0.056 per kWh. Hence, there could be hours for which condition (5.9) is not satisfied and the energy savings are negative.

Given the hourly power demands of the buildings over the entire year, the *annual* energy savings per kW of SOFC system capacity are presented in Table 5.3 for the eight scenarios. The savings per unit of power capacity are calculated as the quotient of the annual energy savings (see (5.7)) and the acquired system capacity ($k_4^{\text{out}} A_4$) for each scenario. Large, positive annual energy savings are achieved in all of the southern

Table 5.3: Annual energy savings per kW of SOFC system capacity provided in each scenario.

Scenario	Annual Energy Savings (\$/kW)
1	341.02
2	454.44
3	341.02
4	454.44
5	-39.82
6	69.27
7	-3.28
8	79.24

California scenarios given the high electricity-to-gas price ratio. On the other hand, positive annual energy savings are only obtained in the southern Wisconsin scenarios that include heat capture. Even with heat capture, the energy savings are relatively small given the low electricity-to-gas price ratio.

Emissions Savings

For Scenarios 1 through 4, because the SOFCs baseload and the power output could be less than or greater than the building demand, conditions (5.13) or (5.14), respectively, could apply. Regardless of which condition applies, the hourly emissions savings are positive when the taxable emissions from the (off-site) utility decrease at a greater rate than the taxable emissions from the (on-site) SOFCs and boiler increase. Based on the 0.18 kg per kWh carbon emissions rate associated with the combustion of natural gas, and the fixed efficiencies of the SOFCs and boiler, the on-site emissions increase at 0.44 kg per kWh for Scenarios 1 and 3 (without heat capture) and 0.34 kg per kWh for Scenarios 2 and 4 (with heat capture). Since the maximum rate of decrease in off-site emissions for Scenarios 1 through 4 is 0.27 kg per kWh, conditions (5.13) and (5.14) are *not* satisfied and the emissions savings are negative in *all* hours.

For Scenarios 5 through 8, only condition (5.13) applies, since the SOFCs load-follow and the power output never exceeds the building demand. As the SOFC power output changes and the electric efficiency varies between 57% and 41%, the on-site emissions increase at a rate between 0.32-0.44 kg per kWh for Scenarios 5 and 7 (without heat capture) and a rate between 0.24-0.34 kg per kWh for Scenarios 6 and 8 (with heat capture). Since the off-site (i.e., utility) emissions decrease at a rate of 0.74 kg per kWh for Scenarios 5 through 8, condition (5.13) is satisfied and positive emissions savings are achieved in *all* hours.

Given the hourly power demands of the buildings over the entire year, and a \$0.02 per kg carbon tax, the *annual* emissions savings per kW of SOFC system capacity are presented in Table 5.4 for the eight scenarios. The savings per unit of power capacity

are calculated as the quotient of the annual emissions savings (see (5.11)) and the acquired system capacity ($k_4^{\text{out}} A_4$) for each scenario. The annual emissions savings

Table 5.4: Annual emissions savings per kW of SOFC system capacity provided in each scenario.

Scenario	Annual Emissions Savings (\$/kW)
1	-36.36
2	-18.93
3	-44.86
4	-27.42
5	44.97
6	57.82
7	37.38
8	47.10

are negative in all of the southern California scenarios given the relatively low carbon emissions rate of the utility in that market. Conversely, positive annual emissions savings are obtained in all of the southern Wisconsin scenarios given the relatively high emissions rate in that market.

O&M Savings

Condition (5.16) cannot be satisfied unless heat capture is included to offset a portion of the thermal energy provided by the boiler. Thus, the hourly O&M savings are negative for Scenarios 1, 3, 5, and 7, since those scenarios do not include heat capture. With heat capture, the hourly O&M savings are positive when the O&M costs per unit of thermal energy produced are higher for the boiler than for the SOFCs. For all scenarios, we assume that the SOFC O&M costs are \$0.02 per kWh of electric energy produced and that the boiler O&M costs are \$0.02 per kWh of thermal energy produced. Hence, the SOFC O&M costs must be converted to units of thermal energy produced, based on the electric and thermal efficiencies of the SOFCs.

For Scenarios 2 and 4, in which the SOFCs baseload, the electric and thermal efficiencies are fixed. Thus, the SOFC O&M costs are fixed at \$0.05 per kWh of thermal energy produced. For Scenarios 6 and 8, in which the SOFCs load-follow, the electric efficiency varies based on the power output. Accordingly, the SOFC O&M costs vary between \$0.05-0.07 per kWh of thermal energy produced. Since the boiler O&M costs are \$0.02 per kWh for all scenarios, condition (5.16) is *not* satisfied and the O&M savings are negative in *all* hours.

Given the hourly power demands of the buildings over the entire year, the *annual* O&M savings per kW of SOFC system capacity are presented in Table 5.5 for the eight scenarios. The savings per unit of power capacity are calculated as the quotient of the annual O&M savings (see (5.15)) and the acquired system capacity ($k_4^{\text{out}}A_4$) for each scenario. The annual O&M savings are negative for all scenarios. The savings

Table 5.5: Annual O&M savings per kW of SOFC system capacity provided in each scenario.

Scenario	Annual O&M Savings (\$/kW)
1	-175.20
2	-102.56
3	-175.20
4	-102.56
5	-137.39
6	-83.84
7	-108.46
8	-67.96

are greater (i.e., less negative) for the scenarios that include heat capture; however, the thermal efficiency of the SOFCs must increase significantly in order to achieve positive O&M savings.

Peak Demand Savings

Because the SOFCs produce power in all hours, whether baseloading or load-following,

condition (5.18) is satisfied and positive peak demand savings are achieved in all scenarios. Additionally, because the SOFC system is sized based on the buildings' average power load, which is less than the peak power load, the SOFCs operate at rated capacity during peak demand hours in all scenarios. As a result, the monthly peak demand savings are calculated as the product of the peak demand charge and the acquired system capacity.

Given the monthly peak power demands of the buildings over the entire year, the *annual* peak demand savings per kW of SOFC system capacity are presented in Table 5.6 for the eight scenarios. The savings per unit of power capacity are calculated as the quotient of the annual peak demand savings (see (5.17)) and the acquired system capacity ($k_4^{\text{out}}A_4$) for each scenario. The annual peak demand savings are positive

Table 5.6: Annual peak demand savings per kW of SOFC system capacity provided in each scenario.

Scenario	Annual Peak Demand Savings (\$/kW)
1	76.68
2	76.68
3	76.68
4	76.68
5	136.25
6	136.25
7	136.24
8	136.24

in all scenarios. However, the savings are larger in the southern Wisconsin market where the peak demand charges are nearly double those of the southern California market.

Total Savings

Based on summing the four types of annual savings listed in the previous tables, the *total* annual savings per kW of SOFC system capacity are presented in Table 5.7 for

the eight scenarios. The total annual savings are positive in all scenarios. However,

Table 5.7: Total annual savings per kW of SOFC system capacity provided in each scenario.

Scenario	Total Annual Savings (\$/kW)
1	206.14
2	409.63
3	197.64
4	401.14
5	4.01
6	179.50
7	61.88
8	194.62

there is a 10,000% increase in operational savings from the worst-case to best-case scenario! Thus, the combination of building type, energy market, and system design and dispatch in a given scenario clearly has a significant impact on the economic viability of the SOFC system.

The worst-case scenario presented in this chapter is the hotel, located in southern Wisconsin, without heat capture for the SOFCs (Scenario 5). Figure 5.5 depicts the total annual savings for Scenario 5 based on the accumulation of annual energy, emissions, O&M, and peak demand savings. For this scenario, the negative energy savings are barely offset by the positive emissions savings, and the negative O&M savings are nearly offset by the positive peak demand savings. Summing the four savings-types results in a total operational savings near zero (\$4.01 per kW). With nearly no operational savings, the SOFC system is not economically viable. In order to increase the viability of the system, we might consider a more favorable energy market for the hotel.

By locating the hotel, with the power-only SOFC system, in the southern California market (Scenario 1), we increase the operational savings by 5,000%. Figure 5.6

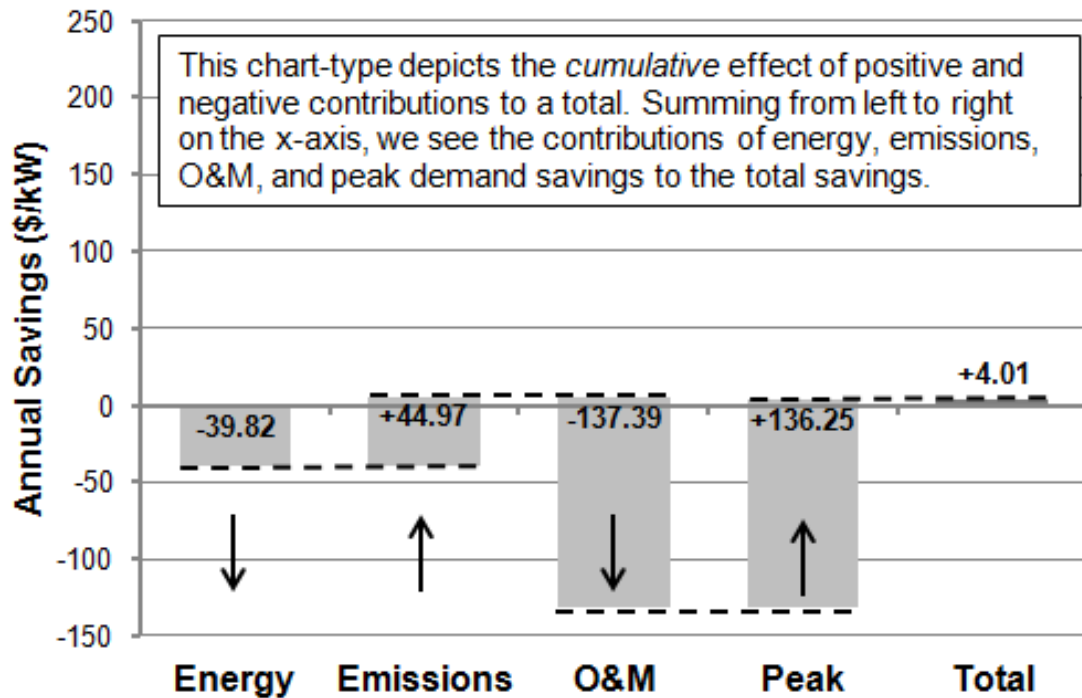


Figure 5.5: Total annual savings for Scenario 5.

demonstrates that Scenario 1 results in total operational savings of \$206.14 per kW. Although the emissions savings in the southern California market are negative, they are more than offset by the large, positive energy savings. In fact, when comparing Scenarios 1 and 5, the emissions, O&M, and peak demand savings are all less in Scenario 1. However, the energy savings are large enough to result in greater *total* savings in Scenario 1. In order to increase the economic viability of the system even further, we might consider upgrading the SOFCs with heat capture.

Adding heat capture to the SOFC system for the hotel in southern California (Scenario 2) increases the operational savings a further 100%. Figure 5.7 depicts the energy, emissions, O&M, and peak demand savings for Scenario 2, which result in total operational savings of \$409.63 per kW. By adding heat capture to the SOFC system in Scenario 2, the energy savings increase by over 30%, the emissions savings increase by nearly 50%, and the O&M savings increase by over 40% compared to Scenario

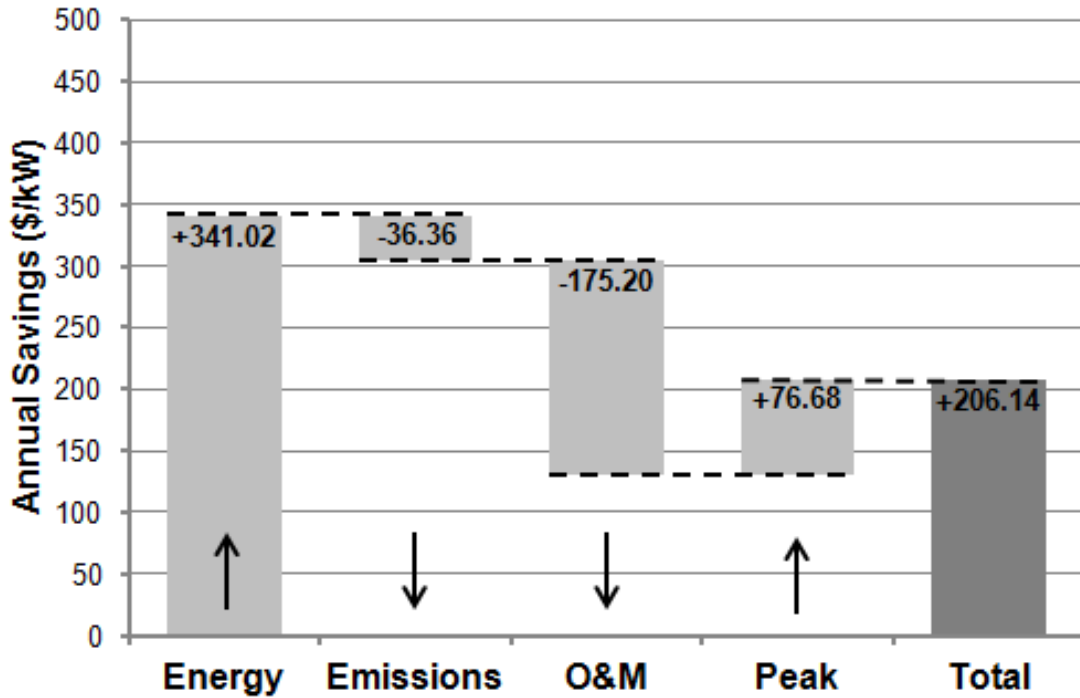


Figure 5.6: Total annual savings for Scenario 1.

1. Of the eight scenarios tested here, Scenario 2 provides the greatest operational savings and, consequently, represents the scenario for which the SOFC system is most economically viable.

Scenario 2 of our analysis results in total annual operational savings of \$81,926, which represents the right-hand side of condition (5.6). By dividing both sides of the inequality in (5.6) by the system capacity ($k_4^{\text{out}}A_4 = 200$), we obtain the economic viability condition $c_4 < 409.63$. The parameter c_4 is the annualized capital and installation cost (\$ per kW) of the SOFC CHP system, while 409.64 is the annual operational savings (\$ per kW) provided by that system. Thus, the annualized capital and installation cost for the SOFC system must be less than \$409.63 per kW in order for the system operation to provide any economic benefit. Various methods of amortization, interest rates, and system lifetimes can be employed to obtain the annualized capital and installation cost. As one example, an initial capital and

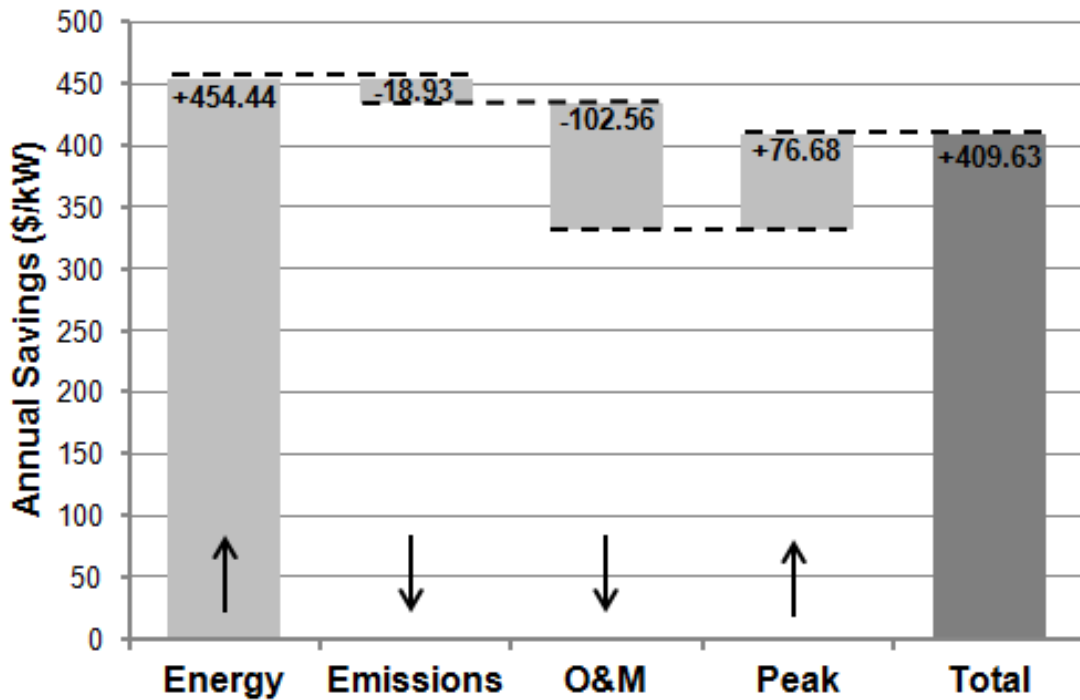


Figure 5.7: Total annual savings for Scenario 2.

installation cost of \$2,900 per kW compounded continuously at 5% interest over a 15-year system lifetime results in an annualized cost of \$409.29 per kW. At this cost, the SOFC CHP system barely achieves economic viability. Lower initial investment costs, a lower interest rate, or a longer system lifetime are required to produce greater viability. Regardless of the method and parameters used to annualize the capital and installation cost, the resulting value must be less than the annual operational savings for the SOFCs to be economically viable.

5.4.2 Savings Sensitivity Within Scenarios

The previous subsection examined the sensitivity of the annual operational savings across the scenarios presented in Table 5.2. This analysis allows us to identify building types, locations, and system configurations for which DG might achieve economic viability. However, within each of these scenarios, the building, market, and system parameters are fixed. By contrast, the analysis presented in this subsection examines

the sensitivity of the annual operational savings to changes in the parameters within a scenario. Specifically, we investigate the impact on the operational savings of varying the SOFCs' rated electric efficiency and the market's carbon tax. We perform this sensitivity analysis for each of the hotel scenarios (i.e., 1, 2, 5, and 6) in order to demonstrate the results over a range from the worst to best-case scenario.

Electric Efficiency

For the analysis presented in Section 5.4.1, the rated electric efficiency (i.e., the efficiency at maximum power output) of the SOFCs is fixed at 41%. Also, the part-load electric efficiency (i.e., the efficiency below maximum power output) increases to a maximum of 57% as the SOFC power output decreases to the maximum turn-down. In this section, we vary the rated electric efficiency of the SOFCs between 40% and 60% to determine the associated impact on the operational savings. Regardless of the rated electric efficiency, we assume the part-load electric efficiency increases linearly to a maximum that is 16% greater than the rated electric efficiency. For example, if the rated electric efficiency is 60%, then the electric efficiency at the maximum turn-down is 76%. The rated thermal efficiency remains fixed at 17% for those scenarios that include heat capture.

The electric efficiency of the SOFCs contributes to the annual energy, emissions, and O&M savings, according to equations (5.7), (5.11), and (5.15), respectively. Figure 5.8 demonstrates the impact on the annual energy savings of increasing the rated electric efficiency from 40% to 60%. The annual energy savings increase as the rated electric efficiency increases. Regardless of the electric efficiency and whether heat capture is included, the southern California scenarios (1 and 2) provide greater energy savings than the southern Wisconsin scenarios (5 and 6). This is due primarily to the high price of utility-purchased electricity in southern California and the favorable net-metering policies that encourage the SOFCs to baseload. The relatively low price of electricity and unfavorable net-metering policies in southern Wisconsin lead

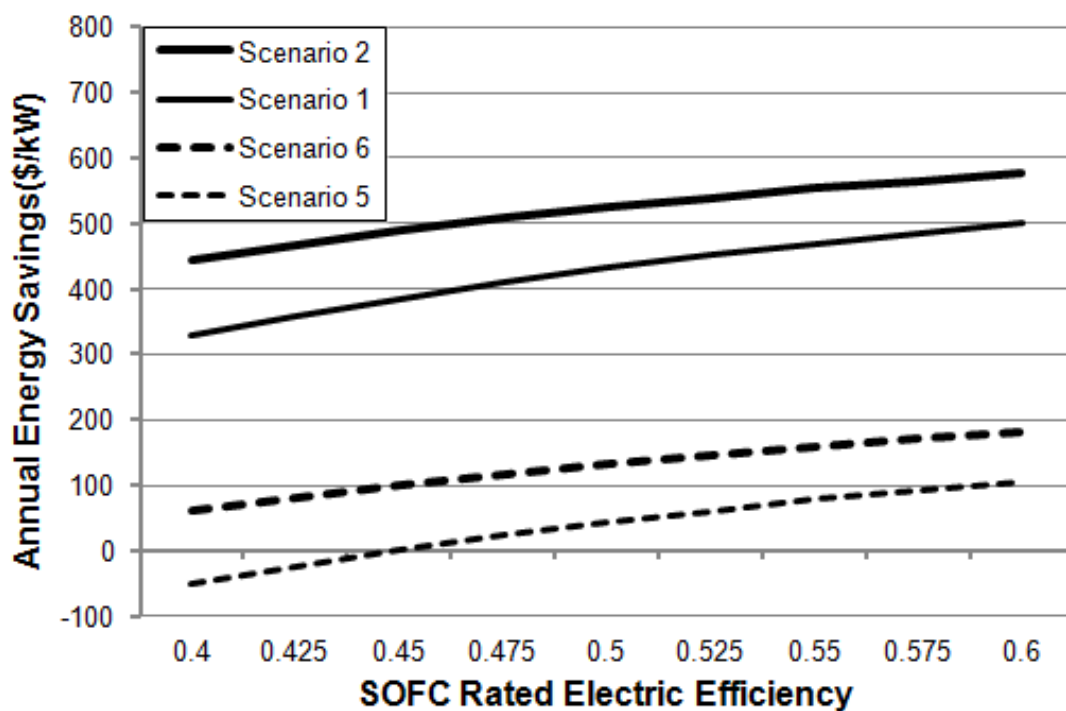


Figure 5.8: Sensitivity of the annual energy savings to changes in the rated electric efficiency of the SOFC.

to lower energy savings. In fact, for the southern Wisconsin scenario (5) without heat capture, the annual energy savings are not positive unless the rated electric efficiency increases beyond 45%.

Increasing the rated electric efficiency also increases the annual emissions savings, as depicted in Figure 5.9. In contrast to the energy savings, the southern Wisconsin scenarios provide greater emissions savings than the southern California scenarios, regardless of the electric efficiency. The average rate of centralized carbon emissions in the southern California market is so low that positive annual emissions savings are only achievable at a rated electric efficiency greater than 60%. On the other hand, the centralized carbon emissions in the southern Wisconsin market are high enough that positive emissions savings are achievable across the entire range of electric efficiencies tested. For both energy markets, however, the scenarios (2 and 6) that include heat

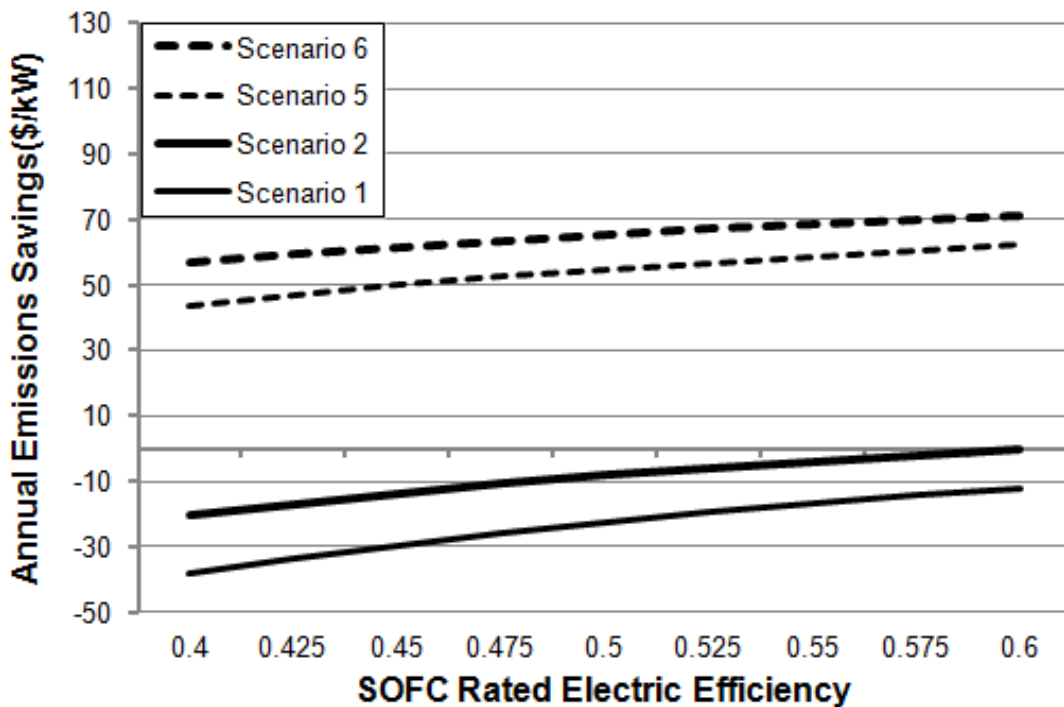


Figure 5.9: Sensitivity of the annual emissions savings to changes in the rated electric efficiency of the SOFC.

capture provide greater savings than those that do not include heat capture due to the decrease in emissions from the boiler.

The final type of savings that is affected by changes in the rated electric efficiency of the SOFCs is O&M. According to Figure 5.10, the O&M savings decrease, or remain the same, as the rated electric efficiency increases. Furthermore, due to the relatively low O&M costs for the boiler, the annual O&M savings are negative regardless of the electric efficiency of the SOFCs. For scenarios (1 and 5) that do not include heat capture, positive O&M savings can never be achieved because there is no reduction in the thermal energy provided by the boiler. However, for scenarios (2 and 6) that include heat capture, the O&M savings decrease as the rated electric efficiency increases. This is due to the fact that increasing the electric efficiency of the SOFCs decreases the amount of natural gas required as input and, therefore, decreases the

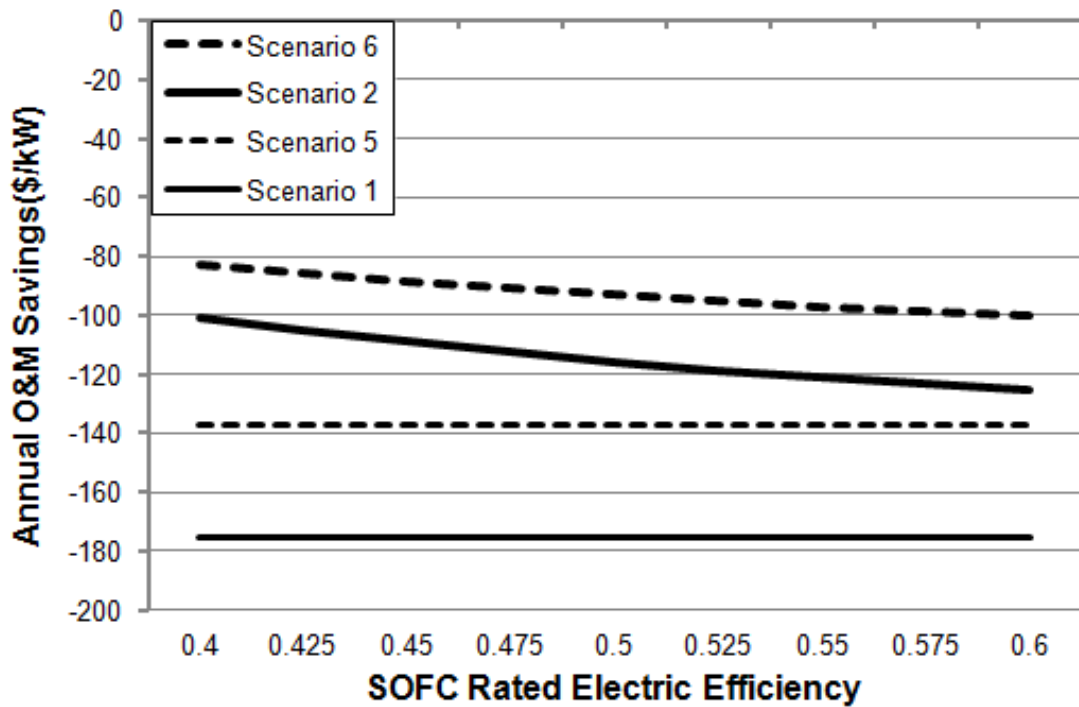


Figure 5.10: Sensitivity of the annual O&M savings to changes in the rated electric efficiency of the SOFC.

amount of exhaust gas output. With less exhaust gas available to offset the thermal energy provided by the boiler, the O&M savings decrease.

Increasing the rated electric efficiency of the SOFCs increases the annual energy and emissions savings, but decreases (or does not impact) the annual O&M savings. The net-effect of these changes in annual energy, emissions, and O&M savings is that the *total* annual savings increase with the rated electric efficiency. According to condition (5.6), SOFCs become economically viable when the total annual savings they provide exceed their annualized capital and installation cost. Thus, as the total annual savings increase, the economic viability of the SOFCs increases. Given the total annual savings for a specific scenario, we refer to the annualized capital and installation cost that precisely equals the annual savings as the annualized “break-even” cost. At capital and installation costs below the break-even cost, positive

net-savings are achievable and the SOFCs are economically viable.

Based on the annualized break-even cost, we calculate an initial (i.e., upfront) break-even cost for the SOFCs by reversing the amortization process (i.e., continuous compounding at 5% interest over the 15-year lifetime). Figure 5.11 demonstrates the effect on the initial break-even cost of increasing the rated electric efficiency of the SOFCs. In terms of economic viability, the southern California scenarios (1

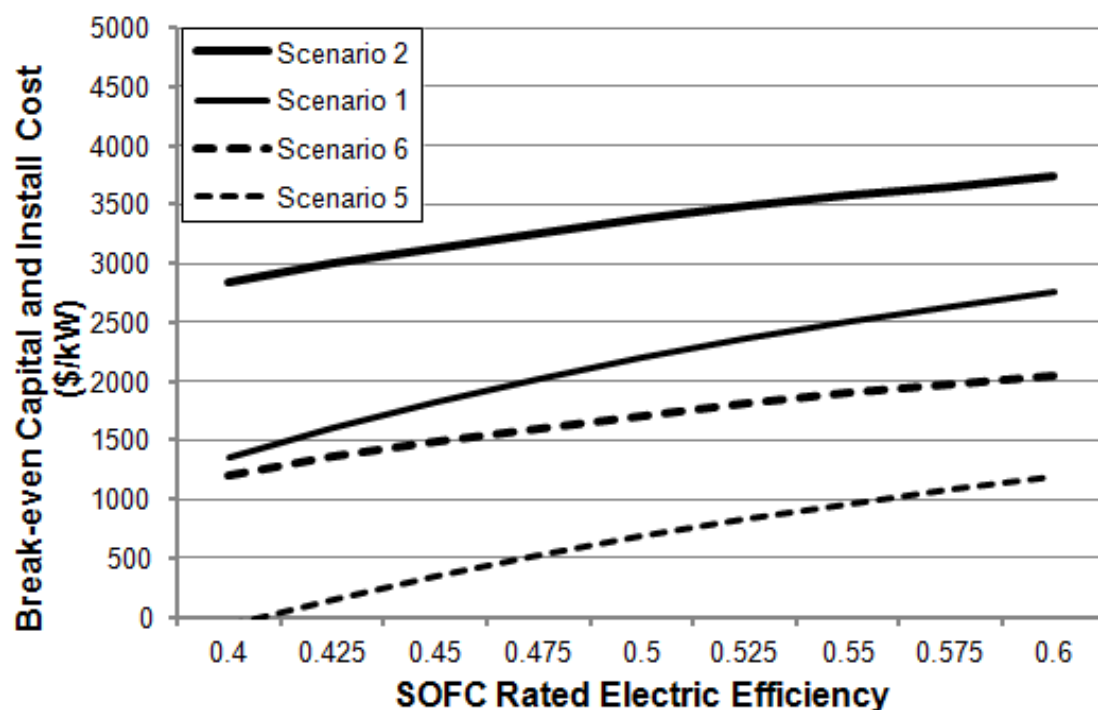


Figure 5.11: Sensitivity of the break-even capital and installation cost to changes in the rated electric efficiency of the SOFC. The break-even cost is the SOFC capital and installation cost that equates exactly to the operational savings provided by the SOFC.

and 2) dominate the southern Wisconsin scenarios (5 and 6) across the range of electric efficiencies. At the lowest rated electric efficiency (i.e., 40%) for the southern Wisconsin scenario (5) without heat capture, the SOFCs are not economically viable because the break-even cost is *negative*. At the highest rated electric efficiency (i.e., 60%) for the southern Wisconsin scenario (6) with heat capture, the SOFCs are only

economically viable for initial capital and installation costs at or below \$2,000 per kW. By contrast, the southern California scenario (2) with heat capture demonstrates economic viability for the SOFCs at costs approaching \$4,000 per kW, when the rated electric efficiency is 60%.

Carbon Tax

In addition to the rated electric efficiency of the SOFCs, the carbon tax rate in the market of interest also affects the economic viability of the SOFC system. For all of the analysis presented up to this point, the carbon tax rate is assumed to be \$0.02 per kg (roughly \$20 per metric ton). For the analysis presented next, we vary the carbon tax rate between \$0.02 per kg and \$0.10 per kg (roughly \$100 per metric ton). In order to isolate the impact of changes in the carbon tax, we return the rated electric efficiency of the SOFCs to the fixed 41%.

Unlike the electric efficiency, the carbon tax rate contributes *only* to the annual emissions savings, according to equation (5.11). Figure 5.12 demonstrates the impact on the annual emissions savings of varying the carbon tax rate between \$0.02-0.10 per kg. As the carbon tax increases, the annual emissions savings in the southern Wisconsin scenarios (5 and 6) increase. On the other hand, the annual emissions savings in the southern California scenarios (1 and 2) decrease as the carbon tax increases. As previously demonstrated in Figure 5.9, the emissions savings are positive in Scenarios 5 and 6, and negative in Scenarios 1 and 2. Thus, increasing the carbon tax causes the annual emissions savings to be *more positive* in Scenarios 5 and 6, and *more negative* in Scenarios 1 and 2. The increase or decrease in the annual emissions savings has implications for the *total* annual savings.

For the southern Wisconsin scenarios, the total annual savings increase as the carbon tax rate increases. By contrast, the total annual savings decrease as the carbon tax rate increases for the southern California scenarios. Applying the same approach as with the electric efficiency sensitivity analysis, we calculate the initial

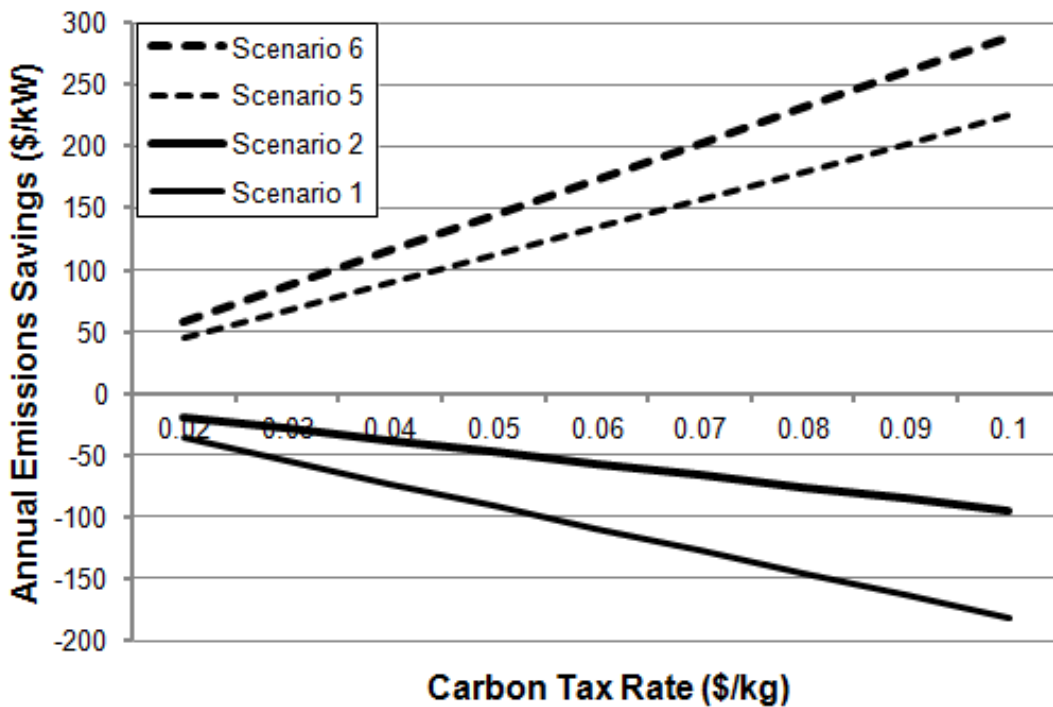


Figure 5.12: Sensitivity of the annual emissions savings to changes in the carbon tax rate.

break-even capital and installation cost for the SOFCs based on the total annual savings. Figure 5.13 depicts the initial break-even cost for the SOFCs as the carbon tax rate varies between \$0.02-0.10 per kg. At a carbon tax rate of \$0.02 per kg, the southern California scenarios dominate the southern Wisconsin scenarios in terms of economic viability. In the best-case scenario (2) at this tax rate, the SOFCs are economically viable at initial capital and installation costs approaching \$3,000 per kW. In the worst-case scenario (5) at this tax rate, the SOFCs are not viable at any positive cost. However, as the carbon tax increases, the SOFCs become more viable in southern Wisconsin and less viable in southern California. In fact, at carbon tax rates greater than \$0.07 and \$0.08 per kg for scenarios without (1 and 5) and with (2 and 6) heat capture, respectively, the SOFCs achieve greater economic viability in southern Wisconsin than in southern California. For a carbon tax rate of \$0.10

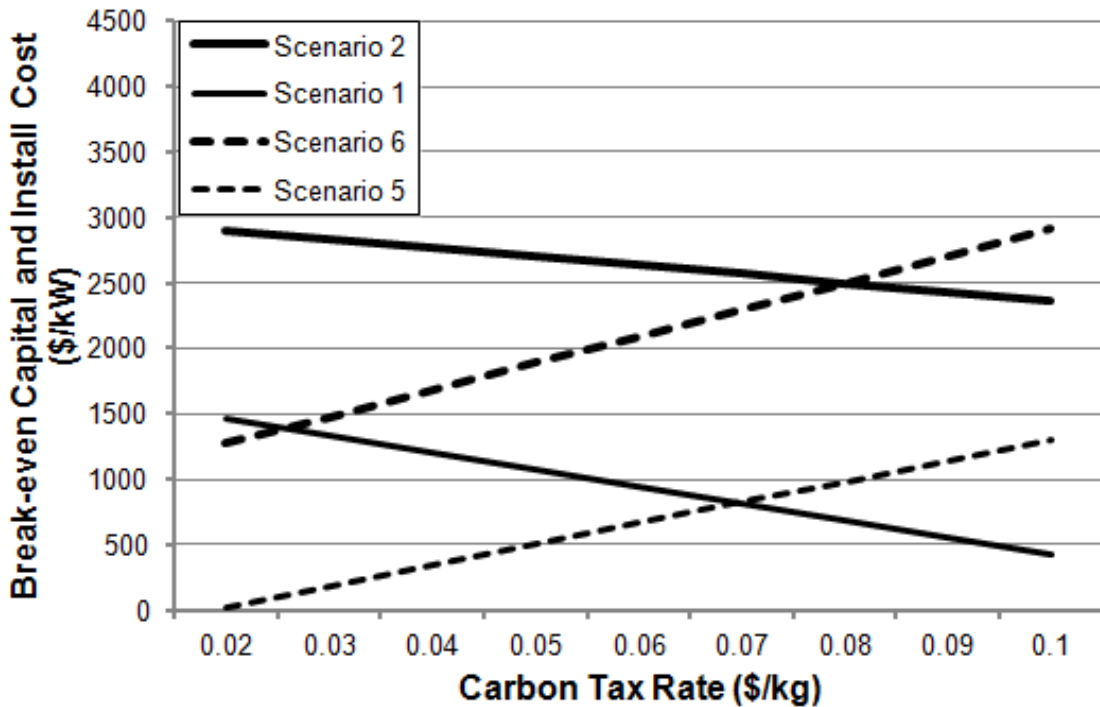


Figure 5.13: Sensitivity of the break-even capital and installation cost to changes in the carbon tax rate. The break-even cost is the SOFC capital and installation cost that equates exactly to the operational savings provided by the SOFC.

per kg, the best-case scenario (6) achieves approximately the same break-even cost (nearly \$3,000 per kW) as the best-case scenario (2) for a carbon tax rate of \$0.02 per kg. However, at the higher tax rate, the best-case scenario is located in southern Wisconsin, rather than in southern California.

The cost versus savings analysis presented in this chapter provides screening criteria for the instances of (\mathcal{P}) we wish to solve. For a given scenario (i.e., a problem instance), if the savings provided by acquiring and operating a DG technology exceed its capital and installation cost, according to (5.6), then the technology is economically viable. If the technology is economically viable, then the optimal system design and dispatch determined by solving the instance of (\mathcal{P}) is likely to include that technology. However, the (\mathcal{P}) -solution could identify a more favorable (i.e., lower-cost)

capacity and operational strategy for the technology than that used to initially assess its economic viability. This is particularly true when the assessed technology can be integrated with other technologies (e.g., electric and thermal storage) in the more robust system (see Figure 2.1) modeled by (\mathcal{P}) . For this reason, our economic viability analysis is a useful complement to, but not a replacement for, (\mathcal{P}) .

In addition to providing screening criteria for instances of (\mathcal{P}) , the cost versus savings analysis presented in this chapter reveals building, market, and technology characteristics for which DG might achieve greater market penetration. The cost analysis, which culminates with (5.6), demonstrates that lower capital and installation costs are likely to encourage greater investment in DG technologies. However, the savings analyses also identify a number of favorable circumstances for DG.

The energy savings analysis indicates that a market with high electricity costs relative to the cost of natural gas, and with net-metering at full market price, is more likely to result in positive operational savings from DG, according to (5.9) and (5.10). The emissions savings analysis demonstrates that a market with a higher rate of carbon emissions, relative to that resulting from the combustion of natural gas, is also more likely to result in positive operational savings, according to (5.13) and (5.14). However, for many markets, it is difficult to achieve *both* positive energy savings and positive emissions savings. The data provided in Appendix B demonstrate that markets with the highest electricity prices often have the lowest carbon emissions rates. We demonstrate such a market with the southern California scenarios. Conversely, markets with low electricity prices often have high emissions rates. The southern Wisconsin scenarios exemplify a market such as this. In general, this phenomenon is due to the higher cost of low-emitting fuel sources, like gas and nuclear, and the lower cost of high-emitting fuel sources, like coal. Thus, the analysis provided in this chapter can help identify markets that balance the trade-off between energy and emissions savings in order to obtain positive *total* savings.

The energy and emissions savings analyses also show the benefits of DG technologies which have higher electric and thermal efficiencies, particularly relative to the technologies they are replacing. The O&M savings analysis similarly indicates that DG is more attractive when the operations and maintenance costs of the new technology are low relative to the technology being replaced, according to (5.16). This information can be used to identify benchmarks for the performance capabilities of new technologies, as well as to select older technologies for upgrade.

Finally, the peak demand savings analysis reveals that buildings with large peak loads are likely to benefit from DG technologies that can operate during peak demand time periods, according to (5.18). Commonly referred to as “peak shaving,” the operation of DG technologies during peak demand time periods has the potential to provide significant savings, particularly in markets with relatively high peak demand charges. Combining all of the insight provided by the cost versus savings analysis, one can discover building-market-technology combinations that are likely to encourage DG investment.

CHAPTER 6

CONCLUSIONS

In this chapter, we review the major findings of our research, and provide recommendations for future work on the design and dispatch problem.

6.1 Major Findings

In **Chapter 1**, we thoroughly review the existing solution approaches to the design and dispatch problem, and the research applications which apply those approaches. The major findings are as follows:

- The primary solution approaches to the design and dispatch problem are simulation, evolutionary algorithms (e.g., genetic algorithms), and traditional mathematical programming algorithms (e.g., branch-and-bound).
- Traditional mathematical programming algorithms can guarantee global optimality of design and dispatch solutions, while simulation and evolutionary algorithms cannot.
- A prominent model (i.e., DER-CAM) which applies traditional mathematical programming algorithms can easily solve large instances of the design and dispatch problem to global optimality, but simplifies or ignores many dynamic performance characteristics of DG technologies.

In **Chapter 2**, we develop a mixed-integer, nonlinear programming (MINLP) formulation, (\mathcal{P}), of the design and dispatch problem which includes dynamic performance characteristics of the DG technologies. The major findings are as follows:

- The minimum turn-down, start-up fuel consumption, power ramping, and part-load electric efficiency of power generation technologies can be modeled in the

context of a mathematical program, but require numerous general integer variables, nonseparable constraints, and nonlinear equality constraints.

- The time-varying temperature of thermal storage technologies can be modeled in the context of a mathematical program, but requires numerous binary variables and nonseparable, nonlinear equality constraints.

In **Chapter 3**, we develop specialized convex underestimation, (\mathcal{U}) , and heuristic linearization, (\mathcal{H}) , techniques to bound and solve instances of (\mathcal{P}) . The major findings are as follows:

- Global lower bounds on instances of (\mathcal{P}) can be obtained by formulating convex underestimators for the bilinear and trilinear terms in the nonlinear equality constraints, and solving the resulting MILP, (\mathcal{U}) .
- Global upper bounds on instances of (\mathcal{P}) can be obtained by fixing the values of the electric efficiency and storage temperature variables, and solving the resulting MILP, (\mathcal{H}) .
- A prominent MINLP solver (i.e., MINOTAUR) is capable of solving (\mathcal{P}) -instances with a time horizon of up to four days, while our bounding techniques can solve (\mathcal{P}) -instances of up to one year.

In **Chapter 4**, we evaluate the qualitative and quantitative impacts of ignoring dynamic performance characteristics by contrasting (\mathcal{P}) with a simpler, linear formulation (\mathcal{S}) . The major findings are as follows:

- The consideration of dynamic performance characteristics is most important for scenarios in which it is beneficial, or required, to dispatch the system in a load-following (i.e., time-varying) manner.
- A representative MILP formulation, (\mathcal{S}) , of the design and dispatch problem includes fewer variables and constraints than (\mathcal{P}) , but models the natural gas

consumption of power generation technologies and the inventory of energy in thermal storage technologies in a fundamentally different manner than (\mathcal{P}) .

- A case study comparing (\mathcal{P}) and (\mathcal{S}) reveals that the simpler formulation overestimates the annual operational costs of the power generation technologies and, as a result, underestimates the optimal acquired power capacity by 15%.

In **Chapter 5**, we determine parametric conditions for the economic viability of a DG technology that can be utilized as screening criteria for the scenarios that are solved by (\mathcal{P}) . The major findings are as follows:

- A comparative static analysis of the economic viability of a DG technology can be performed using the total cost objective function of (\mathcal{P}) ; however, the variables in the total cost function must be replaced with fixed parameters by choosing a specific design and dispatch strategy to evaluate.
- The analysis reveals that a DG technology is economically viable when the operational savings, consisting of energy, emissions, O&M, and peak demand savings, exceed the capital and installation cost.
- Sensitivity analyses across and within a variety of scenarios reveal that the problem instances most likely to result in DG acquisition when solved in (\mathcal{P}) are those that include buildings retrofitted with high-CHP-efficiency technologies and located in markets with either a high electricity-to-gas price ratio or with a high rate of carbon emissions coupled with a high carbon tax rate.

6.2 Future Work

One might pursue a number of extensions to (\mathcal{P}) in future research. For instance, the model might include additional types of building energy demand. In the work presented here, we aggregate the building's space and water heating demands, and

include the cooling demand as part of the power demand. An alternative formulation could treat all of the energy demands of the building separately.

The separation of the building's energy demands affords the opportunity to consider different technologies as part of the DG system. For example, one might integrate absorption chillers with the CHP generators in order to supply a portion of the building's cooling demand. The chillers might then be combined with cold thermal storage, in the form of chilled water, ice, or ice-slurry. The model could also include alternative renewable sources of generation. Wind turbines and solar thermal collectors would provide additional means to offset the power and heating burdens of the existing system.

Other interesting modifications to (\mathcal{P}) might explore how the generators are currently modeled. We treat the electric efficiency of a fuel cell as a decreasing, linear function of its power output. However, one might test other functional forms for alternative technologies. Additionally, in the case of multiple fuel cells, the current formulation aggregates their power output such that each fuel cell supplies an equal share of the total power output. Future work could modify the (\mathcal{P}) formulation, with additional integer variables, to allow each fuel cell to operate at a power output, and therefore efficiency, that is independent of the other fuel cells. This greater flexibility in operational strategy could increase the economic viability of the technology.

Finally, future research could include uncertainty in the building demand, system availability, and utility pricing. We treat each of these parameters as deterministic in (\mathcal{P}) . A stochastic programming version of (\mathcal{P}) could test various parametric scenarios to examine the sensitivity of the optimal system design and dispatch to changes in demand, availability, and pricing. Because the uncertainty in building demand and system availability primarily exists from minute-to-minute, accurately capturing the stochasticity of these parameters could require a greater time fidelity than one hour. Similarly, because the uncertainty in utility pricing exists from year-to-year,

a stochastic model might require a time horizon longer than one year. Greater time fidelity and a longer time horizon increase the size of (\mathcal{P}) -instances and, consequently, make them more difficult to solve. However, the more difficult stochastic model would provide additional real-world insight that could impact the market penetration of DG.

REFERENCES CITED

- [1] EIA. Summary statistics for electric power in the U.S., 1998-2009. Technical report, U.S. Energy Information Administration, January 2011.
- [2] E. Gumerman, R. Bharvirkar, K. LaCommare, and C. Marnay. Evaluation framework and tools for distributed energy resources. Technical Report LBNL-52079, Lawrence Berkeley National Laboratory, February 2003.
- [3] EIA. Annual energy outlook 2011 (AEO2011) early release overview. Technical report, U.S. Energy Information Administration, January 2011.
- [4] M. Manfren, P. Caputo, and Costa G. Paradigm shift in urban energy systems through distributed generation: Methods and models. *Applied Energy*, 88:1032–1048, 2011.
- [5] R. Braun. Techno-economic optimal design of SOFC systems for residential micro-combined heat and power applications in the U.S. *ASME Journal of Fuel Cell Science and Technology*, 7:031018:1–15, June 2010.
- [6] H. Sayyaadi. Multi-objective approach in thermoenviromomic optimization of a benchmark cogeneration system. *Applied Energy*, 86:867–879, 2009.
- [7] A. Toffolo and A. Lazzaretto. Energy, economy and environment as objectives in multi-criteria optimization of thermal system design. *Energy*, 29:1139–1157, 2004.
- [8] A. Azhdari, H. Ghadamian, A. Ataei, and C. Yoo. A new approach for optimization of combined heat and power generation in edible oil plants. *Journal of Applied Sciences*, 9(21):3813–3820, 2009.
- [9] P. Boait, R. Rylatt, and M. Stokes. Optimisation of consumer benefits from microcombined heat and power. *Energy and Buildings*, 38:981–987, 2006.
- [10] P. Mago and A. Hueffed. Evaluation of a turbine driven CCHP system for large office buildings under different operating strategies. *Energy and Buildings*, 42:1628–1636, 2010.
- [11] A. Nosrat and J. Pearce. Dispatch strategy and model for hybrid photovoltaic and trigeneration power systems. *Applied Energy*, 88:3270–3276, 2011.

- [12] P. Subbaraj, R. Rengaraj, and S. Salivahanan. Enhancement of combined heat and power economic dispatch using self adaptive real-coded genetic algorithm. *Applied Energy*, 86:915–921, 2009.
- [13] X. Kong and R. Wang. Energy optimization model for a CCHP system with available gas turbines. *Applied Thermal Engineering*, 25:377–391, 2005.
- [14] Y. Ishida, M. Bannai, T. Miyazaki, Y. Harada, R. Yokoyama, and A. Akisawa. The optimal operation criteria for a gas turbine cogeneration system. *Energies*, 2(2):202–225, 2009. ISSN 19961073.
- [15] R. Firestone, M. Stadler, and C. Marnay. Integrated energy system dispatch optimization. Technical Report LBNL-60591, Lawrence Berkeley National Laboratory, June 2006.
- [16] M. Medrano, J. Brouwer, V. McDonell, J. Mauzey, and S. Samuelsen. Integration of distributed generation systems into generic types of commercial buildings in California. *Energy and Buildings*, 40:537–548, 2008.
- [17] J. Cotrell and W. Pratt. Modeling the feasibility of using fuel cells and hydrogen internal combustion engines in remote renewable energy systems. Technical Report NREL/TP-500-34648, National Renewable Energy Laboratory, September 2003.
- [18] T. Givler and P. Lilienthal. Using HOMER software, NRELs micropower optimization model, to explore the role of gen-sets in small solar power systems. Technical Report NREL/TP-710-36774, National Renewable Energy Laboratory, May 2005.
- [19] M. Khan and M. Iqbal. Pre-feasibility study of stand-alone hybrid energy systems for applications in Newfoundland. *Renewable Energy*, 30(6):835–854, 2005.
- [20] P. Georgilakis. State-of-the-art of decision support systems for the choice of renewable energy sources for energy supply in isolated regions. *International Journal of Distributed Energy Resources*, 2(2):129–150, 2006.
- [21] M. Burer, K. Tanaka, D. Favrat, and K. Yamada. Multi-criteria optimization of a district cogeneration plant integrating a solid oxide fuel cell-gas turbine combined cycle, heat pumps and chillers. *Energy*, 28:497–518, 2003.
- [22] D. Xu, L. Kang, and B. Cao. The elitist non-dominated sorting GA for multi-objective optimization of standalone hybrid wind/PV power systems. *Journal of Applied Sciences*, 6(9):2000–2005, 2006.

- [23] G. Kayo and R. Ooka. Building energy system optimizations with utilization of waste heat from cogenerations by means of genetic algorithm. *Energy and Buildings*, 42:985–991, 2010.
- [24] C. Weber, F. Marechal, D. Favrat, and S. Kraines. Optimization of an SOFC-based decentralized polygeneration system for providing energy services in an office-building in Tokyo. *Applied Thermal Engineering*, 26:1409–1419, 2006.
- [25] Z. Beihong and L. Weiding. An optimal sizing method for cogeneration plants. *Energy and Buildings*, 38:189–195, 2006.
- [26] S. Oh, H. Oh, and H. Kwak. Economic evaluation for adoption of cogeneration system. *Applied Energy*, 84:266–278, 2007.
- [27] A. Siddiqui, C. Marnay, O. Bailey, and K. LaCommare. Optimal selection of on-site generation with combined heat and power applications. *International Journal of Distributed Energy Resources*, 1(1):33–62, January 2005.
- [28] H. Ren and W. Gao. A MILP model for integrated plan and evaluation of distributed energy systems. *Applied Energy*, 87:1001–1014, 2010.
- [29] A. Siddiqui, C. Marnay, J. Edwards, R. Firestone, S. Ghosh, and M. Stadler. Effects of a carbon tax on microgrid combined heat and power adoption. *Journal of Energy Engineering*, 131(1):2–25, April 2005.
- [30] M. Stadler, C. Marnay, A. Siddiqui, J. Lai, and H. Aki. Integrated building energy systems design considering storage technologies. Technical Report LBNL-1752E, Lawrence Berkeley National Laboratory, April 2009.
- [31] N. Greene and R. Hammerschlag. Small and clean is beautiful: Exploring the emissions of distributed generation and pollution prevention policies. *The Electricity Journal*, 13(5):50–60, 2000.
- [32] S. Price and R. Margolis. 2008 solar technologies market report. Technical Report DOE/GO-102010-2867, National Renewable Energy Laboratory, January 2010.
- [33] S. Schoenung and W. Hassenzahl. Long- vs. short-term energy storage technologies analysis: A life-cycle cost study. Technical Report SAND2003-2783, Sandia National Laboratories, August 2003.
- [34] A. Stambouli and E. Traversa. Solid oxide fuel cells (SOFCs): A review of an environmentally clean and efficient source of energy. *Renewable and Sustainable Energy Reviews*, 6:433–455, 2002.

- [35] R. Braun, S. Klein, and D. Reindl. Evaluation of system configurations for SOFC-based micro-CHP systems in residential applications. *Journal of Power Sources*, 158:1290–1305, August 2006.
- [36] A. Hawkes, P. Aguiar, C. Hernandez-Aramburo, M. Leach, N. Brandon, T. Green, and C Adjiman. Techno-economic modelling of a solid oxide fuel cell stack for micro combined heat and power. *Journal of Power Sources*, 156: 321–333, 2006.
- [37] W. Nicholson and C. Snyder. *Microeconomic Theory: Basic Principles and Extensions*. South-Western, 10th edition, 2008.
- [38] G. McCormick. Computability of global solutions to factorable nonconvex programs: Part 1 - convex underestimating problems. *Mathematical Programming*, 10:147–175, 1976.
- [39] C. Adjiman and C. Floudas. α BB algorithm. *Encyclopedia of Optimization*, 1: 61–73, 2008.
- [40] M. Tawarmalani and N. Sahinidis. *Convexification and Global Optimization in Continuous and Mixed-Integer Nonlinear Programming: Theory, Algorithms, Software, and Applications*, volume 65. Kluwer Academic, 2002.
- [41] A. Siddiqui, C. Marnay, R. Firestone, and N. Zhou. Distributed generation with heat recovery and storage. Technical Report LBNL-58630, Lawrence Berkeley National Laboratory, July 2005.
- [42] DOE. Getting Started with EnergyPlus: Basic Concepts Manual-Information You Need about Running EnergyPlus, October 2010.
- [43] SCE. Schedule TOU-GS-3. Technical report, Southern California Edison, 2010.
- [44] SCGC. Schedule G-10. Technical report, Southern California Gas Company, 2010.
- [45] D. Kaffine, B. McBee, and J. Lieskovsky. Empirical estimates of emissions avoided from wind power generation. *USAEE Dialogue*, 19(1), 2011.
- [46] NREL. A performance calculator for grid-connected PV systems (PVWATTSv.1), 2011. URL <http://rredc.nrel.gov/solar/calculators/PVWATTS/version1/>.
- [47] NaturalGas.org. Natural gas and the environment, 2011. URL <http://www.naturalgas.org/environment>.

- [48] IBM. IBM ILOG AMPL Version 12.2 User's Guide: Standard (Command-line) Version including CPLEX Directives, May 2010.
- [49] S. Leyffer, J. Linderoth, J. Luedtke, A. Mahajan, and T. Munson. MINOTAUR User's Manual, 2011.
- [50] J. Czyzyk, M. Mesnier, and J. More. The NEOS Server. *IEEE Journal on Computational Science and Engineering*, 5:68–75, 1998.
- [51] E. Dolan. NEOS Server 4.0 Administrative Guide. Technical Report ANL/MCS-TM-250, Argonne National Laboratory, May 2001. URL <http://www.neos-server.org>.
- [52] WEPC. Volume 19-Electric Rates. Technical Report Cg 2, Wisconsin Electric Power Company, 2011.
- [53] WE-GO. Volume XVI-Firm Sales Service. Technical Report x-100, Wisconsin Electric-Gas Operations, 2011.
- [54] EIA. State electricity profiles 2009. Technical Report DOE/EIA-0348(01)/2, U.S. Energy Information Administration, April 2011.
- [55] EIA. Natural gas annual 2009. Technical Report DOE/EIA-0131(09), U.S. Energy Information Administration, December 2010.
- [56] NNEC. Freeing the Grid: Best and Worst Practices in State Net Metering Policies and Interconnection Procedures. Technical report, Network for New Energy Choices, November 2009.
- [57] WEPC. Volume 19-Electric Rates. Technical Report Cg 3, Wisconsin Electric Power Company, 2010.
- [58] NNEC. Freeing the Grid: Best and Worst Practices in State Net Metering Policies and Interconnection Procedures. Technical report, Network for New Energy Choices, December 2010.
- [59] EIA. State electricity profiles 2010. Technical Report DOE/EIA-0348(01)/2, U.S. Energy Information Administration, January 2012.
- [60] EIA. Natural gas annual 2010. Technical Report DOE/EIA-0131(10), U.S. Energy Information Administration, December 2011.

APPENDIX A - AMPL CODE

This section includes the model, data, run, and out files for a representative one-day instance of (\mathcal{P}) that is solved using (\mathcal{U}) and (\mathcal{H}) . In order to solve instances of multiple months, all of the parameters, variables, objective function components, and constraints that involve the set \mathcal{N} must be used in place of what is shown here. Instructions for doing this are provided in comments prior to the appropriate lines of code.

A.1 Model File

```
#-----  
# Sets, Parameters, and Variables  
#-----  
  
##For one-year instance, remove next three comments and add comment  
##in front of fourth set.  
#set N; #set of all months  
#set Tn{N}; #set of all hours in month n  
#set T = union {n in N} Tn[n]; #set of all hours  
set T; #set of all hours  
  
param tau; #time increment per period in hours  
param de{t in T}; #electricity demand in period t  
param dh{t in T}; #heat demand in period t  
param gpx; #max power capacity of power-only fcells  
param hpx; #max power capacity of CHP fcells  
param vpx; #max power capacity of PV cells
```

```
param pvf{t in T}; #forecasted percent max solar, period t
param gmt; #min turn-down power-only fcells
param hmt; #min turn-down CHP fcells
param gru; #max ramp-up rate for power-only fcell
param grd; #max ramp-down for power-only fcell
param hru; #max ramp-up rate for CHP fcell
param hrd; #max ramp-down for CHP fcell
param gaq; #$/kW of power-only fuel cell
param haq; #$/kW of CHP fuel cell
param vaq; #$/kW of PV cell
param gom; #variable o&m cost power fcell
param hom; #variable o&m CHP fcell
param vom; #variable o&m pv cell
param bom; #variable o&m boiler
param waq; #$/gal of tank
param wx; #initial capacity of tank
param wxx; #max tank capacity
param wd; #decay rate of water temp
param we; #heat x efficiency
param wu; #max water temp
param wh; #hot water delivery temp
param wr; #average return water temp
param wl; #water main temp
param ws; #specific heat of water
param sx; #max storage capacity of battery
param msc; #min state-of-charge of battery
param scr; #max charge rate for battery
```

```

param sdr; #max discharge rate for battery
param sce; #charge efficiency for battery
param sde; #discharge efficiency for battery
param saq; #$/kWh of battery
param ce{t in T}; #price of elec. from grid, hour t
param cg{t in T}; #energy charge for natural gas, hour t
param fe; #elec eff during start-up
param fh; #CHP exhaust output per unit natural gas input
param ft; #average temp of CHP exhaust
param fs; #specific heat of exhaust
param fb; #heat efficiency for boiler
param zt; #carbon tax
param zu; #carbon emission rate from grid
param zg; #carbon emission rate of natural gas

##For one-year instance, remove next comment and add comment
##in front of second param.
#param cd{n in N}; #peak demand charge for electricity, month n
param cd; #peak demand charge for electricity, month n

#-----Underestimator set, bound parameters, vars-----#

set U; #set of all underestimator vars

param GNhi{t in T}; #upper bound for GN
param GNlo{t in T}; #lower bound for GN
param HNhi{t in T}; #upper bound for HN

```

```

param HNlo{t in T}; #lower bound for HN
param GGhi{t in T}; #upper bound for GNG
param GGlo{t in T}; #lower bound for GNG
param HGhi{t in T}; #upper bound for HNG
param HGlo{t in T}; #lower bound for HNG
param GEhi{t in T}; #upper bound for GE
param GElo{t in T}; #lower bound for GE
param HEhi{t in T}; #upper bound for HE
param HElo{t in T}; #lower bound for HE
param WChi{t in T}; #upper bound for WC
param WClo{t in T}; #lower bound for WC
param WDhi{t in T}; #upper bound for WD
param WDlo{t in T}; #lower bound for WD
param Whi{t in T}; #upper bound for W
param Wlo{t in T}; #lower bound for W
param WXhi{t in T}; #upper bound for WX
param WXlo{t in T}; #lower bound for WX
param WYhi{t in T}; #upper bound for WY
param WYlo{t in T}; #lower bound for WY
param WAhi; #upper bound on WA
param WALo; #lower bound on WA

```

```

#initial values for var bounds

```

```

param iGNhi{t in T}; #upper bound for GN
param iGNlo{t in T}; #lower bound for GN
param iHNhi{t in T}; #upper bound for HN
param iHNlo{t in T}; #lower bound for HN

```

```

param iGGhi{t in T}; #upper bound for GNG
param iGGlo{t in T}; #lower bound for GNG
param iHGhi{t in T}; #upper bound for HNG
param iHGlo{t in T}; #lower bound for HNG
param iGEhi{t in T}; #upper bound for GE
param iGelo{t in T}; #lower bound for GE
param iHEhi{t in T}; #upper bound for HE
param iHElo{t in T}; #lower bound for HE
param iWChi{t in T}; #upper bound for WC
param iWClo{t in T}; #lower bound for WC
param iWDhi{t in T}; #upper bound for WD
param iWDlo{t in T}; #lower bound for WD
param jWDlo{t in T}; #tight lower bound for WD
param iWhi{t in T}; #upper bound for W
param jWhi{t in T}; #tight upper bound for W
param iWlo{t in T}; #lower bound for W
param iWXhi{t in T}; #upper bound for WX
param iWXlo{t in T}; #lower bound for WX
param iWYhi{t in T}; #upper bound for WY
param jWYhi{t in T}; #tight upper bound for WY
param iWYlo{t in T}; #lower bound for WY
param iWAhi; #upper bound on WA
param iWAllo; #lower bound on WA

var UE{u in U,t in T}; #new variables to replace NL terms
#trilinear then bilinear
#-----#

```

```

var GA >=0, integer, :=0; #num power-only fuel cells acquired
var HA >=0, integer, :=0; #num CHP fuel cells acquired
var VA >=0, integer, :=0; #num PV cells acquired
var SA >=0, integer, :=0; #num of batteries acquired
var WA >=WAl0, <=WAHi, :=wx; #gallons for tank
var WB binary, :=0; #1 if water tank acquired
var GE{t in T} >=GElo[t], <=GEhi[t], :=fe; #elec eff of power only SOFC
var HE{t in T} >=HElo[t], <=HEhi[t], :=fe; #elec eff of CHP SOFC
var GNG{t in T} >=GGlo[t], <=GGhi[t], :=0; #gas for power SOFCs
var HNG{t in T} >=HGlo[t], <=HGhi[t], :=0; #gas for CHP SOFCs
var BNG{t in T} >=0, :=dh[t]/fb; #gas for boiler
var GN{t in T} integer, >=GNlo[t], <=GNhi[t], :=0;
#num power-only fcells turned on period t
var HN{t in T} integer, >=HNlo[t], <= HNhi[t], :=0;
#num CHP fcells turned on period t
var GY{t in T:t>1} >=0, :=0; #num power fcells turned on t to t-1
var HY{t in T:t>1} >=0, :=0; #num CHP fcells turned on t to t-1
var WY{t in T} binary, >=WYlo[t], <=WYhi[t], :=0;
#1 if water temp is above delivery temp in t
var WX{t in T} binary, >=WXlo[t], <=WXhi[t], :=0;
#1 if water temp is above return temp in t
var P{t in T} >=0, :=0; #power from power-only fuel cells in t
var CP{t in T} >=0, :=0; #power from CHP fuel cells in t
var V{t in T} >=0, :=0; #power from PV cells in t
var W{t in T} >=Wlo[t], <=Whi[t], :=wr; #temp of water tank in t
var WC{t in T} >=WClo[t], <=WChi[t], :=0;

```

```

#flowrate of CHP exhaust into tank in t
var WD{t in T} >=WDlo[t], <=WDhi[t], :=dh[t]/(ws*(wh-wr));
#flow rate of heated water in t
var SC{t in T} >=0, :=0; #state-of-charge of batteries in t
var CR{t in T} >=0, :=0; #charge rate in t
var DR{t in T} >=0, :=0; #depletion rate in t
var EP{t in T} >=0, :=de[t]; #power supplied by grid in period t
var ES{t in T} >=0, :=0; #power sold back to grid in t

##For one-year instance, remove next comment and add comment
##in front of second var.
#var E{n in N} >= 0, :=max{t in Tn[n]}de[t];
var E >= 0, :=max{t in T}de[t]; #max supplied by grid in month n

#-----
# Objective Function (min costs from capital, O&M, fuel, and grid)
#-----

minimize under_cost:
gaq*gpx*GA + haq*hpx*HA + vaq*vpv*VA + saq*sx*SA + waq*(WA-wx) +
tau*sum{t in T}(gom*P[t] + hom*CP[t] + vom*V[t]) +
sum{t in T:t>1}((cg[t]+zt*zg)*(((gmt*gpx)/fe)*GY[t]+
((hmt*hpx)/fe)*HY[t]))+
tau*sum{t in T}((bom*fb+cg[t]+zt*zg)*BNG[t]) +
tau*sum{t in T}((cg[t]+zt*zg)*(GNG[t]+HNG[t])) +
tau*sum{t in T}((ce[t]+zt*zv)*EP[t])- tau*sum{t in T}(ce[t]*ES[t])+

```

```

##For one-year instance, remove next comment and add comment
##in front of second line.
#sum{n in N}(cd[n]*E[n]);
0.03*cd*E;

#-----
# Constraints
#-----

#power and heat demand constraints (2.2a) and (2.2b)
subject to demande{t in T}:
P[t] + CP[t] + V[t] + (sde*DR[t]-CR[t]) + (EP[t]-ES[t]) = de[t];
subject to demandh{t in T}:
-WD[t]*(ws*(wh-wr))*wl + (ws*(wh-wr))*UE[6,t] =
dh[t]*(W[t]-wl-UE[7,t]+wh*WY[t]);

#max monthly grid demand constraint (2.3a)
##For one-year instance, remove next comment and add comment
##in front of second constraint.
#subject to minmax{n in N,t in Tn[n]}: E[n] >= EP[t];
subject to minmax{t in T}: E >= EP[t];

#monthly net generator constraint (2.3b)
##For one-year instance, remove next comment and add comment
##in front of second constraint.
#subject to netgen{n in N}:
sum{t in Tn[n]}ES[t] <= sum{t in Tn[n]}EP[t];

```

subject to netgen: $\sum\{t \text{ in } T\}ES[t] \leq \sum\{t \text{ in } T\}EP[t];$

#max power from PV cells constraint (2.4c)

subject to maxpowv{t in T}: $V[t] \leq pvf[t]*vpv*VA;$

#max/min power from fuel cells constraints (2.4d) and (2.4e)

subject to pow_lo{t in T}: $P[t] \geq gmt*gpx*GN[t];$

subject to pow_hi{t in T}: $P[t] \leq gpx*GN[t];$

subject to pow_buyon{t in T}: $GA \geq GN[t];$

subject to chp_lo{t in T}: $CP[t] \geq hmt*hpx*HN[t];$

subject to chp_hi{t in T}: $CP[t] \leq hpv*HN[t];$

subject to chp_buyon{t in T}: $HA \geq HN[t];$

#ramp-up/down rate for fuel cells constraint (2.7b)

subject to pow_rup{t in T:t<card(T)}:

$P[t+1] - P[t] \leq \tau*gru*GN[t+1];$

subject to pow_rdown{t in T:t<card(T)}:

$P[t] - P[t+1] \leq \tau*grd*GN[t];$

subject to chp_rup{t in T:t<card(T)}:

$CP[t+1] - CP[t] \leq \tau*hru*HN[t+1];$

subject to chp_rdown{t in T:t<card(T)}:

$CP[t] - CP[t+1] \leq \tau*hrd*HN[t];$

#start-up for fuel cells constraint (2.7a)

subject to pow_oninc{t in T:t>1}: $GN[t]-GN[t-1] \leq GY[t];$

subject to chp_oninc{t in T:t>1}: $HN[t]-HN[t-1] \leq HY[t];$

```

#natural gas consumption constraints (2.6a) and (2.6b)
subject to ggas{t in T}: UE[1,t] = P[t];
subject to hgas{t in T}: UE[2,t] = CP[t];
subject to bgas{t in T}:
BNG[t] = (ws/fb)*(wh*WD[t]-wh*UE[5,t]-UE[6,t]+UE[3,t]);

#electric efficiency constraint (2.5a)
subject to pow_eff{t in T}: UE[8,t] = 0.61*GN[t]-0.02*P[t];
subject to chp_eff{t in T}: UE[9,t] = 0.61*HN[t]-0.02*CP[t];

#water tank acquisition constraint (2.11a)
subject to tankacq1: WB <= HA;
subject to tankacq2: HNhi[1]*WB >= HA;

#water tank temp constraints (2.10a)-(2.10e)
subject to tanktemp{t in T:t>1}:
ws*UE[10,t] - ws*UE[10,t-1] + ws*wd*UE[4,t-1] =
tau*we*fs*ft*WC[t-1] - tau*we*fs*UE[11,t-1]
- tau*ws*UE[6,t-1] + tau*ws*wr*WD[t-1];
subject to temp1{t in T}: W[t] <= wr + (wu-wr)*WB;
subject to temp3{t in T}: W[t] <= wr + 0.1 + (wu-wr-0.1)*WX[t];
subject to temp4{t in T}: W[t] >= wr + 0.1*WX[t];
subject to temp5{t in T}: W[t] <= wh+(wu-wh)*WY[t];
subject to temp6{t in T}: W[t] >= wh-(wh-wr)*(1-WY[t]);
subject to temp7: W[1] = W[card(T)];

#water tank heat from fuel cells constraint (2.9a)

```

```

subject to tankheat1{t in T}: WC[t] <= fh*HNG[t];

#battery state-of-charge constraints (2.8a) and (2.8c)
subject to soc{t in T:t>1}:
SC[t] = SC[t-1] + tau*(sce*CR[t-1]-DR[t-1]);
subject to soc_init: SC[1] = SC[card(T)];

#max/min state-of-charge constraint (2.8b)
subject to st_upcap{t in T:t>1}: SC[t] <= sx*SA;
subject to st_locap{t in T:t>1}: SC[t] >= msc*sx*SA;

#battery charge/deplete rate constraints (2.4a) and (2.4b)
subject to charge{t in T}: CR[t] <= scr*SA;
subject to deplete{t in T}: DR[t] <= sdr*SA;

#-----
# Underestimator Constraints
#-----

#trilinear term constraints
subject to under5{t in T}: UE[3,t] >=
(WD[t]*Wlo[t]*WYlo[t])+(WDlo[t]*W[t]*WYlo[t])+(WDlo[t]*Wlo[t]*WY[t])
-2*(WDlo[t]*Wlo[t]*WYlo[t]);
subject to under6{t in T}: UE[3,t] >=
(WD[t]*Whi[t]*WYhi[t])+(WDhi[t]*W[t]*WYlo[t])+(WDhi[t]*Wlo[t]*WY[t])
-(WDhi[t]*Wlo[t]*WYlo[t])-(WDhi[t]*Whi[t]*WYhi[t]);
subject to under7{t in T}: UE[3,t] >=

```

$$(WD[t]*Wlo[t]*WYlo[t])+(WDlo[t]*W[t]*WYhi[t])+(WDlo[t]*Whi[t]*WY[t]) \\ - (WDlo[t]*Whi[t]*WYhi[t])-(WDlo[t]*Wlo[t]*WYlo[t]);$$

subject to under8{t in T}: UE[3,t] >=

$$(WD[t]*Whi[t]*WYlo[t])+(WDhi[t]*W[t]*WYhi[t])+(WDlo[t]*Whi[t]*WY[t]) \\ - (WDlo[t]*Whi[t]*WYlo[t])-(WDhi[t]*Whi[t]*WYhi[t]);$$

subject to under9{t in T}: UE[3,t] >=

$$(WD[t]*Wlo[t]*WYhi[t])+(WDlo[t]*W[t]*WYlo[t])+(WDhi[t]*Wlo[t]*WY[t]) \\ - (WDhi[t]*Wlo[t]*WYhi[t])-(WDlo[t]*Wlo[t]*WYlo[t]);$$

subject to under10{t in T}: UE[3,t] >=

$$(WD[t]*Wlo[t]*WYhi[t])+(WDlo[t]*W[t]*WYhi[t])+(WDhi[t]*Whi[t]*WY[t]) \\ - (WDlo[t]*Wlo[t]*WYhi[t])-(WDhi[t]*Whi[t]*WYhi[t]);$$

subject to under11{t in T}: UE[3,t] >=

$$(WD[t]*Whi[t]*WYlo[t])+(WDhi[t]*W[t]*WYlo[t])+(WDlo[t]*Wlo[t]*WY[t]) \\ - (WDhi[t]*Whi[t]*WYlo[t])-(WDlo[t]*Wlo[t]*WYlo[t]);$$

subject to under12{t in T}: UE[3,t] >=

$$(WD[t]*Whi[t]*WYhi[t])+(WDhi[t]*W[t]*WYhi[t])+(WDhi[t]*Whi[t]*WY[t]) \\ - 2*(WDhi[t]*Whi[t]*WYhi[t]);$$

subject to under13{t in T}: UE[4,t] >=

$$(WA*Wlo[t]*WXlo[t])+(WAllo*W[t]*WXlo[t])+(WAllo*Wlo[t]*WX[t]) \\ - 2*(WAllo*Wlo[t]*WXlo[t]);$$

subject to under14{t in T}: UE[4,t] >=

$$(WA*Whi[t]*WXhi[t])+(Wahi*W[t]*WXlo[t])+(Wahi*Wlo[t]*WX[t]) \\ - (Wahi*Wlo[t]*WXlo[t])-(Wahi*Whi[t]*WXhi[t]);$$

subject to under15{t in T}: UE[4,t] >=

$$(WA*Wlo[t]*WXlo[t])+(WAllo*W[t]*WXhi[t])+(WAllo*Whi[t]*WX[t]) \\ - (WAllo*Whi[t]*WXhi[t])-(WAllo*Wlo[t]*WXlo[t]);$$

subject to under16{t in T}: UE[4,t] >=

$$(WA*Whi[t]*WXlo[t])+(WAhi*W[t]*WXhi[t])+(WAl0*Whi[t]*WX[t])$$

$$-(WAl0*Whi[t]*WXlo[t])-(WAhi*Whi[t]*WXhi[t]);$$

subject to under17{t in T}: UE[4,t] >=

$$(WA*Wlo[t]*WXhi[t])+(WAl0*W[t]*WXlo[t])+(WAhi*Wlo[t]*WX[t])$$

$$-(WAhi*Wlo[t]*WXhi[t])-(WAl0*Wlo[t]*WXlo[t]);$$

subject to under18{t in T}: UE[4,t] >=

$$(WA*Wlo[t]*WXhi[t])+(WAl0*W[t]*WXhi[t])+(WAhi*Whi[t]*WX[t])$$

$$-(WAl0*Wlo[t]*WXhi[t])-(WAhi*Whi[t]*WXhi[t]);$$

subject to under19{t in T}: UE[4,t] >=

$$(WA*Whi[t]*WXlo[t])+(WAhi*W[t]*WXlo[t])+(WAl0*Wlo[t]*WX[t])$$

$$-(WAhi*Whi[t]*WXlo[t])-(WAl0*Wlo[t]*WXlo[t]);$$

subject to under20{t in T}: UE[4,t] >=

$$(WA*Whi[t]*WXhi[t])+(WAhi*W[t]*WXhi[t])+(WAhi*Whi[t]*WX[t])$$

$$-2*(WAhi*Whi[t]*WXhi[t]);$$

#bilinear term constraints

subject to under1{t in T}: UE[1,t] >=

$$(GGlo[t]*GE[t])+(GElo[t]*GNG[t])-(GGlo[t]*GElo[t]);$$

subject to under2{t in T}: UE[1,t] >=

$$(GGhi[t]*GE[t])+(GEhi[t]*GNG[t])-(GGhi[t]*GEhi[t]);$$

subject to under49{t in T}: UE[1,t] <=

$$(GGhi[t]*GE[t])+(GElo[t]*GNG[t])-(GGhi[t]*GElo[t]);$$

subject to under50{t in T}: UE[1,t] <=

$$(GGlo[t]*GE[t])+(GEhi[t]*GNG[t])-(GGlo[t]*GEhi[t]);$$

subject to under3{t in T}: UE[2,t] >=

$(HGlo[t]*HE[t])+(HElo[t]*HNG[t])-(HGlo[t]*HElo[t]);$
 subject to under4{t in T}: UE[2,t] >=
 $(HGhi[t]*HE[t])+(HEhi[t]*HNG[t])-(HGhi[t]*HEhi[t]);$
 subject to under51{t in T}: UE[2,t] <=
 $(HGhi[t]*HE[t])+(HElo[t]*HNG[t])-(HGhi[t]*HElo[t]);$
 subject to under52{t in T}: UE[2,t] <=
 $(HGlo[t]*HE[t])+(HEhi[t]*HNG[t])-(HGlo[t]*HEhi[t]);$

subject to under21{t in T}: UE[5,t] >=
 $(WDlo[t]*WY[t])+(WYlo[t]*WD[t])-(WDlo[t]*WYlo[t]);$
 subject to under22{t in T}: UE[5,t] >=
 $(WDhi[t]*WY[t])+(WYhi[t]*WD[t])-(WDhi[t]*WYhi[t]);$
 subject to under23{t in T}: UE[5,t] <=
 $(WDhi[t]*WY[t])+(WYlo[t]*WD[t])-(WDhi[t]*WYlo[t]);$
 subject to under24{t in T}: UE[5,t] <=
 $(WDlo[t]*WY[t])+(WYhi[t]*WD[t])-(WDlo[t]*WYhi[t]);$

subject to under25{t in T}: UE[6,t] >=
 $(WDlo[t]*W[t])+(Wlo[t]*WD[t])-(WDlo[t]*Wlo[t]);$
 subject to under26{t in T}: UE[6,t] >=
 $(WDhi[t]*W[t])+(Whi[t]*WD[t])-(WDhi[t]*Whi[t]);$
 subject to under27{t in T}: UE[6,t] <=
 $(WDhi[t]*W[t])+(Wlo[t]*WD[t])-(WDhi[t]*Wlo[t]);$
 subject to under28{t in T}: UE[6,t] <=
 $(WDlo[t]*W[t])+(Whi[t]*WD[t])-(WDlo[t]*Whi[t]);$

subject to under29{t in T}: UE[7,t] >=

$$(WYlo[t]*W[t])+(Wlo[t]*WY[t])-(WYlo[t]*Wlo[t]);$$

subject to under30{t in T}: UE[7,t] >=

$$(WYhi[t]*W[t])+(Whi[t]*WY[t])-(WYhi[t]*Whi[t]);$$

subject to under31{t in T}: UE[7,t] <=

$$(WYhi[t]*W[t])+(Wlo[t]*WY[t])-(WYhi[t]*Wlo[t]);$$

subject to under32{t in T}: UE[7,t] <=

$$(WYlo[t]*W[t])+(Whi[t]*WY[t])-(WYlo[t]*Whi[t]);$$

subject to under33{t in T}: UE[8,t] >=

$$(GNlo[t]*GE[t])+(GElo[t]*GN[t])-(GNlo[t]*GElo[t]);$$

subject to under34{t in T}: UE[8,t] >=

$$(GNhi[t]*GE[t])+(GEhi[t]*GN[t])-(GNhi[t]*GEhi[t]);$$

subject to under35{t in T}: UE[8,t] <=

$$(GNhi[t]*GE[t])+(GElo[t]*GN[t])-(GNhi[t]*GElo[t]);$$

subject to under36{t in T}: UE[8,t] <=

$$(GNlo[t]*GE[t])+(GEhi[t]*GN[t])-(GNlo[t]*GEhi[t]);$$

subject to under37{t in T}: UE[9,t] >=

$$(HNlo[t]*HE[t])+(HElo[t]*HN[t])-(HNlo[t]*HElo[t]);$$

subject to under38{t in T}: UE[9,t] >=

$$(HNhi[t]*HE[t])+(HEhi[t]*HN[t])-(HNhi[t]*HEhi[t]);$$

subject to under39{t in T}: UE[9,t] <=

$$(HNhi[t]*HE[t])+(HElo[t]*HN[t])-(HNhi[t]*HElo[t]);$$

subject to under40{t in T}: UE[9,t] <=

$$(HNlo[t]*HE[t])+(HEhi[t]*HN[t])-(HNlo[t]*HEhi[t]);$$

subject to under41{t in T}: UE[10,t] >=

```

(WAlo*W[t])+(Wlo[t]*WA)-(WAlo*Wlo[t]);
subject to under42{t in T}: UE[10,t] >=
(WAhi*W[t])+(Whi[t]*WA)-(WAhi*Whi[t]);
subject to under43{t in T}: UE[10,t] <=
(WAhi*W[t])+(Wlo[t]*WA)-(WAhi*Wlo[t]);
subject to under44{t in T}: UE[10,t] <=
(WAlo*W[t])+(Whi[t]*WA)-(WAlo*Whi[t]);

```

```

subject to under45{t in T}: UE[11,t] >=
(WClo[t]*W[t])+(Wlo[t]*WC[t])-(WClo[t]*Wlo[t]);
subject to under46{t in T}: UE[11,t] >=
(WChi[t]*W[t])+(Whi[t]*WC[t])-(WChi[t]*Whi[t]);
subject to under47{t in T}: UE[11,t] <=
(WChi[t]*W[t])+(Wlo[t]*WC[t])-(WChi[t]*Wlo[t]);
subject to under48{t in T}: UE[11,t] <=
(WClo[t]*W[t])+(Whi[t]*WC[t])-(WClo[t]*Whi[t]);

```

#####Linearization Problem for Upper Bound#####

```

param dGE{t in T};
param dHE{t in T};
param dW{t in T};
param dWX{t in T};
param dWY{t in T};

var dWA >=0;

```

```

var dWB binary;
var dWD{t in T} >=0;
var dWC{t in T} >=0;
var dBNG{t in T} >=0;
var dGA >=0, integer;
var dHA >=0, integer;
var dVA >=0, integer;
var dSA >=0, integer;
var dGNG{t in T} >=0;
var dHNG{t in T} >=0;
var dGN{t in T} >=0, integer;
var dHN{t in T} >=0, integer;
var dGY{t in T:t>1} >=0;
var dHY{t in T:t>1} >=0;
var dP{t in T} >=0;
var dCP{t in T} >=0;
var dV{t in T} >=0;
var dSC{t in T} >=0;
var dCR{t in T} >=0;
var dDR{t in T} >=0;
var dEP{t in T} >=0;
var dES{t in T} >=0;

##For one-year instance, remove next comment and add comment
##in front of second var.
#var dE{n in N} >= 0;
var dE >= 0;

```

```

#-----
# Minimize the cost using fixed efficiencies/temps from (U)
#-----

minimize heuristic_cost:
gaq*gpx*dGA + haq*hpx*dHA + vaq*vpv*dVA + saq*sx*dSA + waq*(dWA-wx) +
tau*sum{t in T}((bom*fb+cg[t]+zt*zg)*dBNG[t])+
tau*sum{t in T}(gom*dP[t] + hom*dCP[t] + vom*dV[t]) +
sum{t in T:t>1}((cg[t]+zt*zg)*(((gmt*gpx)/fe)*dGY[t]+
((hmt*hpx)/fe)*dHY[t]))+
tau*sum{t in T}((cg[t]+zt*zg)*(dGNG[t]+dHNG[t])) +
tau*sum{t in T}((ce[t]+zt*zv)*dEP[t])- tau*sum{t in T}(ce[t]*dES[t])+

##For one-year instance, remove next comment and add comment
##in front of second line.
#sum{n in N}(cd[n]*dE[n]);
0.03*cd*dE;

#-----
# Constraints using fixed efficiencies/temps from (U)
#-----

#power and heat demand constraints
subject to ddemande{t in T}:
dP[t] + dCP[t] + dV[t] + (sde*dDR[t]-dCR[t]) + (dEP[t]-dES[t]) = de[t];
subject to ddemandh{t in T}:

```

```
-dWD[t]*(ws*(wh-wr))*wl + (ws*(wh-wr))*dW[t]*dWD[t] =  
dh[t]*(dW[t]-wl-dW[t]*dWY[t]+wh*dWY[t]);
```

```
#max monthly grid demand constraint
```

```
##For one-year instance, remove next comment and add comment
```

```
##in front of second constraint.
```

```
#subject to dminmax{n in N,t in Tn[n]}: dE[n] >= dEP[t];
```

```
subject to dminmax{t in T}: dE >= dEP[t];
```

```
#monthly net generator constraint
```

```
##For one-year instance, remove next comment and add comment
```

```
##in front of second constraint.
```

```
#subject to dnetgen{n in N}:
```

```
sum{t in Tn[n]}dES[t] <= sum{t in Tn[n]}dEP[t];
```

```
subject to dnetgen: sum{t in T}dES[t] <= sum{t in T}dEP[t];
```

```
#max power from PV cells constraint
```

```
subject to dmaxpowv{t in T}: dV[t] <= pvf[t]*vpv*dVA;
```

```
#max/min power from fuel cells constraints
```

```
subject to dpow_lo{t in T}: dP[t] >= gmt*gpx*dGN[t];
```

```
subject to dpow_hi{t in T}: dP[t] <= gpx*dGN[t];
```

```
subject to dpow_buyon{t in T}: dGA >= dGN[t];
```

```
subject to dchp_lo{t in T}: dCP[t] >= hmt*hpx*dHN[t];
```

```
subject to dchp_hi{t in T}: dCP[t] <= hpx*dHN[t];
```

```
subject to dchp_buyon{t in T}: dHA >= dHN[t];
```

```

#ramp-up/down rate for fuel cells constraints
subject to dpow_rup{t in T:t<card(T)}:
dP[t+1] - dP[t] <= tau*gru*dGN[t+1];
subject to dpow_rdown{t in T:t<card(T)}:
dP[t] - dP[t+1] <= tau*grd*dGN[t];
subject to dchp_rup{t in T:t<card(T)}:
dCP[t+1] - dCP[t] <= tau*hru*dHN[t+1];
subject to dchp_rdown{t in T:t<card(T)}:
dCP[t] - dCP[t+1] <= tau*hrd*dHN[t];

#start-up for fuel cells constraints
subject to dpow_oninc{t in T:t>1}: dGN[t]-dGN[t-1] <= dGY[t];
subject to dchp_oninc{t in T:t>1}: dHN[t]-dHN[t-1] <= dHY[t];

#natural gas consumption constraints
subject to dggas{t in T}: dGE[t]*dGNG[t] = dP[t];
subject to dhgas{t in T}: dHE[t]*dHNG[t] = dCP[t];
subject to dbgass{t in T}:
dBNG[t] = (ws/fb)*(wh*dWD[t]-wh*dWY[t]*dWD[t]-dW[t]*dWD[t]+
dWD[t]*dW[t]*dWY[t]);

#electric efficiency constraints
subject to dpow_eff{t in T}: dGE[t]*dGN[t] = 0.61*dGN[t]-0.02*dP[t];
subject to dchp_eff{t in T}: dHE[t]*dHN[t] = 0.61*dHN[t]-0.02*dCP[t];

#water tank temp constraints
subject to dtanktemp{t in T:t>1}:

```

```

ws*dW[t]*dWA - ws*dW[t-1]*dWA + ws*wd*dWA*dWX[t-1]*dW[t-1] =
tau*we*fs*ft*dWC[t-1] - tau*we*fs*dW[t-1]*dWC[t-1]
- tau*ws*dW[t-1]*dWD[t-1] + tau*ws*wr*dWD[t-1];
subject to dtemp1{t in T}: dW[t] <= wr + (wu-wr)*dWB;

#water tank heating from fuel cells constraint
subject to dtankheat1{t in T}: dWC[t] <= fh*dHNG[t];

#water tank acquisition constraints
subject to dtankacq1: dWB <= dHA;
subject to dtankacq2: HNhi[1]*dWB >= dHA;
subject to dtanksize1: dWA >= wx;
subject to dtanksize2: dWA <= wxx;

#battery state-of-charge constraints
subject to dsoc{t in T:t>1}:
dSC[t] = dSC[t-1] + tau*(sce*dCR[t-1]-dDR[t-1]);
subject to dsoc_init: dSC[1] = dSC[card(T)];

#battery max/min state-of-charge constraints
subject to dst_upcap{t in T:t>1}: dSC[t] <= sx*dSA;
subject to dst_locap{t in T:t>1}: dSC[t] >= msc*sx*dSA;

#battery charge/deplete rate constraints
subject to dcharge{t in T}: dCR[t] <= scr*dSA;
subject to ddeplete{t in T}: dDR[t] <= sdr*dSA;

```

A.2 Data File

#time increment

param tau:= 1;

#carbon emissions tax (\$/kg) and rates (kg/kWh)

param zt:= 0.02;

param zg:= 0.18;

param zu:= 0.27;

#Utility rates, demand, and PV capacity

param cd:= 6.39;

param: T: dh de pvf cg ce:=

1 66 107 0.00 0.02 0.09

2 66 109 0.00 0.02 0.09

3 66 106 0.00 0.02 0.09

4 88 110 0.00 0.02 0.09

5 148 139 0.00 0.02 0.09

6 263 246 0.00 0.02 0.09

7 363 309 0.02 0.02 0.09

8 280 270 0.25 0.02 0.09

9 205 250 0.44 0.02 0.12

10 167 206 0.56 0.02 0.12

11 124 212 0.67 0.02 0.12

12 124 214 0.70 0.02 0.12

13 117 205 0.70 0.02 0.21

14 122 207 0.64 0.02 0.21

15 123 205 0.52 0.02 0.21

16 91 232 0.35 0.02 0.21
17 141 263 0.14 0.02 0.21
18 250 314 0.00 0.02 0.21
19 187 321 0.00 0.02 0.12
20 187 346 0.00 0.02 0.12
21 274 323 0.00 0.02 0.12
22 208 254 0.00 0.02 0.12
23 131 184 0.00 0.02 0.12
24 86 128 0.00 0.02 0.09;

#daily cost/kW or kWh based on initial cost of \$4000/kW,

#\$4,800/kW, \$4,000/kW, \$200/kWh, 5% interest rate,

#15 year lifetime for gens, and 5 years for batteries

#at 70% costs

param gaq:= 1.09;

param haq:= 1.30;

param vaq:= 1.09;

param saq:= 0.10;

param waq:= 0.00;

#variable O&M costs

param gom:= 0.02;

param hom:= 0.02;

param vom:= 0.04;

param bom:= 0.01;

#kW or kWh max capacity

```
param gpx:= 10;  
param hpx:= 10;  
param vpx:= 10;  
param sx:= 10;
```

```
#water tank params
```

```
param wx:= 1000;  
param wxx:=4000;  
param wu:= 85;  
param wh:= 60;  
param wr:= 16;  
param wl:= 15;  
param we:= 0.8;  
param wd:= 0.01;  
param ws:=0.004;
```

```
#CHP exhaust param
```

```
param fh:= 2.05;  
param ft:= 365;  
param fs:= 0.0003;
```

```
#min turn-down fcells and min state-of-charge batteries
```

```
param gmt:= 0.2;  
param hmt:= 0.2;  
param msc:= 0.3;
```

```
#max ramping of fcells and charging of batteries
```

```

param gru:= 4;
param grd:= 4;
param hru:= 4;
param hrd:= 4;
param scr:= 1;
param sdr:= 2.5;

#power-heat efficiencies of fcells
#and charge-discharge of batteries
param fe:= 0.41;
param fb:= 0.75;
param sce:= 0.9;
param sde:= 0.9;

#####

#set of underestimator variables
set U:= 1 2 3 4 5 6 7 8 9 10 11;

#underestimator data
param iWAhi:=4000;
param iWAllo:=1000;

param: iGNhi iGNlo iHNhi iHNlo iGGhi iGGlo iHGhi iHGlo iGEhi iGElo
iHEhi iHElo iWChi iWClo iWDhi iWDlo iWhi iWlo iWXhi iWXlo iWYhi iWYlo:=
1 35 0 35 0 854 0 854 0 0.57 0.41
0.57 0.41 1750 0 375 241 85 16 1 0 1 0

```

2 35 0 35 0 854 0 854 0 0.57 0.41
0.57 0.41 1750 0 375 241 85 16 1 0 1 0
3 35 0 35 0 854 0 854 0 0.57 0.41
0.57 0.41 1750 0 375 241 85 16 1 0 1 0
4 35 0 35 0 854 0 854 0 0.57 0.41
0.57 0.41 1750 0 500 321 85 16 1 0 1 0
5 35 0 35 0 854 0 854 0 0.57 0.41
0.57 0.41 1750 0 841 540 85 16 1 0 1 0
6 35 0 35 0 854 0 854 0 0.57 0.41
0.57 0.41 1750 0 1495 960 85 16 1 0 1 0
7 35 0 35 0 854 0 854 0 0.57 0.41
0.57 0.41 1750 0 2063 1325 85 16 1 0 1 0
8 35 0 35 0 854 0 854 0 0.57 0.41
0.57 0.41 1750 0 1591 1022 85 16 1 0 1 0
9 35 0 35 0 854 0 854 0 0.57 0.41
0.57 0.41 1750 0 1165 748 85 16 1 0 1 0
10 35 0 35 0 854 0 854 0 0.57 0.41
0.57 0.41 1750 0 949 609 85 16 1 0 1 0
11 35 0 35 0 854 0 854 0 0.57 0.41
0.57 0.41 1750 0 705 452 85 16 1 0 1 0
12 35 0 35 0 854 0 854 0 0.57 0.41
0.57 0.41 1750 0 705 452 85 16 1 0 1 0
13 35 0 35 0 854 0 854 0 0.57 0.41
0.57 0.41 1750 0 665 427 85 16 1 0 1 0
14 35 0 35 0 854 0 854 0 0.57 0.41
0.57 0.41 1750 0 694 445 85 16 1 0 1 0
15 35 0 35 0 854 0 854 0 0.57 0.41

0.57 0.41 1750 0 699 449 85 16 1 0 1 0
16 35 0 35 0 854 0 854 0 0.57 0.41
0.57 0.41 1750 0 518 332 85 16 1 0 1 0
17 35 0 35 0 854 0 854 0 0.57 0.41
0.57 0.41 1750 0 802 515 85 16 1 0 1 0
18 35 0 35 0 854 0 854 0 0.57 0.41
0.57 0.41 1750 0 1421 913 85 16 1 0 1 0
19 35 0 35 0 854 0 854 0 0.57 0.41
0.57 0.41 1750 0 1063 683 85 16 1 0 1 0
20 35 0 35 0 854 0 854 0 0.57 0.41
0.57 0.41 1750 0 1063 683 85 16 1 0 1 0
21 35 0 35 0 854 0 854 0 0.57 0.41
0.57 0.41 1750 0 1557 1000 85 16 1 0 1 0
22 35 0 35 0 854 0 854 0 0.57 0.41
0.57 0.41 1750 0 1182 759 85 16 1 0 1 0
23 35 0 35 0 854 0 854 0 0.57 0.41
0.57 0.41 1750 0 745 478 85 16 1 0 1 0
24 35 0 35 0 854 0 854 0 0.57 0.41
0.57 0.41 1750 0 489 314 85 16 1 0 1 0;

param: jWhi jWYhi jWDlo :=

1	85	1	241
2	85	1	241
3	85	1	241
4	85	1	321
5	85	1	540
6	85	1	960

7	48	0	2062
8	74	1	1213
9	85	1	748
10	85	1	609
11	85	1	452
12	85	1	452
13	85	1	427
14	85	1	445
15	85	1	449
16	85	1	332
17	85	1	515
18	85	1	913
19	85	1	683
20	85	1	683
21	83	1	1030
22	85	1	759
23	85	1	478
24	85	1	314;

A.3 Run File

```
param starttime2;  
let starttime2:= time();  
  
model CHP_DG_under2.mod;  
data LA_Hotel_Power1.dat;  
  
option presolve 0;  
option solver cplexamp123;
```

```

option cplex_options 'timing 1 feasibility 0.01 mipgap 0.01
mipdisplay 3 mipemphasis 2 timelimit 36000';
option display_1col 9000;

problem UnderEstimate:
GA,HA,VA,SA,WA,WB,GN,HN,GY,HY,P,CP,V,WC,WD,SC,CR,DR,EP,ES,E,GE,HE,
GNG,HNG,BNG,WY,WX,W,UE,
under_cost,
demande,demandh,minmax,netgen,maxpowv,pow_lo,pow_hi,pow_buyon,
chp_lo,chp_hi,chp_buyon,pow_rup,pow_rdown,chp_rup,chp_rdown,
pow_oninc,chp_oninc,ggas,hgas,bgas,pow_eff,chp_eff,
tankacq1,tankacq2,tanktemp,temp1,tankheat1,temp3,temp4,temp5,temp6,temp7,
soc,soc_init,st_upcap,st_locap,charge,deplete,
under1,under2,under3,under4,under5,under6,under7,under8,under9,under10,
under11,under12,under13,under14,under15,under16,under17,under18,under19,
under20,under21,under22,under23,under24,under25,under26,under27,under28,
under29,under30,under31,under32,under33,under34,under35,under36,under37,
under38,under39,under40,under41,under42,under43,under44,under45,under46,
under47,under48,under49,under50,under51,under52;

problem Heuristic:
dGA,dHA,dSA,dVA,dGN,dHN,dGY,dHY,dP,dCP,dV,dSC,dCR,dDR,dEP,dES,dE,
dGNG,dHNG,dWA,dWB,dWD,dWC,dBNG,
heuristic_cost,
ddemande,dminmax,dnetgen,dmaxpowv,dpow_lo,dpow_hi,dpow_buyon,
dchp_lo,dchp_hi,dchp_buyon,dpow_rup,dpow_rdown,dchp_rup,dchp_rdown,
dpow_oninc,dchp_oninc,dggas,dhgas,dpow_eff,dchp_eff,ddemandh,dbgas,

```

```
dtanktemp, dtemp1, dtankheat1, dtankacq1, dtankacq2, dtanksize1, dtanksize2,  
dsoc, dsoc_init, dst_upcap, dst_locap, dcharge, ddeplete;
```

```
param grid_cost;
```

```
let grid_cost := 0.03*cd*(max{t in T}de[t]) +  
tau*sum{t in T}((ce[t]+zt*zv)*de[t]) +  
tau*sum{t in T}((bom*fb+cg[t]+zt*zg)*(dh[t]/fb));
```

```
##For one-year instance, replace first component
```

```
##of grid_cost with the following:
```

```
#sum{n in N}(cd[n]*(max{t in Tn[n]}de[t]))
```

```
#####Underestimation Problem#####
```

```
let {t in T}GNhi[t] := iGNhi[t];
```

```
let {t in T}GNlo[t] := iGNlo[t];
```

```
let {t in T}GGhi[t] := iGGhi[t];
```

```
let {t in T}GGlo[t] := iGGlo[t];
```

```
let {t in T}GEhi[t] := iGEhi[t];
```

```
let {t in T}GElo[t] := iGElo[t];
```

```
let {t in T}HNhi[t] := iHNhi[t];
```

```
let {t in T}HNlo[t] := iHNlo[t];
```

```
let {t in T}HGhi[t] := iHGhi[t];
```

```
let {t in T}HGlo[t] := iHGlo[t];
```

```
let {t in T}HEhi[t] := iHEhi[t];
```

```
let {t in T}HElo[t] := iHElo[t];
```

```
let {t in T}WChi[t] := iWChi[t];
```

```

let {t in T}WClo[t]:= iWClo[t];
let {t in T}WDhi[t]:= iWDhi[t];
let {t in T}WDlo[t]:= jWDlo[t];
let {t in T}Whi[t]:= jWhi[t];
let {t in T}Wlo[t]:= iWlo[t];
let {t in T}WXhi[t]:= iWXhi[t];
let {t in T}WXlo[t]:= iWXlo[t];
let {t in T}WYhi[t]:= jWYhi[t];
let {t in T}WYlo[t]:= iWYlo[t];

let WAhi:= iWAhi;
let WALo:= iWALo;

solve UnderEstimate;

param lowerbound_totalcost;
let lowerbound_totalcost:= under_cost;

param GA_low;
let GA_low:= GA;

param HA_low;
let HA_low:= HA;

param VA_low;
let VA_low:= VA;

param SA_low;
let SA_low:= SA;

param WA_low;
let WA_low:= WA;

```

```

#####Linearization Heuristic#####

##Without heat capture
let {t in T}dGE[t]:=
(if GN[t]>0 then 0.61-0.02*(P[t]/GN[t]) else 0.41);
let {t in T}dHE[t]:=
(if HN[t]>0 then 0.61-0.02*(CP[t]/HN[t]) else 0.41);
let {t in T}dW[t]:= wr;
let {t in T}dWX[t]:= 0;
let {t in T}dWY[t]:= 0;

solve Heuristic;

param upperbound_totalcost_pow;
let upperbound_totalcost_pow:= heuristic_cost;

param dGA_pow;
let dGA_pow:= dGA;
param dHA_pow;
let dHA_pow:= dHA;
param dVA_pow;
let dVA_pow:= dVA;
param dSA_pow;
let dSA_pow:= dSA;
param dWA_pow;
let dWA_pow:= dWA;

```

```

##With heat capture
let dW[1]:=wh;
let dWX[1]:=1;
let dWY[1]:=0;
param flow{t in T};
let flow[1]:= dh[1]/(ws*(wh-wr));

for {t in T: t>1}{
let dW[t]:= max(wr, min(wu, (1-wd*dWX[t-1])*dW[t-1]+(1/(ws*WA))*
(tau*we*fs*fh*(CP[t-1]/dHE[t-1])*(ft-dW[t-1])-tau*ws*flow[t-1]*
(dW[t-1]-wr))));
let dWX[t]:= (if dW[t]>wr+0.1 then 1 else 0);
let dWY[t]:= (if dW[t]>wh then 1 else 0);
let flow[t]:= (1-(1-((wh-wl)/(dW[t]-wl)))*dWY[t])*(dh[t]/(ws*(wh-wr)));
}

let dW[1]:=dW[card(T)];
let dWX[1]:= (if dW[1]>wr+0.1 then 1 else 0);
let dWY[1]:= (if dW[1]>wh then 1 else 0);
let flow[1]:= (1-(1-((wh-wl)/(dW[1]-wl)))*dWY[1])*(dh[1]/(ws*(wh-wr)));

for {t in T: t>1}{
let dW[t]:= max(wr, min(wu, (1-wd*dWX[t-1])*dW[t-1]+(1/(ws*WA))*
(tau*we*fs*fh*(CP[t-1]/dHE[t-1])*(ft-dW[t-1])-tau*ws*flow[t-1]*
(dW[t-1]-wr))));
let dWX[t]:= (if dW[t]>wr+0.1 then 1 else 0);

```

```

let dWY[t]:= (if dW[t]>wh then 1 else 0);
let flow[t]:= (1-(1-((wh-wl)/(dW[t]-wl)))*dWY[t])*(dh[t]/(ws*(wh-wr)));
}

solve Heuristic;

param upperbound_totalcost_chp;
let upperbound_totalcost_chp:= heuristic_cost;

param dGA_chp;
let dGA_chp:= dGA;
param dHA_chp;
let dHA_chp:= dHA;
param dVA_chp;
let dVA_chp:= dVA;
param dSA_chp;
let dSA_chp:= dSA;
param dWA_chp;
let dWA_chp:= dWA;

param runtime2;
let runtime2:= time() - starttime2;

display runtime2,grid_cost,
lowerbound_totalcost,GA_low,HA_low,VA_low,SA_low,WA_low,
upperbound_totalcost_pow,dGA_pow,dHA_pow,dVA_pow,dSA_pow,dWA_pow,
upperbound_totalcost_chp,dGA_chp,dHA_chp,dVA_chp,dSA_chp,dWA_chp,

```

```
dGN,dGY,dP,dGNG,dGE,dHN,dHY,dCP,dHNG,dHE,dW,dWX,dWY,dWC,dWD,dV,  
dSC,dCR,dDR,dEP,dES>pruitt_solution.out;
```

A.4 Out File

```
runtime2 = 5  
grid_cost = 969.318  
lowerbound_totalcost = 742.747  
GA_low = 3  
HA_low = 21  
VA_low = 0  
SA_low = 5  
WA_low = 2453.13  
upperbound_totalcost_pow = 869.638  
dGA_pow = 29  
dHA_pow = 0  
dVA_pow = 0  
dSA_pow = 5  
dWA_pow = 1000  
upperbound_totalcost_chp = 823.758  
dGA_chp = 3  
dHA_chp = 21  
dVA_chp = 0  
dSA_chp = 7  
dWA_chp = 2453.13
```

```
: dGN dGY dP dGNG dGE dHN dHY dCP dHNG:=  
1 3 . 6 10.5 0.57 21 . 187.1 433.3  
2 3 0 6 10.5 0.57 21 0 108 213.0
```

3	3	0	6	10.5	0.57	21	0	192	449.5
4	3	0	6	10.5	0.57	21	0	204.4	492.2
5	3	0	6	10.5	0.57	21	0	161.8	354.8
6	3	0	6	10.5	0.57	21	0	204.4	492.2
7	3	0	14	26.5	0.52	21	0	204.4	492.2
8	3	0	18	36.7	0.49	21	0	204.4	492.2
9	3	0	30	73.2	0.41	21	0	210	512.2
10	3	0	30	73.2	0.41	21	0	210	512.2
11	3	0	30	73.2	0.41	21	0	210	512.2
12	3	0	30	73.2	0.41	21	0	210	512.2
13	3	0	30	73.2	0.41	21	0	210	512.2
14	3	0	30	73.2	0.41	21	0	210	512.2
15	3	0	30	73.2	0.41	21	0	210	512.2
16	3	0	30	73.2	0.41	21	0	210	512.2
17	3	0	30	73.2	0.41	21	0	210	512.2
18	3	0	30	73.2	0.41	21	0	210	512.2
19	3	0	30	73.2	0.41	21	0	210	512.2
20	3	0	30	73.2	0.41	21	0	210	512.2
21	3	0	30	73.2	0.41	21	0	210	512.2
22	3	0	30	73.2	0.41	21	0	210	512.2
23	3	0	30	73.2	0.41	21	0	204.4	492.2
24	2	0	18	41.9	0.43	13	0	120.4	283.5;

:	dHE	dW	dWX	dWY	dWC	dWD	dV	dSC	dCR:=
1	0.43	35.0	1	0	888.2	375	0	21	7
2	0.51	38.9	1	0	436.6	375	0	27.3	7
3	0.43	38.5	1	0	921.5	375	0	33.6	7

4	0.42	42.0	1	0	1009	500	0	39.9	7
5	0.46	44.3	1	0	727.4	840.9	0	46.2	7
6	0.42	39.8	1	0	1009	1494.3	0	52.5	7
7	0.42	32.9	1	0	1009	2062.5	0	58.8	0
8	0.42	26.6	1	0	1009	1590.9	0	58.1	7
9	0.41	27.8	1	0	1050	1164.78	0	64.4	0
10	0.41	30.6	1	0	1050	948.9	0	64.4	0
11	0.41	33.2	1	0	1050	704.5	0	64.4	6.2
12	0.41	36.5	1	0	1050	704.5	0	70	0
13	0.41	38.7	1	0	1050	664.8	0	70	0
14	0.41	40.5	1	0	1050	693.2	0	70	0
15	0.41	41.5	1	0	1050	698.9	0	70	0
16	0.41	42.1	1	0	1050	517.0	0	67.2	0
17	0.41	44.5	1	0	1050	801.2	0	67.2	0
18	0.41	43.0	1	0	1050	1420.5	0	49.7	0
19	0.41	35.2	1	0	1050	1062.5	0	32.2	7
20	0.41	35.0	1	0	1050	1062.5	0	38.5	0
21	0.41	34.9	1	0	1000	1556.8	0	21	0
22	0.41	30.6	1	0	1050	1181.8	0	21	0
23	0.42	31.9	1	0	1009	744.3	0	21	0
24	0.42	35.0	1	0	0	488.6	0	21	0;

	dDR	dEP	dES:=
1	0	0	79.1
2	0	2	0
3	0	0	85
4	0	0	93.4

5	0	0	21.8
6	0	42.6	0
7	0.7	90.3	0
8	0	54.6	0
9	0	10	0
10	0	0	34
11	0	0	21.8
12	0	0	26
13	0	0	35
14	0	0	33
15	2.8	0	37.5
16	0	0	8
17	17.5	7.3	0
18	17.5	58.3	0
19	0	88	0
20	17.5	90.3	0
21	0	83	0
22	0	14	0
23	0	0	50.4
24	5.3	0	15.1;

APPENDIX B - STATE PRICING, EMISSIONS, AND GRID DATA

Table B.1 and Table B.2 list the average price of commercial-sector electricity, the primary fuel source for all-sector power generation, and the average carbon emissions rate for all-sector power generation according to the Energy Information Administration (EIA) 2009 State Electricity Profiles report (see [54]). The average carbon emissions rate is calculated as the quotient of the all-sector total carbon emissions (thousand metric tons) and the all-sector net-generation (MWh).

The net-metering policy and interconnection procedure grades are obtained from the Network for New Energy Choices (NNEC) 2009 Freeing the Grid report (see [56]). A grade of “A” indicates that the state policies and procedures actively encourage DG interconnection and use by, among other reasons, offering full retail credit for exported power and presenting few barriers to system integration. A grade of “F” indicates that state policies and procedures deter, or completely block, the interconnection and use of customer-sited DG systems. A grade of “n/a” indicates there are no state-wide net-metering or interconnection standards. The NNEC report offers further details on the methodology used to grade each state.

The average price of commercial-sector natural gas is derived from the EIA 2009 Natural Gas Annual report (see [55]), along with a conversion factor of 302.08 kWh per thousand cubic feet. Table B.3 and Table B.4 provide the same data for 2010, based on the EIA reports (see [59] and [60]) and NNEC report (see [58]) for that year.

Table B.1: 2009 state energy pricing, carbon emissions rates, and net-metering grades for Alabama through Missouri

State	Electricity Price [\$/kWh]	Prime Fuel Source	Carbon Rate [kg/kWh]	Net-meter Policy	Inter-connect Procedure	Gas Price [\$/kWh]
AL	0.101	coal	0.483	n/a	n/a	0.049
AK	0.145	gas	0.633	n/a	n/a	0.031
AZ	0.094	coal	0.478	A	C	0.040
AR	0.076	coal	0.530	C	F	0.035
CA	0.134	gas	0.290	A	B	0.026
CO	0.082	coal	0.771	A	B	0.025
CT	0.169	nuclear	0.258	A	D	0.033
DE	0.120	coal	0.856	A	D	0.053
FL	0.108	gas	0.527	A	C	0.037
GA	0.089	coal	0.598	F	F	0.039
HI	0.219	petro	0.787	C	F	0.099
ID	0.065	hydro	0.078	F	n/a	0.032
IL	0.090	nuclear	0.511	B	B	0.029
IN	0.083	coal	0.952	F	D	0.030
IA	0.076	coal	0.829	C	F	0.026
KS	0.079	coal	0.776	B	F	0.033
KY	0.076	coal	0.951	B	F	0.036
LA	0.077	gas	0.585	B	F	0.035
ME	0.126	gas	0.288	B	n/a	0.046
MD	0.120	coal	0.586	A	B	0.036
MA	0.154	gas	0.505	B	B	0.043
MI	0.092	coal	0.727	B	C	0.031
MN	0.079	coal	0.642	C	F	0.026
MS	0.095	gas	0.482	n/a	n/a	0.031
MO	0.070	coal	0.846	C	F	0.036

Table B.2: 2009 state energy pricing, carbon emissions rates, and net-metering grades for Montana through Wyoming

State	Electricity Price [\$/kWh]	Prime Fuel Source	Carbon Rate [kg/kWh]	Net-meter Policy	Inter-connect Procedure	Gas Price [\$/kWh]
MT	0.083	coal	0.657	C	F	0.031
NE	0.073	coal	0.703	B	F	0.025
NV	0.106	gas	0.485	B	B	0.036
NH	0.146	nuclear	0.273	C	C	0.048
NJ	0.138	nuclear	0.260	A	B	0.034
NM	0.084	coal	0.844	B	B	0.025
NY	0.155	nuclear	0.286	D	B	0.035
NC	0.080	coal	0.548	D	B	0.038
ND	0.068	coal	0.954	D	n/a	0.025
OH	0.097	coal	0.846	B	C	0.034
OK	0.068	gas	0.693	D	n/a	0.035
OR	0.075	hydro	0.166	A	B	0.039
PA	0.095	coal	0.531	A	B	0.039
RI	0.137	gas	0.413	B	n/a	0.050
SC	0.087	nuclear	0.381	n/a	F	0.037
SD	0.071	hydro	0.428	n/a	B	0.025
TN	0.096	coal	0.545	n/a	n/a	0.035
TX	0.097	gas	0.611	n/a	D	0.027
UT	0.070	coal	0.839	A	F	0.025
VT	0.129	nuclear	0.001	B	C	0.043
VA	0.081	nuclear	0.516	B	A	0.034
WA	0.070	hydro	0.129	C	D	0.041
WV	0.068	coal	0.931	D	n/a	0.047
WI	0.096	coal	0.738	D	D	0.030
WY	0.073	coal	0.971	B	F	0.027

Table B.3: 2010 state energy pricing, carbon emissions rates, and net-metering grades for Alabama through Missouri

State	Electricity Price [\$/kWh]	Prime Fuel Source	Carbon Rate [kg/kWh]	Net-meter Policy	Inter-connect Procedure	Gas Price [\$/kWh]
AL	0.102	coal	0.522	n/a	n/a	0.044
AK	0.140	gas	0.610	B	n/a	0.029
AZ	0.095	coal	0.498	A	n/a	0.035
AR	0.073	coal	0.558	B	n/a	0.029
CA	0.131	gas	0.271	A	B	0.027
CO	0.091	coal	0.798	A	B	0.025
CT	0.165	nuclear	0.276	A	B	0.032
DE	0.114	gas	0.744	A	F	0.044
FL	0.098	gas	0.540	A	B	0.035
GA	0.091	coal	0.600	F	n/a	0.036
HI	0.259	petro	0.765	B	F	0.121
ID	0.066	hydro	0.101	n/a	n/a	0.027
IL	0.089	nuclear	0.512	B	B	0.029
IN	0.084	coal	0.929	D	C	0.025
IA	0.079	coal	0.821	B	B	0.026
KS	0.083	coal	0.758	B	n/a	0.032
KY	0.079	coal	0.949	B	F	0.029
LA	0.085	gas	0.571	B	n/a	0.033
ME	0.125	gas	0.291	B	A	0.039
MD	0.118	coal	0.605	A	B	0.033
MA	0.145	gas	0.474	A	A	0.040
MI	0.098	coal	0.668	A	C	0.030
MN	0.084	coal	0.614	B	D	0.025
MS	0.093	gas	0.493	n/a	n/a	0.029
MO	0.075	coal	0.854	C	n/a	0.034

Table B.4: 2010 state energy pricing, carbon emissions rates, and net-metering grades for Montana through Wyoming

State	Electricity Price [\$/kWh]	Prime Fuel Source	Carbon Rate [kg/kWh]	Net-meter Policy	Inter-connect Procedure	Gas Price [\$/kWh]
MT	0.086	coal	0.684	C	C	0.028
NE	0.076	coal	0.668	B	n/a	0.023
NV	0.098	gas	0.484	B	B	0.032
NH	0.143	nuclear	0.250	B	D	0.042
NJ	0.139	nuclear	0.292	A	B	0.033
NM	0.086	coal	0.810	B	B	0.025
NY	0.163	gas	0.304	B	B	0.036
NC	0.082	coal	0.569	D	B	0.034
ND	0.072	coal	0.894	D	n/a	0.023
OH	0.097	coal	0.849	A	C	0.031
OK	0.075	gas	0.686	F	n/a	0.032
OR	0.076	hydro	0.183	A	B	0.033
PA	0.101	coal	0.535	A	B	0.035
RI	0.131	gas	0.416	B	n/a	0.048
SC	0.089	nuclear	0.397	F	F	0.034
SD	0.076	hydro	0.359	n/a	B	0.024
TN	0.097	coal	0.585	n/a	n/a	0.031
TX	0.092	gas	0.611	n/a	C	0.026
UT	0.072	coal	0.841	A	A	0.023
VT	0.134	nuclear	0.001	B	C	0.039
VA	0.077	nuclear	0.544	B	A	0.032
WA	0.074	hydro	0.135	B	D	0.035
WV	0.077	coal	0.919	A	B	0.034
WI	0.100	coal	0.734	C	D	0.028
WY	0.074	coal	0.950	B	n/a	0.024